# Identification of novel genes involved in prostate and Schwann cell malignancies utilizing a *Sleeping Beauty* transposon somatic cell mutagenesis screen

A DISSERTATION
SUBMITTED TO THE FACULTY OF THE GRADUATE SCHOOL
OF THE UNIVERSITY OF MINNESOTA
BY

**Eric Patrick Rahrmann**

IN PARTIAL FULFILLMENT OF THE REQUIREMENTS
FOR THE DEGREE OF
DOCTOR OF PHILOSOPHY

Dr. David A. Largaespada

June 2011

**Acknowledgements**

I would like to thank my advisors during my graduate school career Dr. Paul C. Marker and Dr. David A. Largaespada for teaching me how to become an independent research scientist. I would like to thank members and former members of the Marker lab: Dr. Sheri Kuslak, Dr. Meg Joesting, Kat Volzing and Todd Knutson for technical and scientific help. I would also like to thank members of the Largaespada lab: Dr. Timothy Starr, Dr. Vincent Keng, Branden Moriarity, Adrienne Watson, Luke Manlove, Caitlin Conboy, Dr. Rachel Bergerson, Dr. Zohar Sachs, Sue Rathe, Micki Diers, Dr. Julia Hatler for all their scientific and technical assistance during the course of my graduate career. I would also like to thank Dr. Clint Matson for his mentorship/friendship during my graduate career. I would also like to give a special thanks to Dr. Christopher Moertel and Dr. David Largaespada for going beyond the basic science and providing me opportunities to directly interact with the general community to really understand how the diseases we study directly effect people.

**Dedication**

This dissertation is dedicated to my family. Thank you for sticking with me as the spring season of my life has come to pass and the summer season of my life is about to begin.

**Table of Contents**

**List of Tables**

**List of Figures**

# Chapter 1.
# Introduction

The focus of this thesis is the identification of new therapeutic targets for prostate and Schwann cell cancers using the *Sleeping Beauty* (SB) transposon system. The main emphasis will be in describing new mouse models of prostate cancer (chapters 2 & 3) and malignant peripheral nerve sheath tumor formation (chapters 4 & 5).

This chapter will be an overview on current status of cancer and cancer treatments available. The last section of this chapter will discuss the use of the *Sleeping Beauty* transposon system for identifying novel genes involved in cancer initiation and progression. The introduction of each chapter will highlight the current status and background of each cancer type being modeled with the *Sleeping Beauty* transposon system.

**What is Cancer?**

Cancer is simply described as the uncontrolled growth of abnormal cells in the body. Normal cells within our bodies respond to signals that provide information about when to proliferate and when to die. Genes called proto-oncogenes and tumor suppressor genes tightly regulate these signals within the cell. It is when normal cells acquire mutations in these genes allowing them to 'avoid' regulation of growth and death that they become abnormal.

These mutations can be divided into two classes: 1) inherited genetic causes and 2) environmental causes. Inherited genetic causes are mutations within genes that are passed through generations that give rise to cancer [reviewed Anand, P. 2008]. These causes generally make up only a small portion of cancer incidence. Largely, cancer is most often caused by carcinogens, cancer causing factors, found in the environment. These environmental factors include but are not limited to: chemicals (benzene), excess alcohol, tobacco, environmental toxins/pollutants, excessive sunlight, obesity, radiation, and viruses [reviewed Anand, P. 2008]. The overall mechanism by which these environmental factors induce cancer is to mutate genes within our cells and cause them to become abnormal. However, many environmental factors that cause cancer and the sum of specific genetic loci that are mutated remain unknown.

**Cancer incidence in the United States.**

Cancer is the second leading cause of death in the United States after heart disease. In 2010, the American Cancer Society projected 1.5 million people were diagnosed with cancer [Jemal, A. 2010]. However, this number does not reflect individuals who were diagnosed with non-invasive cancers or basal and squamous cell skin cancers. Based on American Cancer Society 2006 reports that over 2 million people were treated for skin cancers, the estimates of newly diagnosed overall cancer incidents may truly be closer to 3.5 million Americans in 2010 [Jemal, A. 2010]. Furthermore, there were 569,490 cancer related deaths in 2010 which accounted for 1 in every 4 deaths recorded in the United States [Jemal, A. 2010]. Analysis of cancer sup-types demonstrated that epithelial cell based cancers (lung, colon, prostate, breast, and pancreas) were the principle component of the cancer related deaths (Figure 1). Though the number of reported cancer cases are increasing, the survival rates are improving for many cancers [Jemal, A. 2010].

**Current cancer treatments.**

Survival rates for cancer patients are increasing steadily over the years from a 50% 5-year survival from 1975-1977 to a 68% 5-year survival rate from 1999-2005 based on the National Cancer Institute Surveillance Epidemiology and End Results (SEER) data (Figure 2) [Jemal, A. 2010]. The largest contributing factors to this increase in survival are better earlier cancer detection and improved treatments. Improvements in cancer detection has allowed surgeons to remove cancerous masses prior to the cancer spreading throughout the body, metastasizing. In addition to surgical resection of tumors, the use of non-targeted chemotherapeutic agents such as 5-Fluorouracil-leucovorin (incorporates into DNA), oxaliplatin (Cross-links DNA), and irinotecan (topoisomerase inhibitor) have been effective in some cancers (colon cancer) providing improved survival [Hind, D. 2008]. However, current chemotherapeutic treatments are not effective for all cancer types. Therefore, there is a need for improved and newly targeted therapies for cancer treatment.

Currently, targeted therapies using Bevacizumab (anti-VEGF) and Cetuximab &

Panitummumab (anti-EGFR) have been used in combination with non-targeted therapies and have elicited better responses yet efficacy again has not been observed in all cancer types [Willett, C.G. 2004;Van Cutsem, E. 2008;Tawbi,H. 2008]. One great success story for targeted therapy is Imatinib (BCR-ABL inhibitor) for treatment of chronic myeloid leukemia (CML). Nearly ~95% of people with CML possess the *BCR-ABL* translocation [Sawyers, C.L. 1999]. Identification of a specific translocation (*BCR-ABL*) in CML patients allowed the drug Imatinib to selectively induce cytotoxic effects on T-cells with this mutation [Schindler, T. 2000; Sawyers, C.L. 1999; Druker, B.J. 2000]. This success story may in part be due to the possibility that CML originates from a single genetic alteration upon which the cells are totally dependent. This suggests that the method of success in creating targeted therapies for cancer treatment relies on identifying genetic alterations that give rise to the disease, and possibly also having few driver genetic alterations.

**The Genetic Landscape of Human Cancer**

With recent advances in sequencing technologies, much emphasis has been placed on sequencing all the exons of all the annotated genes (exome) in a wide variety of cancers. In particular, Sjoblom et al, resequenced 13,023 genes in 11 colorectal cancer and 11 breast cancer samples and identified on average ~90 genes mutated per tumor [Sjoblom, T. 2006]. Statistical analyses of the mutations identified suggested that a minimum of 15 driver mutations, mutations that directly contribute to tumor formation, were needed for tumor formation. In addition, Sjoblom et al. also assessed DNA copy number changes and observed that 500 genes had >2 fold changes in 10% of the tumors assessed [Sjoblom, T. 2006]. Taken together, this suggests that numerous changes occur that can give rise to tumorigenesis. Moreover, based on these changes it is difficult to discern which of the genetic alterations are driver for tumor formation. In addition, this problem is amplified by the fact that the majority of annotated genes have not been studied (Figure 3) [Huss, J.W. 2010]. Huss et al., scoured through PubMed Database and found that 78% of the annotated genes have five or fewer references [Huss, J.W. 2010]. Also, re-sequencing approaches have limitations in that all relevant genetic alterations cannot be

detected: amplification of genes, complete deletions of genes that lead to haploinsufficiency, and epigenetic changes. Taken together, these large hurdles bring us back to the question of how do we identify the genetic drivers of tumor formation in order to create targeted therapies for cancer treatment?

**Utilizing the *Sleeping Beauty* transposon system to model human cancers in mice.** Forward somatic cell mutagenesis screens in model organisms are powerful tools to identify genes and highlight genetic pathways altered in human cancer [Jonkers, J. 1996; Johansson, F.K 2004; Callahan, R. 2000]. Insertional mutagenic approaches either by retroviral mutagenesis or by transposon-based mutagenesis are favored over classic mutagenic approaches such as chemical and radiation induced mutagenesis due to the ease of identifying the mutations induced by the mutagens [de Angelis, M.H. 2000; Justice, M.J. 1999]. These insertional mutagens provide a 'molecular tag' to easily identify where mutagenic events in the genome occur which in turn allows for rapid identification of mutagenized genomic loci. These regions of the genome that are repeatedly found mutated in tumors from many mice are deemed common insertion sites (CISs). Retroviral and transposon based insertional mutagenic studies have demonstrated that CISs identify known oncogenes and tumor suppressor genes (TSGs) [Jonkers, J. 1996; Johansson, F.K. 2004; Callahan, R. 2000; Collier, LS. 2005; Dupuy, A.J. 2005].

The *Sleeping Beauty* (SB) transposon system is a bipartite system comprised of a mobilized piece of DNA called a transposon and enzyme that catalyzes the transposition reaction called a transposase [Ivics,Z. 1997]. SB is a DNA based transposon that functions via a 'cut-and-paste' and paste mechanism [Ivics,Z. 1997]. The transposase enzyme binds to specific Inverted Repeat Direct Repeat (IRDR) sequences that flank the transposon at a 2:1 ratio. Upon binding the IRDRs, the transposase induces a DNA double strand break, excises the transposon from the donor location, and mobilizes the transposon to randomly be reinserted into a 'TA' dinucleotide with in the genome [Ivics,Z. 1997]. The DNA double strand break is repaired by the non-homologous endjoing repair mechanisms leaving a 7 bp footprint. At the new insertion site, there is a duplication of the 'TA' nucleotide (Figure 4). A unique feature of this system is that the

transposon can contain virtually any cargo (DNA elements) with the only requirement being the cargo is flanked by IRDR sequences for the transposase to bind. These features of the transposon have made the SB system amenable to many uses including gene therapy, germline studies, and cancer gene discovery screens [Dupuy,A.J. 2002; Belur,L.R. 2003; Ohlfest,J.R. 2005; Dupuy,A.J. 2009; Keng,V.W. 2009; Starr,T.K. 2009; Collier, L.S. 2005; Dupuy, A.J. 2005].

Recent studies have shown that genome-wide somatic mutagenesis with a *Sleeping Beauty* transposon called T2/onc can also be used to induce tumors and identify cancer genes at CISs. T2/onc was engineered with features similar to slow transforming retroviruses that allow it to activate and/or disrupt endogenous genes [Collier, L.S. 2005]. These features include a gene disruption cassette, bidirectional splice acceptors followed by stop codons/poly-adenylation signals, and an overexpression cassette, constitutively active murine stem cell virus promoter followed by a splice donor (Figure 5). In practice, T2/onc can reduce expression of TSGs or overexpress proto-oncogenes giving rise to tumor formation.

The SB system has been used to generate mouse models of variety of cancers. Using this transposon, transgenic mice have been generated that harbor a concatemer of ~25-300 copies of the T2/Onc transposon [Collier, L.S. 2005;Dupuy, A.J. 2005]. Mouse studies in which ubiquitous mobilization of T2/Onc by SB under the control of the *Rosa26* promoter occurred caused robust tumor formation and in some cases embryonic lethality [Dupuy, A.J. 2005; Collier, L.S. 2009]. The majority of tumors formed were of hematopoietic origin with some solid tumors including medulloblastomas, gliomas, pituitary tumors as well as neoplasias in the intestines and prostate [Collier, L.S. 2009; Rahrmann, E.P. 2009].

In order to selectively target SB mutagenesis to study specific cancers, a conditional SB transposition system was developed utilizing the Cre-lox technology [Dupuy,A.J. 2009]. The *Rosa26-SB11* allele was modified to include a loxP-stop/eGFP-loxP cassette, stop cassette, immediately upstream of the SB11 cDNA creating the *Rosa26-lsl-SB11* allele. When the stop cassette is present, the transposase will not be transcribed. By supplying the enzyme Cre-recombinase (Cre), Cre will bind to the loxP

sites and remove the stop cassette allowing for *SB11* expression from the *Rosa26* promoter (Figure 6). This expression can be controlled in a tissue specific manner by placing the Cre allele under the control of a tissue specific promoter thereby restricting transposition to the cell type of interest. This technology has been utilized to successfully model colorectal cancer using *Villin-Cre,* hepatocellular carcinoma using *Albumin-Cre*, and germinal center B-cell lymphoma using *Aid-Cre* [Dupuy,A.J. 2009; Keng, V.W. 2009; Starr, T.K. 2009]. In each of these studies, the SB system identified known oncogenes and TSGs involved in tumorigenesis, validating the screen, as well as many novel genes not previously implicated. Taken together, the SB system is a powerful tool for identifying oncogenes and TSGs involved in human cancers.

When I started my thesis work, there were many important facts not known about the use of *Sleeping Beauty* somatic mutagenesis for cancer gene discovery. It was not known whether epithelial tumors could be induced, if genetically 'predisposed' backgrounds for screens were needed, if the conditional SB-system worked well, and could the SB-system be used to model all stages of human cancer progression. A culmination of my thesis work, described in the following chapters, and work from many others has been able address these fundamental questions.

**Thesis Statement**

The goals of my thesis were to model human prostate cancer and MPNST development in mice to identify new therapeutic targets for treatment of these diseases. In the following chapters, I will describe how we successfully utilized the *Sleeping Beauty* transposon system to identify new candidate genes involved in prostate cancer and MPNST formation.

**Figure 1. Cancer-related deaths based on cancer type.** Graph depicts the percent breakdown of people who have died from cancer-related deaths and the type of cancer the patient possessed. Data is based on 2010 statistics from SEER data.

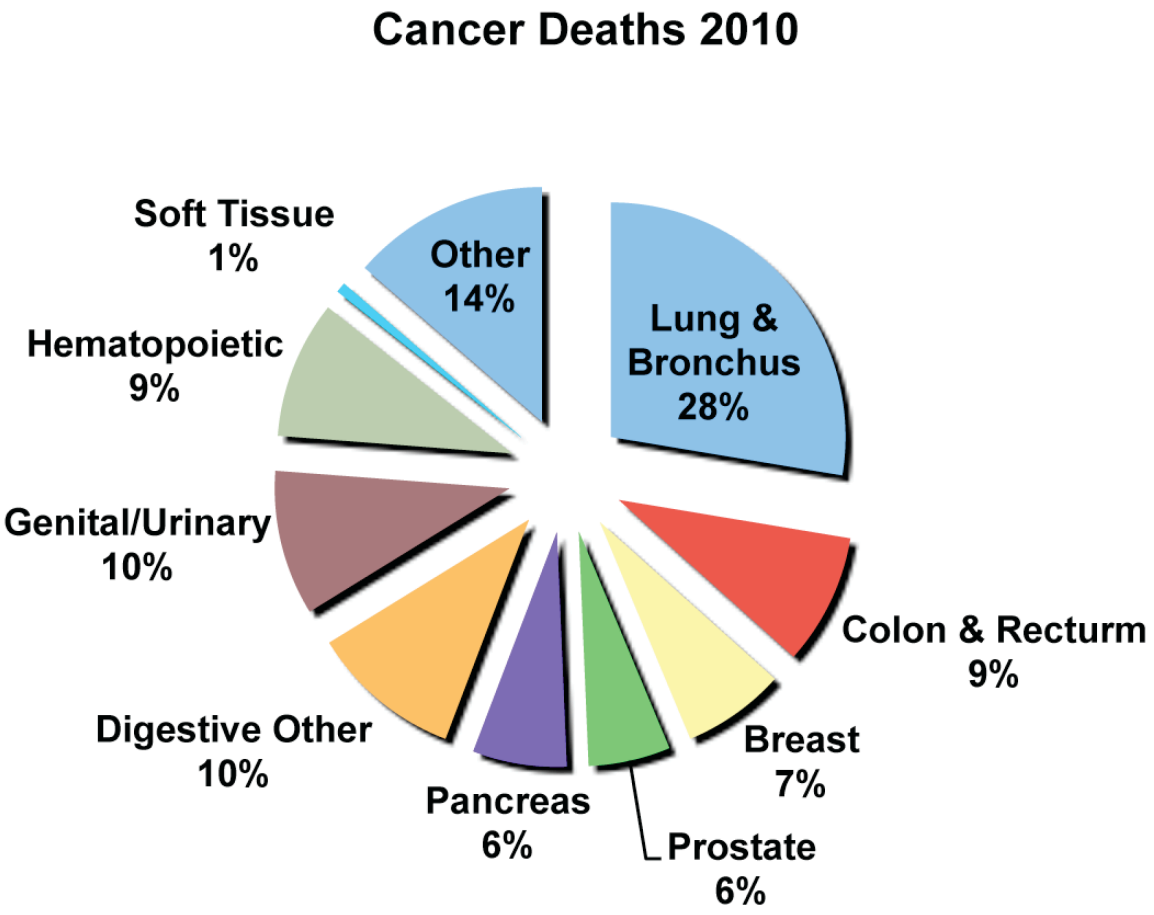
Cancer Deaths 2010
Soft Tissue
1%
Other
14%
Lung &
Bronchus
28%
Hematopoietic
9%
Genital/Urinary
10%
Colon & Recturm
9%
Digestive Other
10%
Breast
7%
Pancreas
6%
Prostate
6%

**Figure 2. SEER 5-year cancer survival rates over time.** The graph depicts 5-year survival rates from SEER data gathered by National Cancer Institute (NCI). Illustrated is the 5-year survival rate of all cancer types as well as select subtypes of cancer that are the most prevalent (prostate, breast, ovarian, colon/rectum, lung/bronchus, female genital tract) www.seer.cancer.gov/statistics/.

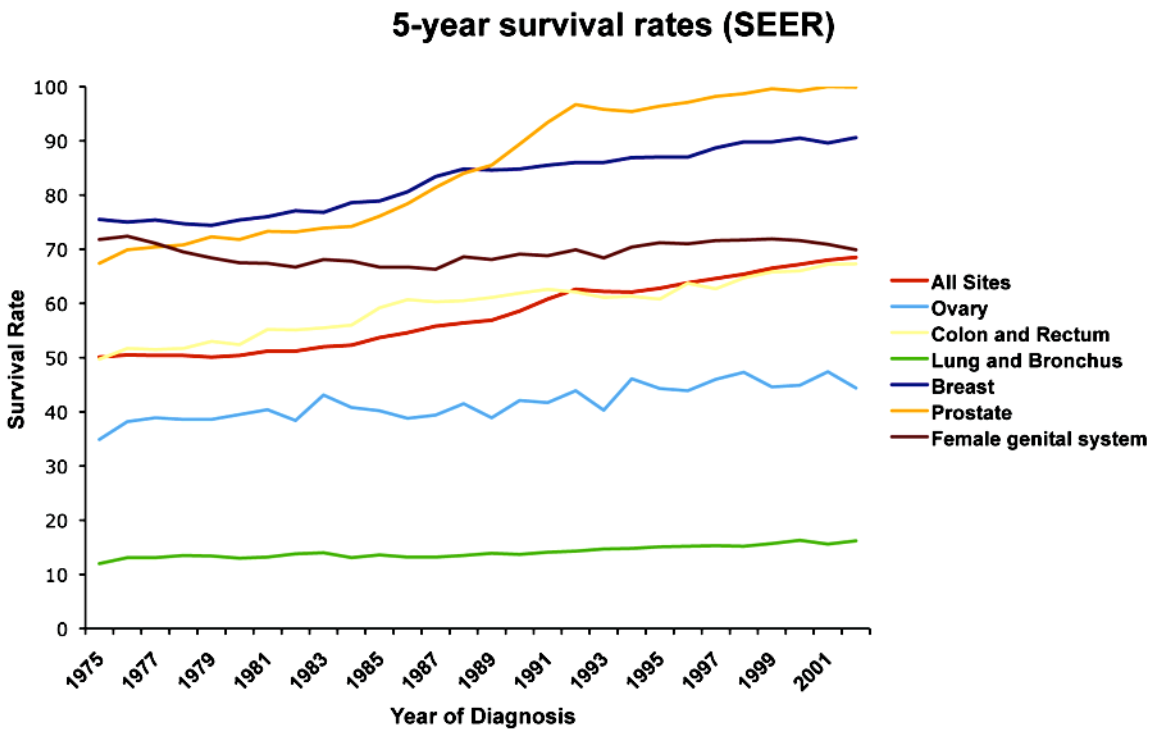
5-year survival rates (SEER)
Survival Rate
100
90
80
70
60
50
40
30
20
10
0
1975
1977
1979
1981
1983
1985
1987
1989
1991
1993
1995
1997
1999
2001
Year of Diagnosis
All Sites
Ovary
Colon and Rectum
Lung and Bronchus
Breast
Prostate
Female genital system

**Figure 3. PubMed annotations of genes based on literature results.** This graph was modified from *Huss et al., Nucleic Acids Research, 2009.* Their work depicts that a majority of annotated genes have few to no publications describing their function.

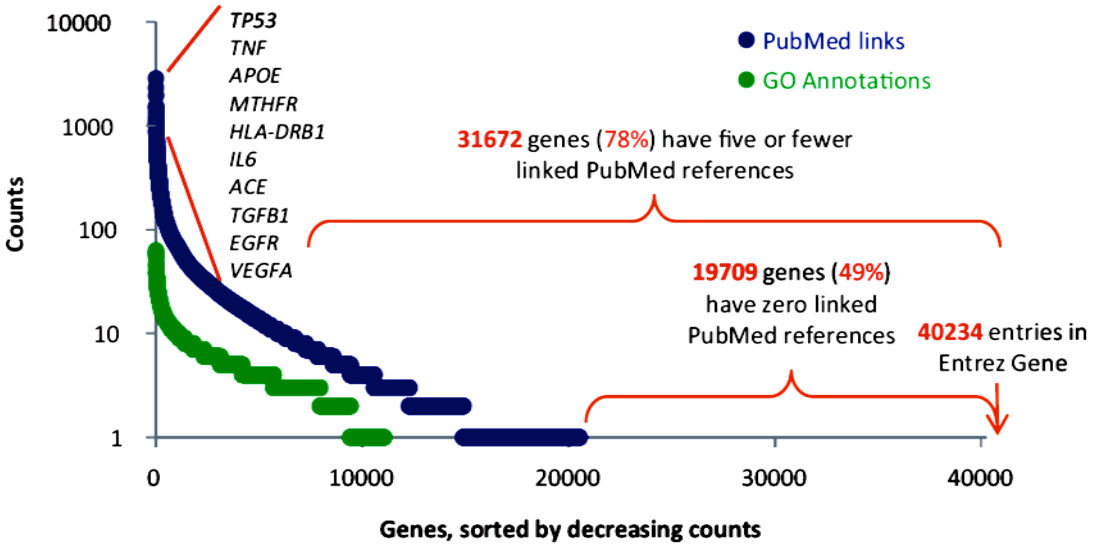
10000
1000
100
10
1
Counts
TP53
TNF
APOE
MTHFR
HLA-DRB1
IL6
ACE
TGFB1
EGFR
VEGFA
PubMed links
GO Annotations
31672 genes (78%) have five or fewer linked PubMed references
19709 genes (49%) have zero linked PubMed references
40234 entries in Entrez Gene
0
10000
20000
30000
40000
Genes, sorted by decreasing counts

**Figure 4. Schematic depicting the mechanism of *Sleeping Beauty* transposition.** SB binds the IRDRs (gray arrows) flanking the transposon. Upon binding, SB excises the transposon from a donor location leaving behind a 7-bp footprint. The transposon is mobilized throughout the genome and randomly integrated back into the genome with the only requirement being a 'TA' dinucleotide.

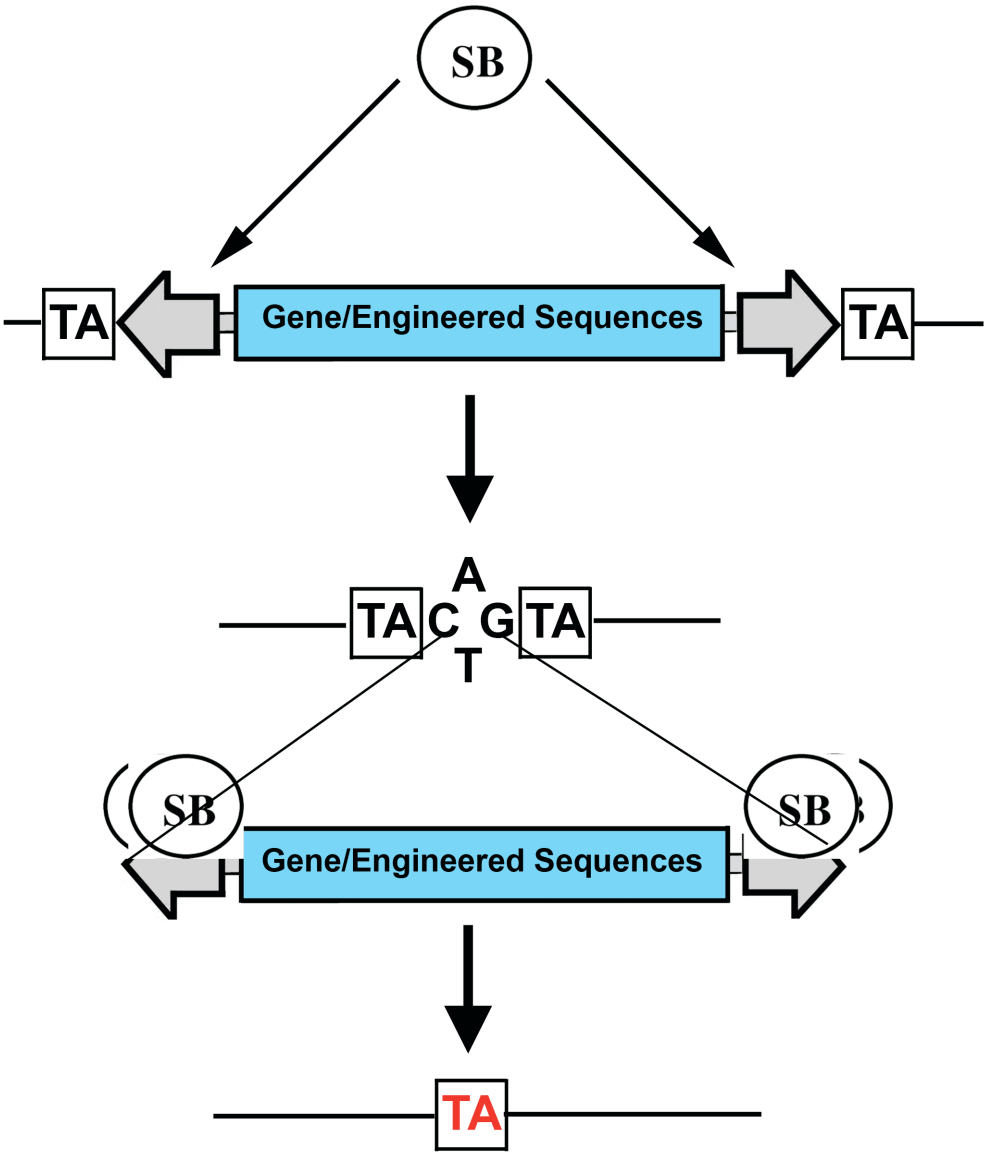
SB
TA
Gene/Engineered Sequences
TA
A
TA C G TA
T
SB
SB
Gene/Engineered Sequences
TA

**Figure 5. Schematic depicting T2/Onc.** T2/Onc transposon contains elements to induce gain-of-function mutations (Murine Stem Cell Virus 5' Long Terminal Repeat (MSCV 5'LTR) and splice donor (SD)) by inserting upstream of a gene and splicing into downstream exons causing aberrant expression of a proto-oncogene. In addition, T2/Onc contains elements to cause loss-of-function mutations (bi-directional splice acceptor (SA), and poly-Adenylation signals (pA). T2/Onc could insert within an intron of a tumor suppressor gene and reduced expression of the gene by altering the normal pattern of splicing.

**Overexpression of genes**

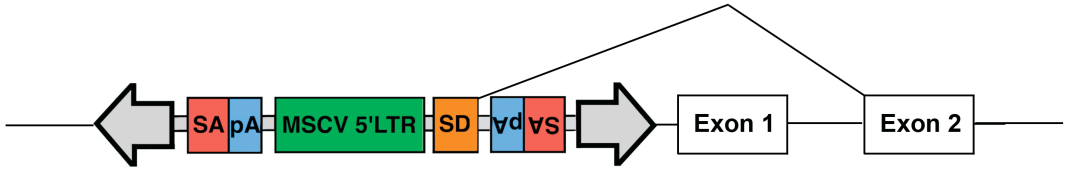


**Redcued expression of genes**

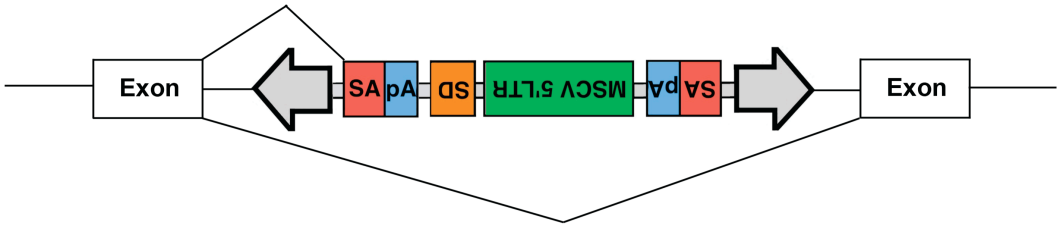

**Figure 6. Schematic depicting conditional expression of SB using the Cre/lox technology.** This two-part system illustrates the conditional knock-in allele of *SB11* (transposase) downstream of the ubiquitously expressed *Rosa26* promoter. Between the promoter and *SB11* cDNA, a stop cassette that expresses *GFP* was introduced flanked by two *LoxP* sites (red blocks). Expression of Cre-recombinase under the control of a tissue specific promoter will cause Cre to bind to the *LoxP* sites, removing the stop cassette and allowing for transposase expression to occur in your cell type of interest.

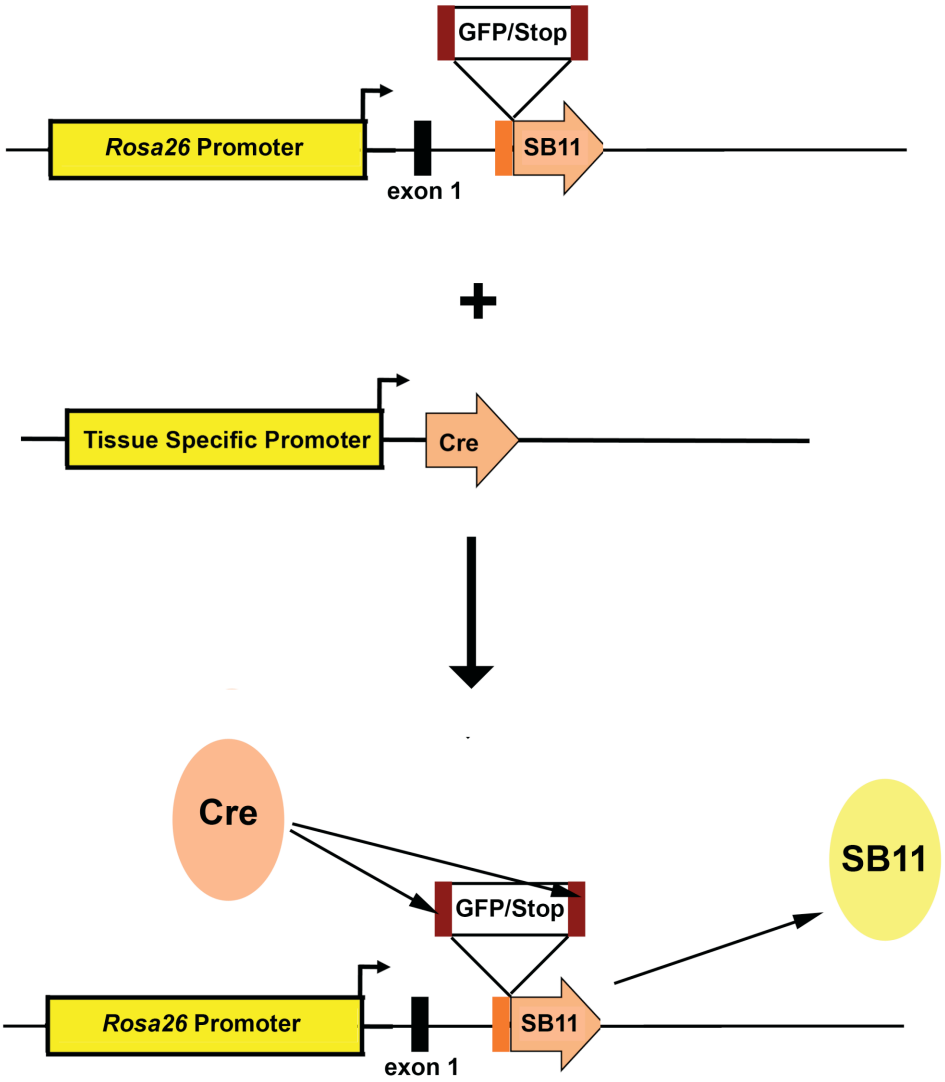
GFP/Stop
Rosa26 Promoter
SB11
exon 1
Tissue Specific Promoter
Cre
Cre
GFP/Stop
SB11
Rosa26 Promoter
SB11
exon 1

# Chapter 2.

## Identification of *PDE4D* as a proliferation promoting factor in prostate cancer using a *Sleeping Beauty* transposon based somatic mutagenesis screen

Eric P. Rahrmann*[1], Lara S. Collier*[2], Todd P. Knutson[1], Meghan E. Doyal[1], Sheri L. Kuslak[1], Laura E. Green[1], Rita L. Malinowski[2], Laura Roethe[2], Keiko Akagi[3], Michelle Waknitz[4], Wei Huang[4], David A. Largaespada[1], and Paul C. Marker[2]

[1] Department of Genetics, Cell Biology, and Development and Masonic Cancer Center, University of Minnesota, Minneapolis, Minnesota, 55455, USA
[2] Division of Pharmaceutical Sciences, School of Pharmacy and UW Carbone Comprehensive Cancer Center, University of Wisconsin-Madison, Madison, Wisconsin, 53705, USA
[3]Mouse Cancer Genetics Program, National Cancer Institute in Frederick, Frederick, MD, 21702, USA
[4]Department of Pathology and Laboratory Medicine, University of Wisconsin-Madison, Madison, Wisconsin, 53705, USA

Financial Support: This study was supported by award W81XWH-05-1-053 (proposal PC050617) to PCM from the Department of Defense Congressionally Mandated Research Program, grant AG024278 to PCM from the NIH/NIA, and grant CA118600 to DAL from the NCI/NIH. LSC was supported by postdoctoral fellowship PF-05-153-01 (MGO) from the American Cancer Society and by CA122183 from the NCI/NIH. EPR and SLK were supported by training grant CA09138 from the NCI/NIH.

Corresponding Author: Paul C. Marker, Division of Pharmaceutical Sciences, School of Pharmacy, University of Wisconsin, Madison, 777 Highland Ave., Madison, WI 53705 (608)890-2150 (voice), (608)262-5345 (FAX), marker@wisc.edu

Running Title: Transposon screen implicates *Pde4d* in prostate cancer

*equal contribution

**AUTHOR CONTRIBUTIONS**

Eric Rahrmann: His work contributed to the majority of the data published. He performed the histological and genetic analysis of the proliferative lesions identified in SB mutagenized prostates. In addition, he performed the cell culture based assays utilizing shRNAs and xenograft models of PDE4D knockdown.

Lara Collier: She developed the SB mutagenized mice.

Todd Knutson: developed initial shRNAs against PDE4D

Meghan Doyal: performed histological analysis not presented in the paper

Sheri Kuslak: sequence analysis of the PDE4D isoform sequences mentioned in figure 2.

Laura Green: isolated prostates from SB mutagenized mice.

Rita Malinowski and Laura Roethe: performed the 5' RACE of PDE4D from human patient samples and sequence analysis.

Keiko Akagi: performed the statistical analysis of cloned insertion sites to develop a CIS list.

Micelle Waknitz and Wei Huang: performed the histologic analysis of human prostate samples for PDE4D expression utilizing the AQUA system.

David Largaespada and Paul Maker: co-principle investigators on the grant for this work.

Retroviral and transposon-based mutagenesis screens in mice have been useful for identifying candidate cancer genes for some tumor types. However, many of the organs that exhibit the highest cancer rates in humans, including the prostate, have not previously been amenable to these approaches. This study demonstrates for the first time that the *Sleeping Beauty* transposon system can be used to identify candidate prostate cancer genes in mice. Somatic mobilization of a mutagenic transposon resulted in focal epithelial proliferation and hyperplasia in the prostate. Efficient methods were established to identify transposon insertion sites in these lesions, and analysis of transposon insertions identified candidate prostate cancer genes at common insertion sites, including *Pde4d*. *PDE4D* was also over-expressed in human prostate cancer patient samples and cell lines, and changes in *PDE4D* mRNA isoform expression were observed in human prostate cancers. Furthermore, knockdown of *PDE4D* reduced the growth and migration of prostate cancer cells *in vitro*, and knockdown of *PDE4D* reduced the growth and proliferation rate of prostate cancer xenografts *in vivo*. These data indicate that *PDE4D* functions as a proliferation promoting factor in prostate cancer, and the *Sleeping Beauty* transposon system is a useful tool for identifying candidate prostate cancer genes.

## INTRODUCTION

Forward somatic mutagenesis screens using murine retroviruses as insertional mutagens have been effective tools for cancer gene discovery in mammary tumors, hematopoietic neoplasms, and brain tumors in mice [Jonkers, J. 1996; Johansson, F.K. 2004; Callahan, R. 2000]. However, many tissue types that are commonly transformed into tumors in humans are not affected by known retroviruses. Two studies have shown that genome-wide somatic mutagenesis using the *Sleeping Beauty* (SB) transposon system can be used to induce tumors and identify cancer genes for hematopoietic tumors and sarcomas [Dupuy, A.J. 2005; Collier,L.S. 2005]. Candidate cancer genes were identified in these studies by finding sites in the genome of SB-induced tumors that were recurrently mutated by transposon insertions in multiple independent tumors. Such sites are called common insertion sites (CISs), and past experience with retroviral-based and transposon-based screens has shown that the genes located at CISs act as oncogenes or tumor suppressors. A major unresolved question for this approach is whether or not SB will be more broadly applicable for cancer gene discovery in epithelial cancers, which are responsible for 80% of human cancer deaths [Jemal, A. 2006].

Prostate adenocarcinoma is the most commonly diagnosed male cancer and is one of the leading causes of male cancer death [Jemal, A. 2006]. Prior to the development of invasive adenocarcinoma, several histologic abnormalities can sometimes be observed that are considered potential precursor lesions for prostatic adenocarcinoma. These include prostatic intraepithelial neoplasia (PIN), atypical small acinar proliferation (ASAP), and proliferative inflammatory atrophy (PIA) [Schlesinger, C. 2005; De Marzo, A.M. 1999]. Features associated with one or more of these candidate precursor lesions include focal areas of increased proliferation, stratification of the epithelium, loss of basal cells, and changes in nuclear morphology. Several genetic and gene expression alterations have been identified as common events in early prostate cancers. The transcription factor *Nkx3.1* is commonly lost in early stage tumor epithelial cells, including loss in 20% of high grade PIN cases examined [Bowen, C. 2000]. This loss of expression is likely due to heterozygous deletions of the genomic locus and epigenetic silencing mechanisms [Asatiani, E. 2005]. Recurrent deletions and translocations that

create fusion genes involving transcription factors ERG, ETV1, or ETV4 in prostate epithelial cells have been reported to occur in a majority of prostate cancers, and are also detected as early as PIN [Tomlins, S.A. 2006; Tomlins, S.A. 2005; Cerveira, N. 2006]. Although these genetic alterations clearly play a role in early prostate cancers, the genetic basis for prostate cancer initiation remains poorly understood [Abate-Shen, C. 2000]. In this study, transposon-based somatic mutagenesis caused foci of altered histology and elevated proliferation in the prostatic epithelium that resembled features associated with prostate cancer precursor lesions. Analysis of transposon insertion sites in these lesions identified candidate cancer genes that may play a role in prostate cancer initiation, including *PDE4D*. PDE4D was also over-expressed in human prostatic adenocarcinomas, and shRNA knockdown of PDE4D reduced the proliferation of prostate cancer cells *in vitro* and *in vivo*, supporting its potential role as a proliferation promoting factor in human prostate cancer.

## MATERIALS AND METHODS

**Mice.** The mouse strains utilized for this study have previously been described including CAGGS-SB10 transgenic, *Rosa26*-SB11 knock-in, and low-copy T2/onc transgenic [Collier,L.S. 2005; Dupuy, A.J. 2005].

**Immunohistochemistry.** Tissues were stained for the Ki67 antigen as previously described [Kuslak, S.L. 2007]. A modified staining protocol was used for laser capture microscopy as follows: tissues were dissected into cold PBS, embedded directly into Tissue Freezing Medium (Triangle Biomedical Sciences) and stored at -80°C. Tissue sections (5mm) were cut at -20°C with a cryostat and immediately mounted onto PEN membrane slides (Leica) and air-dried for 30 minutes followed by fixation in 100% ethanol at -20°C. Slides were washed with PBS, blocked with 2.5% sheep serum in PBS, stained for 3 hours with anti-phospho-Histone-H3 (Upstate Cell Signaling Solutions) 1:150 in 2.5% sheep serum in PBS, and washed in PBT (PBT = 1X PBS with 0.1% Tween 20). The primary antibody was visualized with an anti-rabbit IgG horseradish peroxidase conjugate (Chemicon) diluted 1:500 in 2.5% sheep serum in PBS followed by PBT washes and staining with the DAB reagent (Vector Laboratories) according to the manufacturer's instructions. Slides were counter stained with Hematoxylin, dehydrated into 100% ethanol, and air dried for 1 hour prior to laser capture.

**Laser capture microscopy and Liner-mediated PCR.** Cells of interest were captured from tissue sections using a Leica LMD6000 laser capture microdisection microscope. DNA was isolated from the captured cells using a Qiagen Qiamp DNA Micro Kit according to the manufacturer's instructions except GenomiPhi DNA amplification sample buffer was substituted for the Qiagen elution buffer during the last step of DNA purification. Samples were then amplified using the GenomiPhi DNA Amplification Kit (GE Healthcare) according to the manufacturer's instructions. Transposon-genomic DNA junctions were amplified as previously described [Largaespada,D.A. 2008], cloned into plasmids, and sequenced by Functional Biosciences Inc.

**AQUA Analysis of PDE4D expression.** The AQUA analysis was conducted on a previously assembled tissue microarray (TMA) of prostate tissues from patients treated at the University of Wisconsin-Madison using an established protocol [Warren, M. 2009]. Epithelial compartment visualization was achieved with a 30 minute incubation of a mouse anti-cytokeratin AE1/AE3 1:200 (Dako North America, Carpinteria, CA) and mouse anti-E-cadherin 1:50 (Abcam, Cambridge, MA) cocktail, followed by a 30 minute incubation of Invitrogen Alexa Fluor 555 donkey anti-mouse IgG 1:200. Goat anti-PDE4D IgG 1:100 (Santa Cruz, Santa Cruz, CA) was preincubated with PDE4D protein (5x wt:wt) (Santa Cruz, Santa Cruz, CA) for 2 hr 30 min. prior to application. Both PDE4D antibody 1:100 and PDE4D with 5x protein were incubated for 60 minutes followed by a 15 minute incubation with Invitrogen biotinylated swine anti-goat IgG 1:200. Staining on the TMA was visualized as previously described [Warren, M. 2009]. There were 336 tissue cores from 168 patients (2 cores from each patient) in the TMA stained for this study. In addition to an automated image acquisition and analysis as previously described [Camp, R.L. 2002], all cores for this study were examined for staining and morphology by surgical pathologist, Wei Huang, MD. TMA cores without sufficient epithelium (<5%) or with poor staining quality (i.e., section folding, excess trapping of fluorochrome, etc.) were excluded from analysis. In total, 282 of the 336 cores stained for PDE4D passed this quality control and were included in the final data set.

**RLM-5'-RACE.** The RNA analyzed in the RLM-5'-RACE experiment was isolated from human prostate samples obtained by the University of Minnesota Cancer Center Tissue Procurement Facility (TPF). For the study, prostate tissue samples were bisected. One piece was provided to our laboratory as a fresh sample that was used for the isolation of RNA. The adjacent piece of tissue was retained by the TPF for examination by a TPF staff pathologist who provided us with a pathology report that indicated the presence/absence and pathological grade of prostate cancer in each tissue sample. RNAs were analyzed using the FirstChoice RLM-RACE kit (Ambion) according to the

manufacturer's instructions. The PDE4D outer and inner primers were 5-TAGGCCACATCAGCATGGTAATGGTCT-3' and 5'-ACCACTAGTTCACATCTTCTAGTTCCTTGGCAAGGA respectively.

**Cell Culture.** DU145-derived cell lines were grown in 1xRPMI (Invitrogen Gibco) supplemented with 5% activated charcoal USP (Sigma) treated fetal bovine serum (Hyclone), 100mg/ml antibiotic/antimycotic (Invitrogen Gibco), and $10^{-8}$M 5α-androsten-17β-ol-3-one (Sigma). PC3-derived cell lines were grown in 1xMEM (Invitrogen Gibco) supplemented with 5% activated charcoal USP (Sigma) treated fetal bovine serum (Hyclone), 100mg/ml antibiotic/antimycotic (Invitrogen Gibco), 1xNon-essential amino acids (Invitrogen Gibco), and 1xSodium Pyruvate (Invitrogen Gibco). All cell lines were grown at 37°C in 5% $CO_2$. Stable *PDE4D* shRNA knockdown and scrambled sequence shRNA control cell lines were generated using lentiviral transduction with GIPZ shRNAs from Open Biosystems. Cells were transduced at a multiplicity of infection of 10 following manufacturers protocol and then underwent G418 selection for stable integrants. Immunoblots of cell line extracts were conducted as previously described using the anti-PDE4D antibody (Abcam) diluted 1:1500 in 2.5% milk [Kuslak, S.L. 2007].

**Growth Assays.** Cells were plated at an initial density of 5,000 cells/$cm^2$ on 4-well plates (Costar). After the growth period, cells were trypsinzed, neutralized in media, and trypan blue was added. The number of viable cells was determined by counting the number of cells that exclude trypan blue on a hemacytometer. Alternatively, cells were plated at an initial density of 500 cells per well on a 96 well plate in triplicate, and cell viability was evaluated using an MTS assay (the CellTiter96 Aqueous One Solution Cell Proliferation Assay from Promega) according to the manufacturer's instructions.

**Xenograft assay.** Cultured cells were trypsinzed, resuspended at $10^6$ cells in 500ml of Matrigel (BD Biosciences 356230), and injected subcutaneously into CD-1 nu/nu mice. After 1 month, xenografts were fixed in formalin and processed for IHC. Following Ki67

staining, 8 random 20X fields were photographed and the ratio of Ki67 positive nuclei to total nuclei was determined using a previously described computer-assisted method for image analysis [Wild, R. 2000].

**Migration (Wound Healing) assay.** shRNA-PDE4D transduced human prostate cancer cells were plated at 250,000 cells per well on 24-well plates (Costar) and allowed to grow until 100% confluent. Once confluent, media serum levels were reduced to 1% serum for 24hours followed by a 1 hours treatment with the proliferation inhibitor Mitomycin C (Sigma) at 10ug/ml. A 200ul pipet tip was used to generate a scratch devoid of cells in the center of the wells. A photograph was taken immediately after making the scratch for the initial (0hr) time point. Photographs were taken subsequently at 3hrs and 5hrs post scratch. Changes in the area devoid of cells were quantified using the Leica Application Suite V3.0.0 software (Leica). Nonsilencing-shRNA transduced cells served as a control. Data was analyzed using an ANOVA with least significant difference post-hoc analysis.

## RESULTS

**Focal hyperplasia in the prostatic epithelium of transposon mutagenized mice.** Previous studies showed that two mouse strains with active transposition of a mutagenic transposon, T2/onc, became moribund due to the formation of tumors with a limited tissue distribution [Collier,L.S. 2005; Dupuy, A.J. 2005]. The two strains used in these experiments differed in the transgene driving transposase expression (CAGGS-SB10 or *Rosa26*-SB11). In addition, the CAGGS-SB10;T2/onc mice were null for the *Arf* tumor suppressor gene. We examined the morphology and histology of prostate glands from CAGGS-SB10;T2/onc low-copy;*Arf-/-* mice, and the only prostatic abnormalities identified were infrequent sarcomas (data not shown). We also evaluated *Rosa26*-SB11;T2/onc low-copy (approximately 25 copies of T2/onc) mice. Unlike the previously reported high rate of embryonic lethality in *Rosa26*-SB11;T2/onc high-copy (148+ copies of T2/onc) mice [Dupuy, A.J. 2005], the ratio of *Rosa26*-SB11;T2/onc low-copy mice to single transgenic littermates was consistent with little or no embryonic lethality. However, these mice succumbed to tumor formation, primarily leukemias, with a median latency of 6-7 months (Lara Collier, unpublished observation). Examination of the histology of prostate glands from moribund *Rosa26*-SB11;T2/onc low-copy mice revealed focal areas of epithelial hyperplasia in the anterior prostate (data not shown) and dorsolateral prostate (Supplemental Fig. 1A, B). Immunohistochemistry (IHC) suggested that the difference in prostatic phenotype for the two models could be explained by differences in transposase expression in the prostate gland (Supplemental Fig. 2).

The prostates of *Rosa26*-SB11;T2/onc low-copy mice were also evaluated using proliferation markers Ki67 [Gallee, MP 1989] and phospho-(ser10)-histone H3 [Nowak, S.J. 2004].In single transgenic control prostates (*Rosa26*-SB11 or T2/onc low-copy only), Ki67 positive cells were rare and typically found as single positive cells or a pair of positive cells (Supplemental Fig. 1C-D). In contrast, *Rosa26*-SB11;T2/onc low-copy double transgenic mice contained focal areas with many Ki67 positive cells (Fig. 1). A quantitative analysis of the distribution of Ki67 positive cells confirmed the increased clustering of Ki67 positive cells into focal areas of elevated proliferation in *Rosa26*-

SB11;T2/onc low-copy prostates relative to controls (Fig. 2A). In addition to the change in the distribution of proliferating cells, an overall increase in the number of proliferating prostatic epithelial cells was observed in *Rosa26*-SB11;T2/onc low-copy mice with both Ki67 and phospho-(ser10)-histone H3 (data not shown).

**Identification of transposon insertion sites in prostatic hyperplasia.**

After failed initial attempts to identify transposon insertion sites present in the prostatic lesions using laser capture microscopy, the limits of the published linker-mediated PCR (LM-PCR) method were evaluated using DNA from two mice with well characterized transposon insertions inherited through the germline [Collier,L.S. 2005; Dupuy, A.J. 2005; Geurts, A.M. 2006]. These mice lacked transposase expression so all somatic cells from each animal harbored identical transposon insertions. LM-PCR on serial dilutions of high quality DNA showed that the isolation of transposon-flanking sequences became unreliable in the low-ng range (Fig. 2B). A modified protocol (see Materials and Methods) allowed the reliable identification of the known transposon insertion sites from approximately 100 laser captured cells isolated from these animals (data not shown). When this protocol was used to identify the transposon insertion sites present in foci of proliferation (clusters of 3 or more phospho-ser10-histone H3 positive cells) from *Rosa26*-SB11;T2/onc low-copy prostates, complex banding patterns were observed following LM-PCR that varied from sample to sample (Fig. 2C).

In order to identify genes that can initiate proliferation/hyperplasia in the prostatic epithelium, 100 proliferating clusters of prostatic epithelial cells were laser captured from the prostates of 20 transposon-mutagenized mice on an otherwise wild type genetic background (median animal age 6 months), and 85 proliferating clusters of prostatic epithelial cells were captured from the prostates of 17 transposon mutagenized mice deficient for *Arf* (median animal age 11 weeks). The laser-captured lesions were analyzed by LM-PCR, and the LM-PCR products were sequenced to determine the transposon insertion sites. Unique genomic sequences were mapped back onto the mouse genome using the mouse genome database maintained by the Wellcome Trust Sanger Institute at www.ensembl.org. This analysis identified 77 unique insertions isolated from prostatic

lesions generated by mutagenesis on a wild type genetic background and 27 unique insertions isolated from prostatic lesions generated by mutagenesis on the *Arf*-null background. Insertions were distributed across most mouse chromosomes (Fig. 2D). The two chromosomes that harbored T2/onc concatomers in the experiment (chromosomes 1 and 15) had an increased frequency of insertions that was expected due to the tendency of transposons to mobilize at higher frequency to locations linked to the donor transposon concatomer, a phenomenon called local hopping [Carlson, C.M. 2003]. The prostate insertions were evaluated using previously proposed criteria for CIS identification [Mikkers, H. 2002]. Using these criteria, 3 CISs were found in the prostate data set. The three genes at prostate CISs in the experiment were *Rabgap1l, Pde4d,* and *Klhl13* (Supplemental Table 1). *Rabgap1l* is known to be located very close to the chromosome 1 T2/onc donor concatomer [Collier, L.S. 2005]. Consequently, this gene may have been repeatedly mutated due to local hopping. The other two genes located at CISs were not linked to the T2/onc concatomers utilized in the experiment so mutation of these genes likely contributed to the abnormal proliferation observed in the prostatic epithelium. Insertions in *Pde4d* were observed in proliferating lesions isolated from three independent mice. However, all of the insertions were in intron 5 with the MSCV promoter in T2/onc oriented toward exon 6 of *Pde4d*. *Pde4d* encodes several alternatively spliced transcripts including short-isoform transcripts that initiate translation at an in-frame AUG codon with a strong Kozak consensus located in exon 6 (Fig. 3). Thus, the T2/onc insertions would be predicted to cause over-expression of one or more endogenous short isoforms of *Pde4d* in prostatic epithelial cells. Transposon insertions in *Klhl13* were observed in both promoter orientations.

The prostate insertion sites observed in this experiment were also compared to previously reported retroviral and transposon insertions from other cancer screens by searching the Retroviral Tagged Cancer Gene Database [RTCGD; Akagi, K. 2004]. Both *Rabgap1l* and *Pde4d* have been previously observed as CISs in other somatic mutagenesis screens for cancer genes [Collier, L.S. 2005; Bijl, J. 2005] while *Klhl13* is a novel CIS. Since many oncogenes and tumor suppressor genes function in multiple tumor types, we hypothesized that the combined prostate and RTCGD data sets may

identify new CISs. Using the criteria proposed by Mikkers et al. for the approximately 8700 insertions in the combined data sets, five novel CISs were identified (Supplemental Table 2) [Mikkers, H. 2002]. Among the remaining insertion sites isolated from prostatic lesions, eleven were insertions into genes previously reported as CISs (Supplemental Table 3).

**Overexpression and mRNA isoform changes for *PDE4D* in human prostate cancer.** To investigate the possibility that PDE4D is involved in human prostate cancer, we collaborated with the laboratory of a board-certified surgical pathologist, Wei Huang, MD. The Huang laboratory had previously assembled a tissue microarray (TMA) of prostate tissues from patients treated at the University of Wisconsin-Madison including patients with benign prostatic hyperplasia (BPH) and patients with prostatic adenocarcinomas [Warren, M. 2009]. The approach used for analyzing PDE4D protein expression on the TMA was a previously described method for automated quantitative analysis (AQUA) [Camp, R.L. 2002]. For the AQUA approach, proteins were detected using fluorescence-based immunohistochemistry. The TMA was co-stained with the antibody against PDE4D, an epithelial cytoplasm-specific antibody cocktail (E-cadherin and anti-cytokeratin antibodies), and a nuclear stain (DAPI). The stained TMA was then imaged using a series of fluorescent filters corresponding to each stain, and the images were analyzed using previously developed algorithms to determine relative expression levels of PDE4D [Camp, R.L. 2002]. A parallel TMA was analyzed in which the anti-PDE4D antibody was blocked with a PDE4D peptide to confirm specificity of the PDE4D signal. A strong PDE4D-specific signal was observed for the PDE4D antibody that co-localized with the E-cadherin/cytokeratin stains in human prostatic adenocarcinomas (Figure 4A). The prostate TMA cores from patients with prostatic adenocarcinoma varied in pathological grade (as scored by surgical pathologist Wei Huang, MD) and included cores that were primarily composed of non-invasive epithelial cells (normal or PIN), cores that were primarily invasive cancer, and cores from sites of metastasis. When the AQUA data was quantified and stratified by these pathologic features, all prostate tissues from patients with adenocarcinomas had higher PDE4D

expression than tissues from patients with BPH (Figure 4B). No significant differences in PDE4D expression level were observed among the different pathological grades for tissue cores from prostate cancer patients. PDE4D expression in prostate cancer was also evaluated by immunoblotting in normal primary prostatic epithelial cells and 5 common prostate cancer epithelial cell lines. PDE4D protein expression was increased in the human prostate cancer cell lines compared to normal primary prostatic epithelial cells (Supplemental Fig. 3).

To further understand the expression of *PDE4D* in human prostate cancer, pooled RNA from samples of pathologically normal prostate and prostatic adenocarcinomas were evaluated by RNA ligase-mediated 5' Rapid Amplification of cDNA Ends [RLM-5'-RACE, [Liu, X. 1993]]. The predominant RLM-5'-RACE products from normal prostate and prostate cancer RNAs were distinct (Fig. 4C), suggesting altered *PDE4D* isoform expression in human prostate cancer. Sequencing of the predominant RLM-5'-RACE product obtained from the pooled prostatic adenocarcinoma RNA identified a cDNA with a first exon that began at base pair 349 of the Genbank deposited sequence for the *PDE4D5* isoform (accession AF12073.1) and was spliced to exon 2 of *PDE4D* in a manner identical to the other *PDE4D* long isoform transcripts.

**_PDE4D_ knockdown reduces the growth rate of human prostate cancer cells and xenografts.**

As an initial test of the functional role of PDE4D in prostate cancer cells, PDE4D protein expression was reduced in DU145 and PC3 cells using three different shRNAs targeting sequences in *PDE4D* (Fig 5). Based on densitometry of immunoblots with an anti-PDE4D antibody, these shRNAs achieved 70-97% knockdown of PDE4D protein expression (data not shown). In all cases, the knockdown cell populations had significantly reduced *in vitro* growth rates compared to control cells with stable transfection of scrambled sequence shRNAs (Fig. 5A-C). The impact of PDE4D knockdown on cell migration was also evaluated using an *in vitro* wound healing assay, and PDE4D knockdown significantly decreased the migration rate of DU145 cells (Supplemental Fig. 4).

To further evaluate the role of PDE4D in prostate cancer cells, we used the exon 14/15 PDE4D knockdown and scrambled shRNA control DU145 cell lines in a xenograft model. PDE4D knockdown resulted in smaller xenografts compared to control tumors (Fig. 6A; Supplemental Fig. 5A). The reduction in wet weight of the PDE4D knockdown xenografts was statistically significant, but there was considerable variability in wet weight among the xenografts in each group due to the presence of large cysts lacking viable tumor cells in many of the xenografts (Supplemental Fig. 5B-D). Consequently, we also assayed tumor cell proliferation using immunostaining for the Ki67 antigen. Analysis of the Ki67 labeling index for PDE4D knockdown and control xenografts found a statistically significant 39.0% reduction ($p<0.01$, by T-Test) in the Ki67 labeling index for knockdown tumors relative to controls (Fig. 6B-D) indicating a reduced proliferation rate in response to PDE4D knockdown. We also examined apoptosis in the xenografts using a TUNEL assay. While moderate rates of apoptosis were observed in all xenografts, no significant differences were observed between the control shRNA and PDE4D knockdown tumors (data not shown) suggesting that the reduction in tumor size was primarily due to decreased proliferation in response to PDE4D knockdown.

## DISCUSSION

Genetic screens in model organisms have been an important strategy for understanding the molecular genetics of several cancers. For many years, one of the most productive screening approaches has been the use of slow transforming retroviruses as insertional mutagens to tag and identify endogenous oncogenes and tumor suppressor genes in mice [reviewed in [Uren, AG 2005]]. Screens using retroviruses have investigated several tumor types including mammary tumors, hematopoietic neoplasms, and brain tumors. These screens have identified genes and genetic interactions that have proven to be directly relevant for understanding the equivalent human cancers. One of the major limitations of retroviruses as a screening tool is their cell-type specificity that defines the types of tumors they can induce. This has prevented retroviral-based screens for many of the most common tumor types in humans.

Recently, the SB transposon system has been shown to function as an insertional mutagen to discover cancer genes for hematopoietic tumors, medulloblastomas, and sarcomas in genetically modified mice [Collier,L.S. 2005; Dupuy, A.J. 2005]. These initial proof-of-principle studies showed that mobilization of transposons engineered to have gain- and loss-of-function elements could accelerate tumor formation, and cloning transposon insertion sites identified candidate cancer genes at CISs. Transposon-based screening has great potential because mobilization of the transposon is not cell-type restricted so screens are possible in tissues not amenable to retroviral screens such as the sarcomas investigated by Collier, Carlson *et al.* However, it had previously not been determined if transposon-based screens can be used to investigate epithelial tumors that constitute the majority of human cancers. In addition, although the candidate cancer genes at the CISs observed by Dupuy *et al.* and Collier, Carlson *et al.* included genes not previously implicated in cancer, it is not yet clear whether these candidate cancer genes will prove to be relevant for understanding disease processes in humans.

The current study addresses these issues by investigating transposon-mutagenized mice for prostate cancer related phenotypes. The prostates of *Rosa26*-SB11;T2/onc low-copy mice had focal areas of epithelial hyperplasia and elevated epithelial proliferation that resembled features of prostate cancer precursor lesions. Cloning transposon insertion

sites from these lesions identified candidate cancer genes at transposon CISs. We conducted our screen using both wild type and *Arf*-null genetic backgrounds. Insertions were observed at newly identified and previously known CISs on both genetic backgrounds. Based on the CISs in the Retroviral Tagged Cancer Gene Database, about 2.2% of all genes have been identified as CISs in one or more cancer screens [Akagi, K. 2004]. For our screen, 19% of insertions on a wild type genetic background were into CIS genes reflecting a 9-fold enrichment over what would be predicted by chance. For insertions on the *Arf*-null background, 41% of insertions were into CIS genes reflecting a 19-fold enrichment over what would be predicted by chance. These data suggest that most of the insertions into CIS genes in our screen were likely to be selected insertions that contributed to the focal prostate epithelial hyperplasia and proliferation observed in *Rosa26*-SB11;T2/onc low-copy mice. Further investigation of one of the CIS genes, *Pde4d*, showed that it is a mitogenic factor for prostatic epithelial cells that is also over-expressed in human prostate cancers. Thus, transposon-based screens in mice can discover novel genes that are directly relevant for understanding human prostate cancer.

*PDE4D* is a gene encoding several phosphodiesterase enzymes that cleave cAMP and are expressed in multiple tissues [Uckert, S. 2006; Richter, W. 2005; Bolger, G.B. 1997; Bolger, G. 1993; N‰ moz, G. 1996]. *PDE4D* encodes at least nine protein isoforms that all possess the phosphodiesterase catalytic domain in the C-terminus but differ at the N-terminus. The nine isoforms are categorized into two groups: long isoforms (3, 4, 5, 7, 8, 9) and short isoforms (1, 2, 6). In our study, we identified multiple transposon insertions into the mouse *Pde4d* gene that are predicted to cause overexpression of one or more short isoforms. A previous investigation of rats that had increased susceptibility to prostate carcinogenesis due to developmental exposure to estrogens found increased expression of *PDE4D4,* one of the long isoforms, in the prostates of susceptible rats [Ho, S.M. 2006]. This led the authors to hypothesize that *PDE4D* overexpression had a causal role in prostate cancer susceptibility in the rat model. Our finding that PDE4D protein is overexpressed in the prostatic epithelial cells of patients with prostatic adenocarcinoma relative to patients with the benign disease BPH regardless of the histopathology of the epithelial cells in the adenocarcinoma

patients (normal, PIN, invasive cancer, metastasis) suggests PDE4D overexpression in the aging human prostate may also be a permissive event that increases susceptibility to prostate cancer.

The status of PDE4D in human prostate cancer had not previously been specifically investigated, but genome-wide expression profiling studies of human prostate cancer often included probes against *PDE4D* transcripts. We reviewed *PDE4D* for expression changes in the available prostate cancer expression profiling studies using the Oncomine Database [Rhodes, D.R. 2004]. The available expression profiling studies generally observed no change for *PDE4D* mRNA expression or a decrease in expression with increasing pathologic grade of prostate cancer. The potential discrepancy between our finding of an increase in PDE4D protein expression in prostate cancer patients and the decreased *PDE4D* mRNA expression observed in some expression profiling studies may reflect post-transcriptional regulation of PDE4D. Comprehensive side-by-side analyses of mRNA and protein expression for multiple *PDE4D* isoforms in the rat have found a poor correlation between mRNA and protein expression levels for multiple *PDE4D* isoforms. This has led to the hypothesis that these *PDE4D* isoforms are post-transcriptionally regulated [Richter, W. 2005]. A more dramatic finding in our study was a shift in *PDE4D* isoform usage in prostate cancer that we identified in RLM-5'-RACE experiments (Fig. 4C, D). The RLM-5'-RACE protocol includes ligation of an RNA adaptor to mRNAs prior to reverse transcription in a reaction that requires the presence of a 7-methylguanosine cap at the 5'-terminus of the mRNA [Liu, X. 1993]. This allows RLM-5'RACE to selectively amplify full-length cDNA 5'-ends. We infer from our data that the predominant *PDE4D* transcript in prostatic adenocarcinomas is initiated at base pair 349 of the Genbank deposited sequence for the *PDE4D5* isoform (accession AF12073.1). Transcripts initiated at this location would not include the normal translation initiation codon for the published *PDE4D5* transcript and would presumably initiate translation at one of the in frame AUG codons present in the truncated mRNA transcript. This possibility is consistent with the size of the PDE4D protein bands observed by immunoblot in prostate cancer cell lines (Supplemental Fig. 3).

Collectively, the increased expression of PDE4D and altered isoform usage in prostate cancer cells indicate that there will be lower cAMP levels in at least some sub-cellular compartments of prostate cancer cells relative to normal prostatic epithelial cells. This correlates with previous *in vitro* studies in prostate cancer cell lines that have found that increasing levels of cAMP by stimulating adenylate cyclase with Forskolin, using cAMP analogs, or treatment with general PDE inhibitors led to growth arrest and apoptosis of prostate cancer cell lines [Niles, RM 1976; Bang, YJ 1994; Bang, Y.J. 1992]. Our data that selectively targeting PDE4D with shRNAs also limits prostate cancer cell growth suggests that future studies with PDE4D selective inhibitors as potential anti-prostate cancer agents are warranted.

Considered more broadly, pharmacologic inhibition of the PDE4 family of enzymes induces apoptosis or inhibits growth in a variety of cancer cell types. However, the role of *PDE4D* specifically in human cancer has not been widely investigated. PDE4 family inhibition induces apoptosis in Chronic Lymphocytic Leukemia (CLL) cells [Kim, D.H. 1998]. However, this effect may not be due to PDE4D specifically, as *PDE4D* mRNA expression was found to be lower in CLL cells than in normal peripheral blood mononuclear cells [Zhang, L. 2008]. Analysis of genomic copy number changes in human lung adenocarcinoma has detected homozygous deletions at the *PDE4D* locus [Weir, B.A. 2007]. Similar studies on esophageal adenocarcinoma identified both homozygous deletions and loss of heterozygosity at the *PDE4D* locus, implicating *PDE4D* as a tumor suppressor gene in these two tumor types [Nancarrow, D.J. 2008]. As regulation of PDE4D activity is complex, close examination of its genomic sequence, transcriptional regulation, alternative splicing and other post-transcriptional/translational modifications will be necessary to address the contribution of *PDE4D* to tumor formation in humans. In addition, it is possible that the ability of *PDE4D* to enhance or limit tumor growth may be cell type dependent, a phenomenon that has been observed for other cancer genes such as *NOTCH1* [Dotto, G.P. 2008].

Prostate cancer is the most common cancer in men and there is considerable genetic heterogeneity among individual prostate cancers [Jemal, A. 2006; Abate-Shen, C. 2000]. Transposon-based somatic mutagenesis is a promising strategy for uncovering the

genetically diverse ways that prostate tumors can evolve. This study refined the methodology for transposon-based screening to allow investigation of small lesions that resembled the initial steps of prostate cancer progression. This identified *Pde4d* as a proliferation promoting factor in the prostates of mice and humans. In addition to *Pde4d*, this study identified 18 other genes as candidate prostate cancer genes including genes at CISs in the prostate data set (Supplemental Table 1), genes at CISs for the combined prostate + RTCGD data sets (Supplemental Table 2), and prostate insertions at genes that had previously been identified as CISs (Supplemental Table 3). Among the 19 candidate prostate cancer genes identified in our study were 5 genes that have previously been investigated for their potential roles in prostate cancer including *Dpt, Notch1, Runx3, Igf1r,* and *Ghr* [representative studies: [Takeuchi, T. 2006; Hellawell, G.O. 2002; Fowler, M. 2006; Shou, J. 2001; Weiss-Messer, E. 2004]]. The remaining 14 candidate prostate cancer genes have not previously been investigated for their potential roles in prostate cancer. Future studies are anticipated to include evaluation of these genes in human prostate cancers and additional screening for candidate cancer genes using the refined methods developed for this study.

**Supplemental Figure 1. Prostatic phenotypes in *Rosa26*-SB11;T2/onc mice.** (A,B) Hematoxylin and eosin stained tissue section from Rosa26-SB11;T2/onc prostates revealed that most of the prostate gland had a normal glandular histology [examples at arrows in A (100X magnification) and B (400X magnification)], but focal areas of epithelial hyperplasia were also observed [examples at arrowheads in A (100X magnification) and B (400X magnification)]. The possibility that the focal areas of hyperplasia in Rosa26-SB11;T2/onc double transgenic mice resulted from focal areas of increased proliferation was investigated by staining Rosa26-SB11;T2/onc double transgenic mice and single transgenic littermate (Rosa26-SB11 only or T2/onc only) controls with an antibody against the proliferation-associated Ki67 antigen (citations). Single transgenic control prostatic tissue sections contained rare Ki67 positive cells (brown stained nuclei) that typically appeared as individual cells or a pair of positive cells (examples at arrows in C-F). The arrows in C and D indicate the same Ki67 positive cell at 100x and 400x magnification respectively. The arrows in E and F indicate the same Ki67 positive cell at 100x and 400x magnification respectively. Double transgenic experimental prostatic tissue sections contained clusters of multiple Ki67 positive cells in addition to occasional single positive cells (see Figure 1 of the main paper). Tissue sections in A-D show the dorsolateral prostate (DLP) while section in E and F show the anterior prostate (AP).

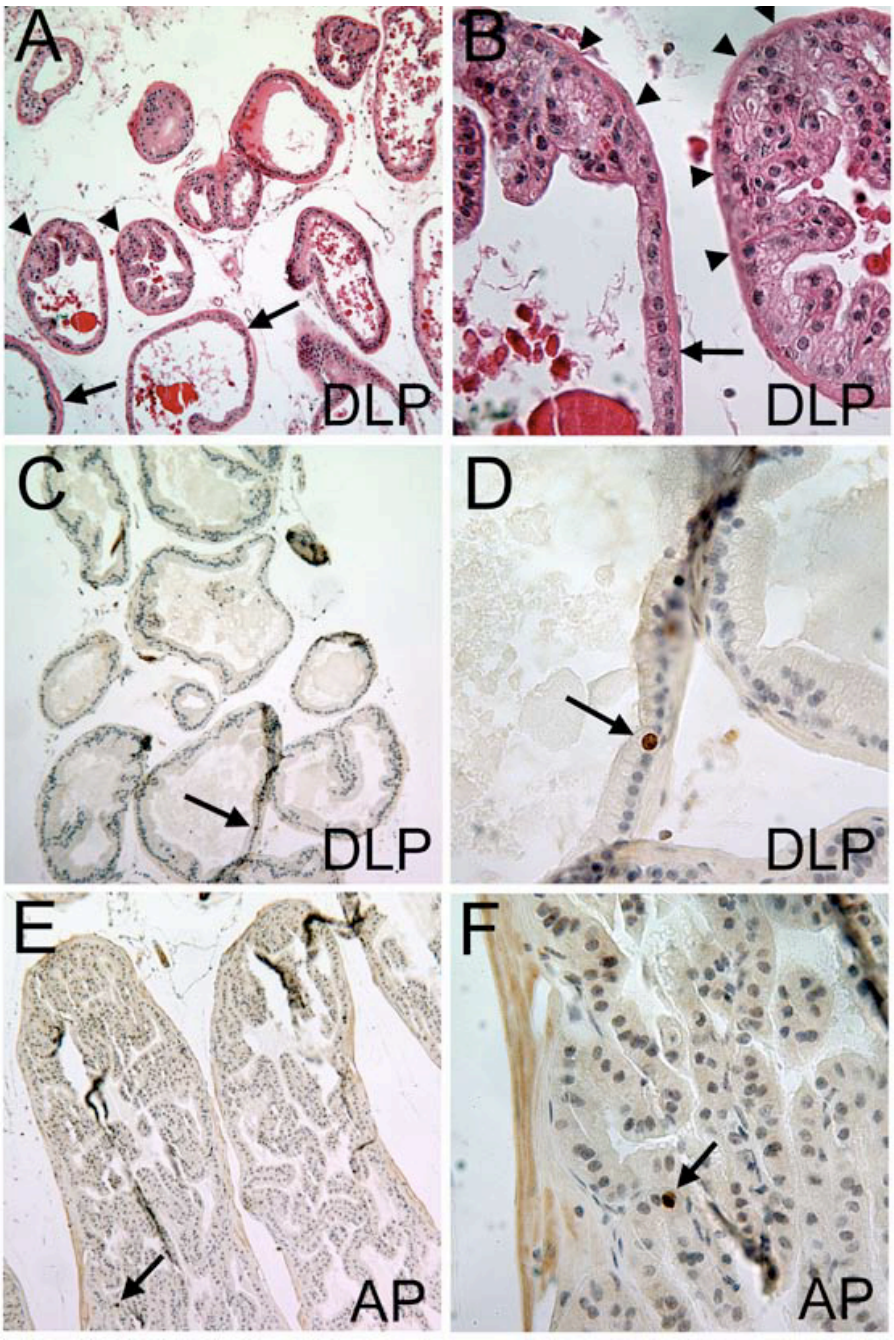
A
DLP
B
DLP
C
DLP
D
DLP
E
AP
F
AP

**Supplemental Figure 2. Transposase expression in *CAGGS-SB10;T2/onc;Arf*$^{-/-}$ and *Rosa26-SB11;T2/onc* mice.** A monoclonal antibody against the Sleeping Beauty transposase was used to evaluate transposase expression in CAGGS-SB10 transgenic mice and Rosa26-SB11 knock-in mice [Collier,L.S. 2005;Dupuy, A.J. 2005]. (A) Minimal background staining was observed in non-transgenic testis. (B) Strong nuclear staining (brown stain) was observed in the testis of CAGGS-SB10 transgenic mice that have previously been shown to exhibit high rates of transposition in the male germline [Carlson, C.M. 2003; Dupuy, A.J. 2001]. (C) Very few prostatic cells stained positive for transposase expression in CAGGS-sB10 transgenic mice. (D) Essentially all prostatic cells stained positive for transposase expression in Rosa26-SB11 mice.

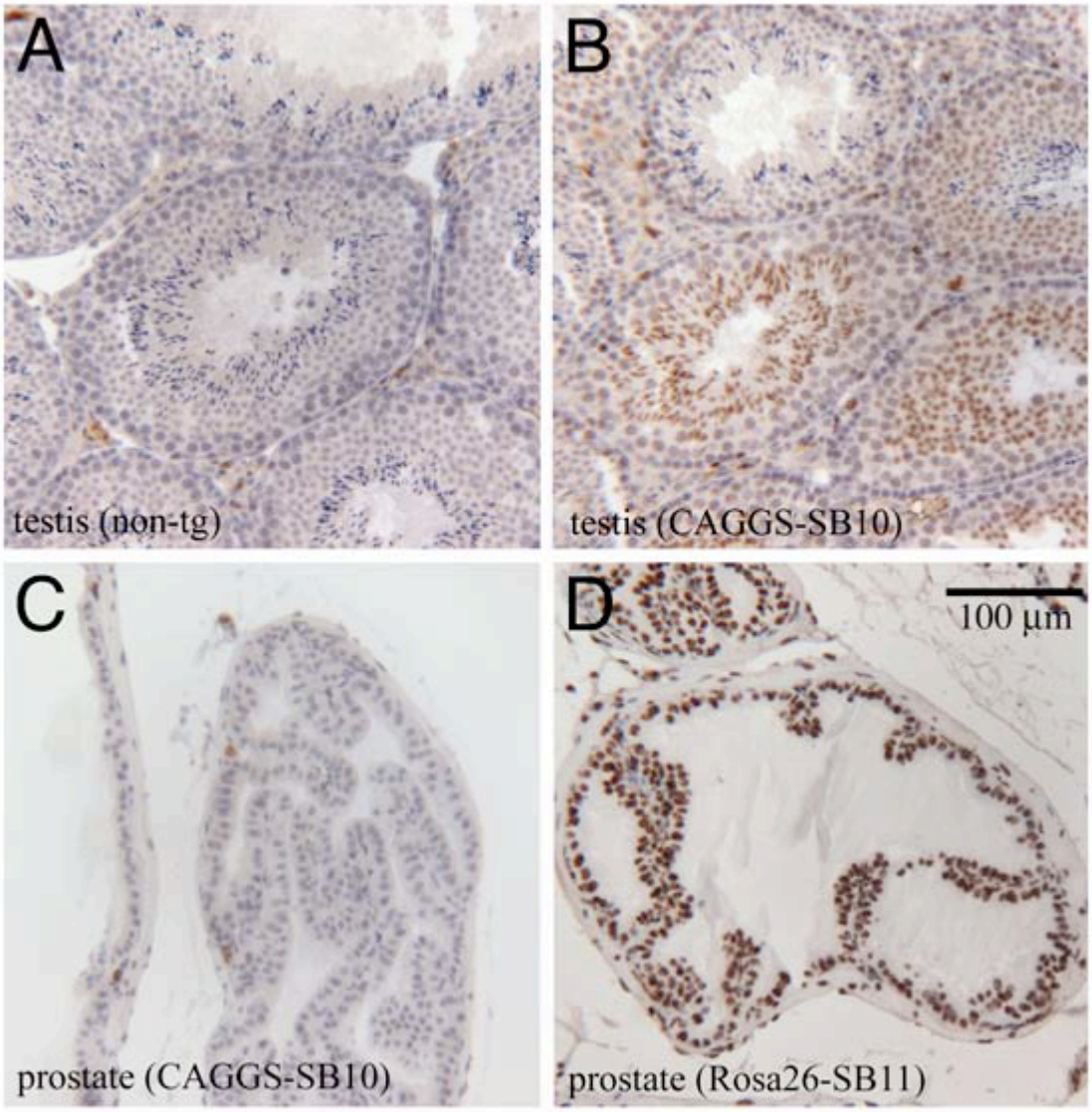
A
testis (non-tg)
B
testis (CAGGS-SB10)
C
prostate (CAGGS-SB10)
D
100 µm
prostate (Rosa26-SB11)

**Figure 1. Focal areas of elevated proliferation in the prostates of *Rosa26*-SB11;T2/onc mice.** The possibility that the focal areas of hyperplasia in *Rosa26*-SB11;T2/onc low-copy double transgenic mice resulted from focal areas of increased proliferation was investigated by staining *Rosa26*-SB11;T2/onc low-copy double transgenic mice and single transgenic littermate (*Rosa26*-SB11 only or T2/onc low-copy only) controls with an antibody against the proliferation-associated Ki67 antigen (20, 21). Single transgenic control prostatic tissue sections contained rare Ki67 positive cells that typically appeared as individual cells or a pair of positive cells (see Supplemental Fig. 1). (A, B) Double transgenic *Rosa26*-SB11;T2/onc low-copy prostatic tissue sections contained clusters of multiple Ki67 positive cells in the dorsolateral prostate (example indicated by the arrow in A and shown at higher magnification in B). (C, D) Similar clusters of multiple Ki67 positive cells were observed in the anterior prostate (example indicated by the arrow in C and shown at higher magnification in D). Scale bars are shown for A and C in A, and for B and D in B.

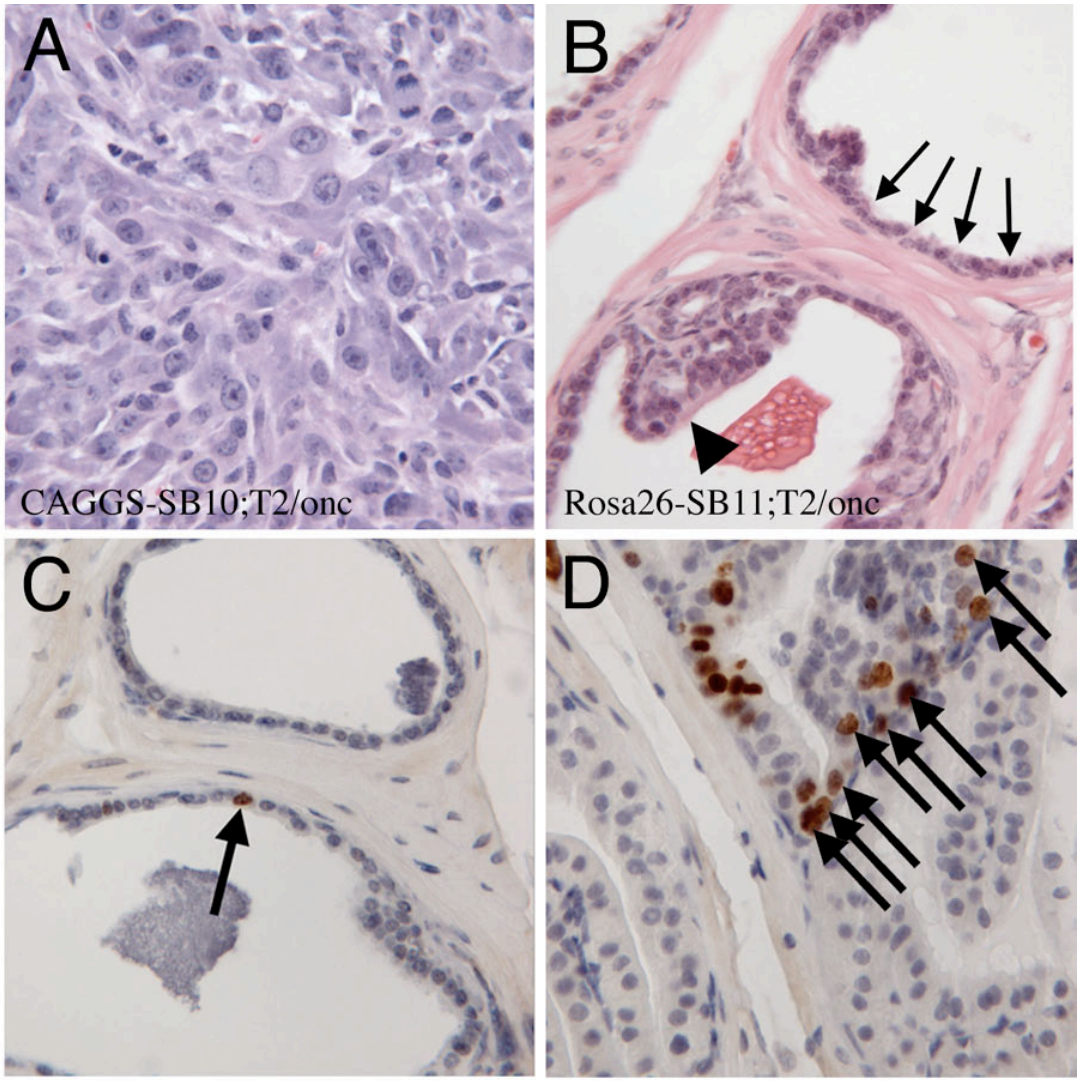
A
CAGGS-SB10;T2/onc
B
Rosa26-SB11;T2/onc
C
D

**Figure 2. Analysis of proliferating prostatic lesions in *Rosa26*-SB11;T2/onc low-copy mice.** To quantify the altered pattern of proliferation in the prostates of *Rosa26*-SB11;T2/onc low-copy mice, Ki67 positive cells were photographed and additional Ki67 positive cells within 25 mm were counted (n=61 for single transgenic controls, n=133 for double transgenic experimental mice). (A) Plot of the distribution of Ki67 positive cells relative to the number of additional Ki67 positive cells within 25 mm is shown. In single transgenic control prostates, there were an average of 0.62 additional Ki67 positive cells within 25 mm of a Ki67 positive cell. In *Rosa26*-SB11;T2/onc low-copy prostates, there were an average of 7.3 additional Ki67 positive cells within 25 mm of a Ki67 positive cell. The altered distribution of Ki67 positive cells for *Rosa26*-SB11;T2/onc low-copy prostates relative to single transgenic controls was highly significant ($P<0.0001$ by T-test). (B) When initial attempts to isolate transposon-genomic DNA junctions from laser captured proliferating prostatic lesions failed, the limitations of published linker mediated PCR protocols for cloning transposon-genomic DNA junctions were evaluated using serial dilutions of genomic DNA isolated from two mice with defined transposon insertions inherited through the germline [Collier,L.S. 2005; Dupuy, A.J. 2005; Wu, X. 2003]. Animal #1 (left 4 lanes) harbored a single insertion while animal #2 (right 4 lanes) harbored 5 insertions. All insertions were reproducibly amplified from either 1mg (lanes 1 and 5) or 100ng (lanes 2 and 6) of genomic DNA, but amplification was unreliable at low-ng quantities of DNA (lanes 3, 4, 7, and 8) and failed when DNA samples were isolated from approximately 100 laser-captured prostatic cells (data not shown). (C) Modified protocols for linker-mediated PCR and immunohistochemistry were used to achieve efficient amplification of transposon-genome junction fragments from laser captured cells isolated from tissue sections stained with an antibody against proliferation-associated marker phospho-(ser10)-Histone H3. When laser-captured proliferating lesions from the prostates of *Rosa26*-SB11;T2/onc low-copy double transgenic mice were analyzed by linker-mediated PCR, a variety of flanking genomic sequences were amplified and the pattern of amplified genomic fragments varied from lesion-to-lesion (samples 1-8). (D) The chromosome distribution of unique genomic insertion sites (n=104) isolated from laser-captured proliferating lesions is shown with the asterisks

indicating chromosomes harboring the T2/onc transgenic concatomers used in the experiment. Approximately 34% of the insertions were linked to the donor T2/onc concatomers while the remaining insertions were distributed across 17 of the 18 other chromosomes.

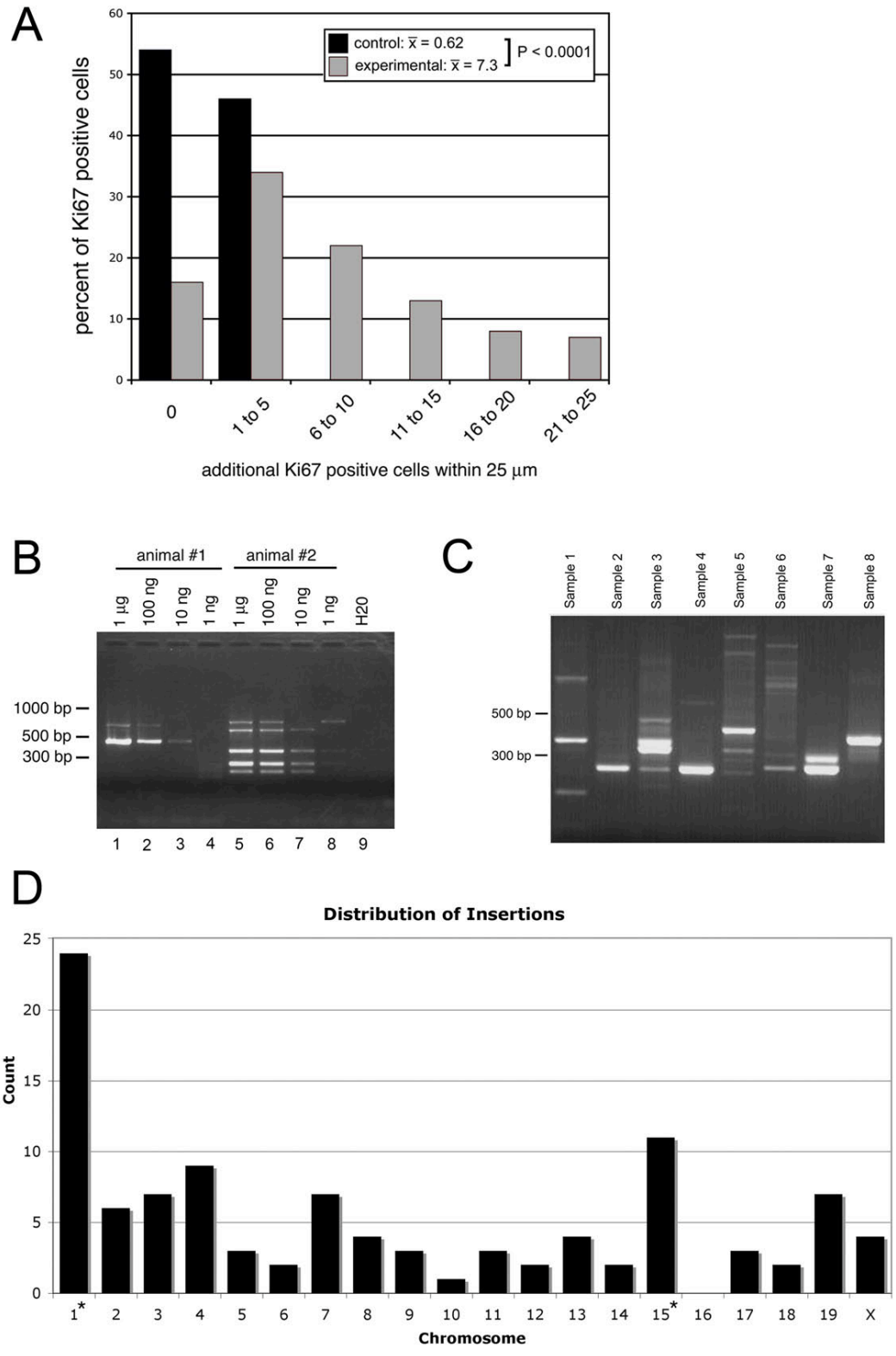
A
percent of Ki67 positive cells
control: x̄ = 0.62
experimental: x̄ = 7.3
P < 0.0001
0
1 to 5
6 to 10
11 to 15
16 to 20
21 to 25
additional Ki67 positive cells within 25 μm
B
animal #1
animal #2
1 μg
100 ng
10 ng
1 ng
H20
1000 bp
500 bp
300 bp
1 2 3 4 5 6 7 8 9
C
Sample 1
Sample 2
Sample 3
Sample 4
Sample 5
Sample 6
Sample 7
Sample 8
500 bp
300 bp
D
Distribution of Insertions
Count
Chromosome
1* 2 3 4 5 6 7 8 9 10 11 12 13 14 15* 16 17 18 19 X

**Figure 3. Transposon insertion sites in *PDE4D*.** The *PDE4D* gene produces multiple protein isoforms by using alternative promoters and alternative splicing. At least 9 isoforms are made in rodents (31) and human orthologues for 8 of the 9 rodent isoforms have been reported and deposited in GenBank. The human pattern of *PDE4D* mRNA alternative splicing is similar to the rodent pattern and is depicted in the figure based on investigator-deposited GenBank transcripts (accession numbers: U50157.1, U50158.1, U50159.1, AF012073.1, AF536975.1, AF536976.1, AF536977.1, AY245867.1). There are 7 alternatively used first exons shown as 1a-1g that initiate transcription for the 8 mRNA isoforms *PDE4D1-3* and *PDE4D5-9*. All isoforms include exons 7-15 that contain coding sequences for the PDE4D catalytic domain. Long isoforms (*PDE4D 3, 5, 7, 8, 9*) also include conserved sequences from exons 2-5 that encode regulatory phosphorylation sites and a dimerization domain while short isoforms (*PDE4D 1, 2, 6*) lack these domains. The position of the T2/onc insertions observed in the prostate screen relative to alternatively used exons is also shown. Activity of the promoter in T2/onc would be predicted to over-express one or more short *PDE4D* isoforms. The location of primers used for RLM-5'-RACE experiments presented in Fig. 4 are indicated below the diagram of the PDE4D as is the transcriptional start site for PDE4D in human prostatic adenocarcinomas as determined by the experiments presented in Fig. 4.

A

Prostate Common Insertion Sites

| Gene | Chr. | # insertions | insertion locations | gene transcription | transposon promoter | prostate genotype |
|---|---|---|---|---|---|---|
| *Rabgap1l* | 1 | 5 | introns 15, 17; 3'-UTR | centromeric | both | wt (4), Arf-/- (1) |
| *Pde4d* | 13 | 3 | intron 5 | telomeric | telomeric | Arf-/- (3) |
| *Klhl13* | X | 2 | intron 1 | centromeric | both | wt (1), Arf-/- (1) |

B

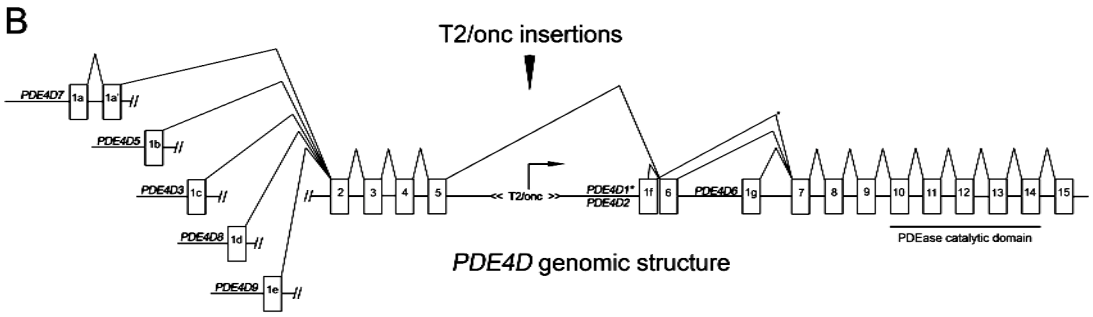

**Supplemental Table 1. Novel CISs for combined prostate and RTCGD data**. The prostate insertion sites observed in our prostate study were compared to previously reported retroviral and transposon insertions from other cancer screens by searching the Retroviral Tagged Cancer Gene Database [RTCGD; [Akagi, K. 2004]]. Using the criteria proposed by Mikkers et al. for a CIS, five novel CISs were identified for the combined data in the prostate study and the RTCGD database [Mikkers, H. 2002].

Supplemental Table 1: Novel CISs for combined prostate and RTCGD data

| Gene | Chr. | # prostate insertions | prostate genotype | # RTCGD insertions | RTCGD tumor types |
|---|---|---|---|---|---|
| *Psen2* | 1 | 1 | wt | 3 | mammary, brain |
| *Slc9a1* | 4 | 1 | Afr-/- | 1 | brain |
| *Lrrc27* | 7 | 1 | Arf-/- | 2 | B-cell, lymphoma |
| *March1* | 8 | 1 | wt | 2 | B-cell |
| *Snx14* | 9 | 1 | wt | 1 | B-cell |

**Supplemental Table 2. Prostate insertions at known CISs.** In addition to insertions at novel CISs listed in supplemental table 1, several prostate insertions were observed in genes previously identified as CISs by the data collected in the RTCGD database.

Supplemental Table 2: Prostate insertions at known CISs

| Gene | Chr. | prostate genotype | CIS mutagen | CIS tumor type | CIS study |
|---|---|---|---|---|---|
| *Dpt* | 1 | Arf-/- | transposon | sarcoma | Collier et al., 2005 |
| *Tnr* | 1 | wt | retrovirus | B-cell | Suzuki et al., 2002 |
| *B4galt5* | 2 | Arf-/- | retrovirus | mammary | Theodorou et al., 2007 |
| *Notch1* | 2 | wt | retrovirus, transposon | lymphoma, myeloid | Suzuki et al., 2002; Dupuy et al., 2005 |
| *Runx3* | 4 | wt | retrovirus | lymphoma, leukemia | Mikkers et al., 2002; Miething et al., 2007 |
| *Zpf644* | 5 | wt | retrovirus | lymphoma | Sauvageau et al., 2008 |
| *Igf1r* | 7 | wt | retrovirus | T-cell | Hwang et al., 2002 |
| *Ghr* | 15 | wt | retrovirus | lymphoma | Suzuki et al., 2002 |
| *Trhr* | 15 | Arf-/- | transposon | sarcoma | Collier et al., 2005 |
| *St6gal1* | 16 | wt | retrovirus | brain | Johansson et al., 2004 |
| *Dym* | 18 | Arf-/- | retrovirus | myeloid | Suzuki et al., 2002 |

**Figure 4. PDE4D is overexpressed and has altered mRNA isoform expression in human prostate cancer patient samples.** (A) Fluorescent images from a prostate cancer core on a human prostate tissue microarray (TMA). The TMA was co-stained with an anti-E-cadherin/anti-cytokeratin cocktail (green channel) to identify the epithelial cell cytoplasm, DAPI (blue channel) to identify nuclei, and anti-PDE4D (red channel). PDE4D was detected in prostate cancer and co-localized with the epithelial cytoplasm-specific stain (yellow signal in top right panel). A parallel TMA was stained in the presence of a PDE4D peptide (lower row) and the anti-PDE4D signal was blocked, indicating that the anti-PDE4D signal reflected specific staining for PDE4D. (B) Graph showing the results of automated quantitative analysis for PDE4D staining on the TMA. The higher PDE4D expression level in patients with prostatic adenocarcinoma relative to patients with benign prostatic hyperplasia (BPH) was statistically significant ($P<0.001$ by T-test). Error bars show the 95% confidence interval. When the tissues from adenocarcinoma patients were stratified by the histopathology of the tissue core into cores that contained primarily non-invasive epithelium (normal ducts or PIN), primarily invasive cancer, or cores from sites of metastasis, the PDE4D expression level differences among the different samples from adenocarcinoma patients were not statistically significant. (C) RNA pools made from 10 prostatic adenocarcinoma samples (left lane) or 10 histologically normal prostate patient samples (right lane) were analyzed by RLM-5'-RACE using primers in exon 10 of *PDE4D* that would allow all known *PDE4D* isoforms to be amplified (location of the primers shown in Fig 3B), and the resulting pattern of amplified 5'-cDNA ends was distinct for the two pools. (D) Sequencing data are shown for the major RLM-5'-RACE product amplified from human prostatic adenocarcinoma RNA. This data showed that the first exon of the amplified transcripts began at base pair 349 of the Genbank deposited sequence for the *PDE4D5* isoform (accession AF12073.1) and was spliced to exon 2 of *PDE4D* in a manner identical to the other *PDE4D* long isoforms. The location of the inferred transcriptional start site is indicated in the diagram in Fig. 3B.

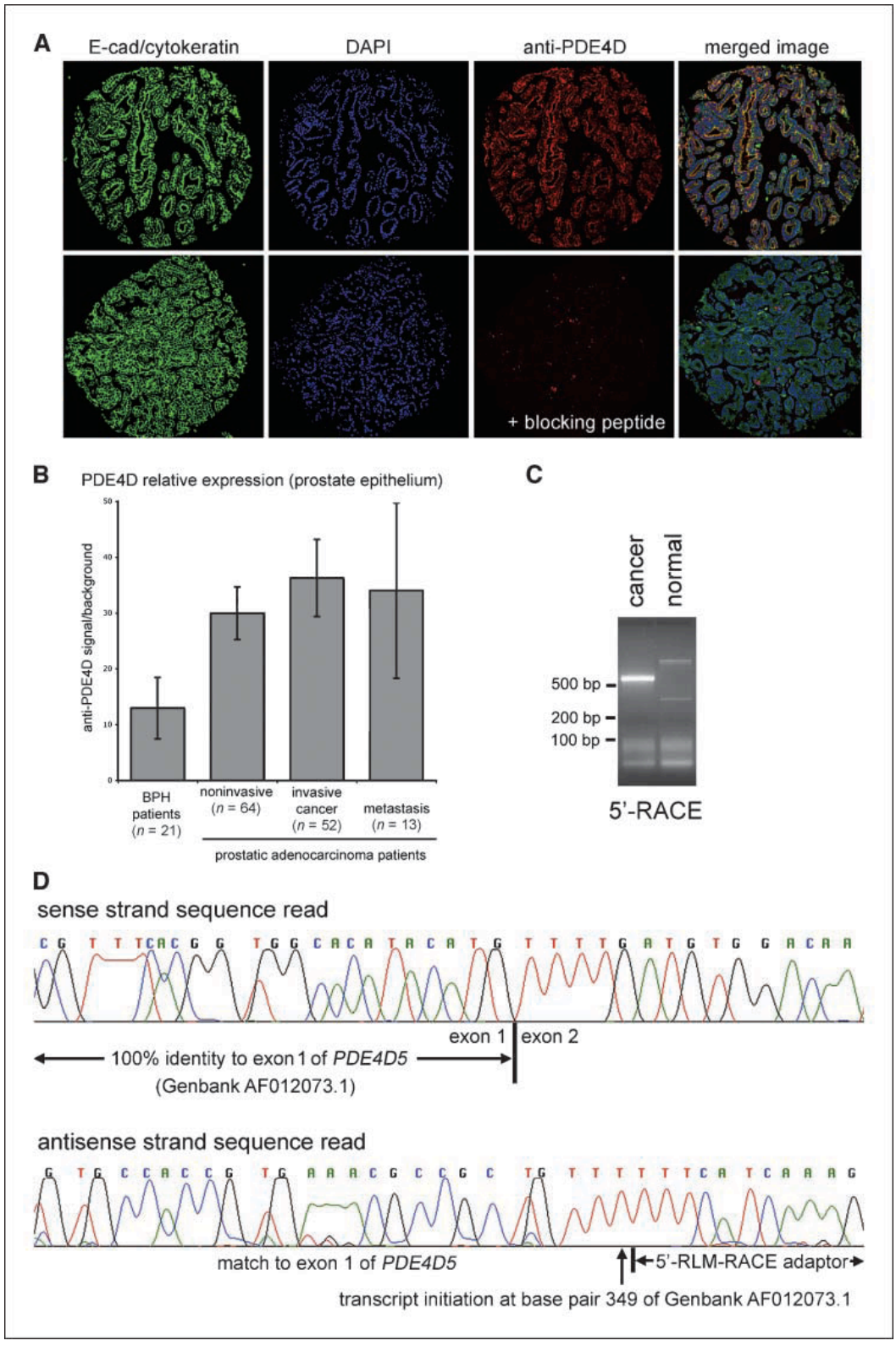
A
E-cad/cytokeratin
DAPI
anti-PDE4D
merged image
+ blocking peptide
B
PDE4D relative expression (prostate epithelium)
anti-PDE4D signal/background
BPH patients (n = 21)
noninvasive (n = 64)
invasive cancer (n = 52)
metastasis (n = 13)
prostatic adenocarcinoma patients
C
cancer
normal
500 bp
200 bp
100 bp
5'-RACE
D
sense strand sequence read
exon 1
exon 2
100% identity to exon 1 of PDE4D5
(Genbank AF012073.1)
antisense strand sequence read
match to exon 1 of PDE4D5
5'-RLM-RACE adaptor
transcript initiation at base pair 349 of Genbank AF012073.1

**Supplemental Figure 3. PDE4D protein expression in primary prostate epithelial cells and prostate cancer cell lines.** Immunoblots with an anti-PDE4D antibody were used to examine protein expression in normal primary human prostatic epithelial cells (PrE) and in a series of commonly used prostate cancer epithelial cell lines (DU145, PC3, LNCaP, C4-2b, and 22Rv1). All of the prostate cancer cell lines over-expressed both long and short PDE4D isoforms relative to the normal primary prostatic epithelial cells. The blots were also evaluated with an antibody against ACTIN as a loading control.

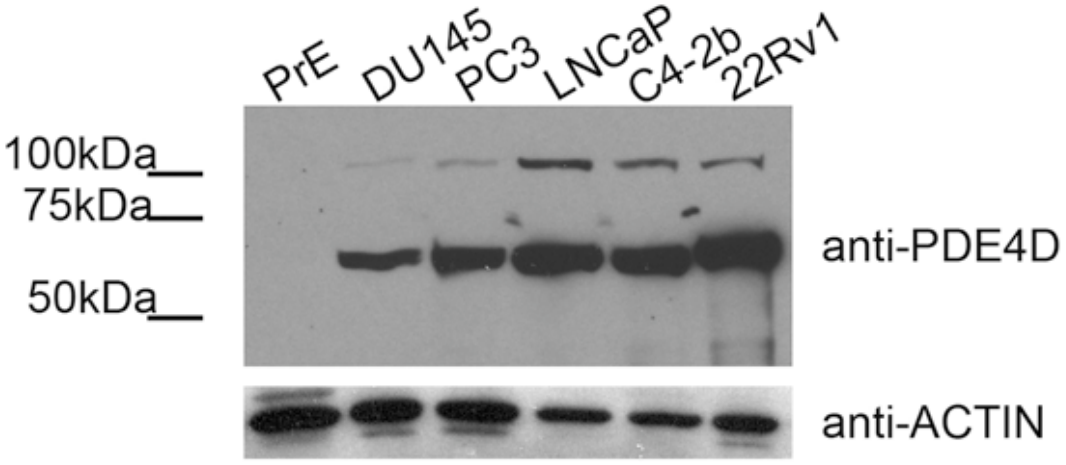
PrE
DU145
PC3
LNCaP
C4-2b
22Rv1
100kDa
75kDa
50kDa
anti-PDE4D
anti-ACTIN

**Figure 5. PDE4D shRNA knockdown reduces prostate cancer cell growth.** (A) Stable transfectant variants of the DU145 prostate epithelial cell line expressing either a shRNA against a sequence in exon 8 of *PDE4D* or a scrambled control shRNA were evaluated by immunoblot for PDE4D protein expression. The control shRNA (SC) did not affect PDE4D expression while two stable transfectant pools for the *PDE4D* shRNA (KD1, KD2) had decreased expression (A, top panel). The same immunoblot was also probed with an anti-ACTIN antibody as a loading control (A, lower blot). The growth rates of the *PDE4D* shRNA and control shRNA transfectant DU145 cells were evaluated using a trypan blue exclusion assay to quantify viable cells, and a significant decrease in growth rate was observed for cells with *PDE4D* knockdown relative to controls (A, graph). (B) The same control and *PDE4D* exon 8 shRNAs were also used to create stable transfectant variants of the PC3 prostate epithelial cell line, and PDE4D knockdown was confirmed by immunoblot (B, upper panels). The growth rates of the *PDE4D* shRNA and control shRNA transfectant PC3 cells were evaluated using a trypan blue exclusion assay to quantify viable cells, and a significant decrease in growth rate was observed for cells with *PDE4D* knockdown relative to controls (B, graph). (C) To control for off-target shRNA effects, additional shRNAs targeting other *PDE4D* exons were designed and used to create stable transfectant variants of the DU145 cell line. These variants were evaluated for PDE4D expression by immunoblot, and the most significant knockdown was observed for shRNAs directed against sequences in *PDE4D* exons 14-15 and 7 (C, upper panel). The growth rates of the exon 14-15 *PDE4D* shRNA, exon 7 *PDE4D* shRNA, and control shRNA transfectant DU145 cells were evaluated using an MTS assay to quantify viable cells, and a significant decrease in growth rate was observed for cells with *PDE4D* knockdown relative to controls (C, graph). Statistically significant differences between experimental and control data points were determined by ANOVA with least significant difference post-hoc analysis and are indicated on the graphs as follows: * $P<0.05$, ** $P<0.001$ (A and C, n=3 per data point; B, n=4 per data point).

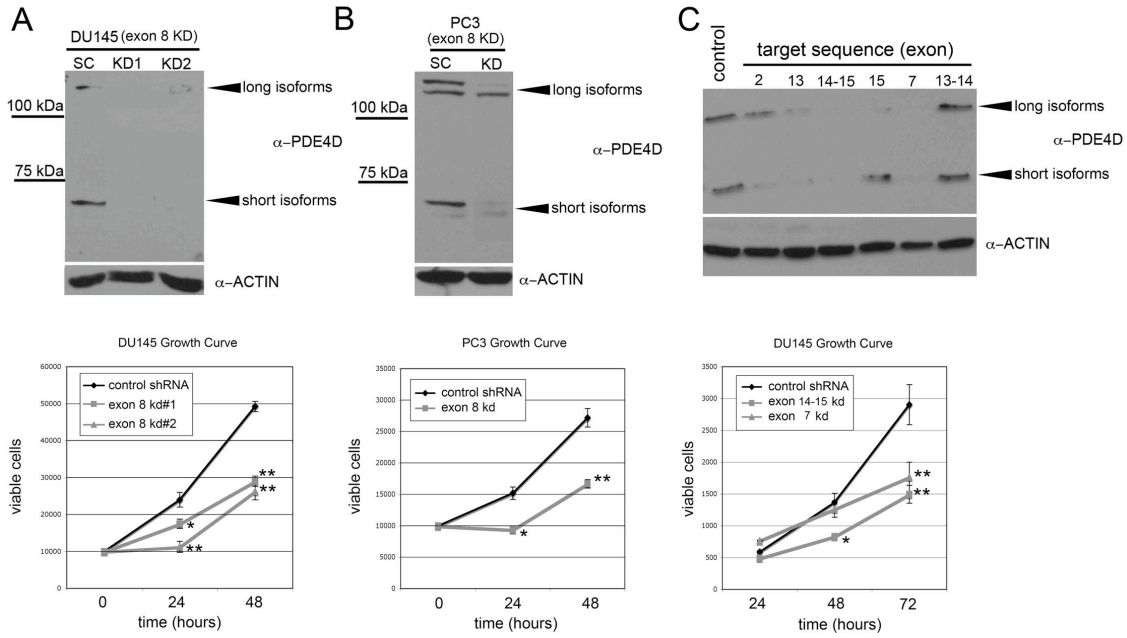
A
DU145 (exon 8 KD)
SC
KD1
KD2
100 kDa
75 kDa
long isoforms
α–PDE4D
short isoforms
α–ACTIN
B
PC3
(exon 8 KD)
SC
KD
100 kDa
75 kDa
long isoforms
α–PDE4D
short isoforms
α–ACTIN
C
control
target sequence (exon)
2
13
14-15
15
7
13-14
long isoforms
α–PDE4D
short isoforms
α–ACTIN
DU145 Growth Curve
control shRNA
exon 8 kd#1
exon 8 kd#2
viable cells
time (hours)
PC3 Growth Curve
control shRNA
exon 8 kd
viable cells
time (hours)
DU145 Growth Curve
control shRNA
exon 14-15 kd
exon 7 kd
viable cells
time (hours)

**Supplemental Figure 4. PDE4D shRNA knockdown reduces prostate cancer cell migration.** The effects of PDE4D knockdown on prostate epithelial cell migration were evaluated using an in vitro wound healing assay. Confluent monolayers of control shRNA and PDE4D shRNA (exon 7 KD, exon 13 KD, and exon 14-15 KD) stable transduced cell lines were scratched with a pipet tip to create an area devoid of cells, and the same area of the scratch wound was photographed at time = 0 (immediately after the scratch wound was created), at 3 hours post-wound, and at 5 hour post-wound (examples of sequential photos for a control and PDE4D exon14-15 shRNA shown in A). The area devoid of cells in the photographs was quantified and used to determine the rate at which cells migrated into the void to close the scratch wound. PDE4D knockdown caused a decrease in the rate at which DU145 cells migrated to close the scratch wound for all three PDE4D-directed shRNAs tested (B). Statistically significant differences between experimental and control data points were determined by ANOVA with least significant difference post-hoc analysis and are indicated on the graphs as follows: * $P<0.05$, ** $P<0.001$ (n=3 per data point).

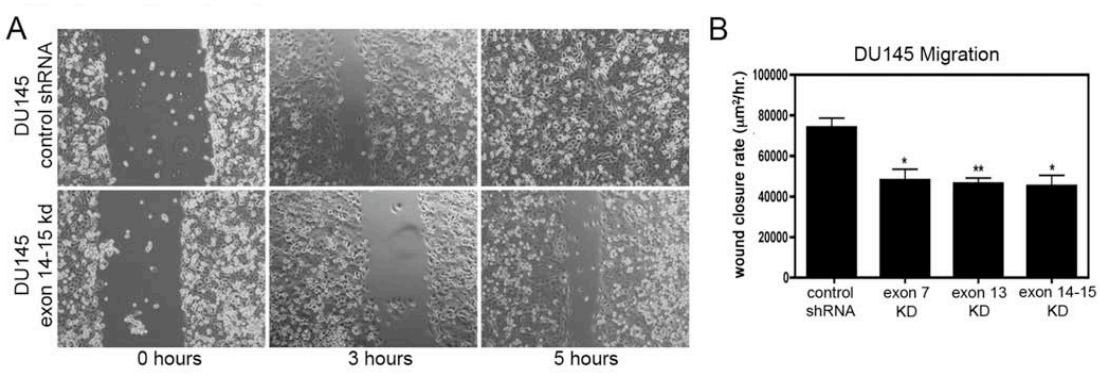
A
DU145 control shRNA
DU145 exon 14-15 kd
0 hours
3 hours
5 hours
B
DU145 Migration
wound closure rate (μm²/hr.)
100000
80000
60000
40000
20000
0
*
**
*
control shRNA
exon 7 KD
exon 13 KD
exon 14-15 KD

**Figure 6: *PDE4D* knockdown reduces the growth of DU145 cells *in vivo*.** Xenografts were made by injecting derivative DU145 cell lines expressing a *PDE4D*-targeting shRNA (n=7) or a scrambled sequence control shRNA (n=7) sub-cutaneously into CD-1 nu/nu male host mice ($10^6$ cells co-injected with matrigel). After 4 weeks of growth *in vivo*, the xenografts were harvested and photographed (examples in A). The xenograft tumors were processed for immunohistochemistry and tissue sections were stained with an antibody against proliferation-associated antigen Ki67 (brown stain in B and C). Sections were also counter stained with hematoxylin (purple stain in B and C). A high percentage of cells in the control shRNA xenografts stained positive for Ki67 (B) while a relatively lower number of cells in the *PDE4D* knockdown xenografts were Ki67 positive (C). To quantify any differences in Ki67 labeling between the two groups, 8 random 20X microscopic fields were photographed for Ki67-stained slides from each xenograft tumor (7 *PDE4D*-targeting shRNA tumors and 7 scrambled sequence control shRNA tumors) and the percentage of Ki67 positive nuclei to total nuclei was determined in the photographed areas of each tumor. The average Ki67 labeling index for control and *PDE4D* knockdown tumors is shown (D). The reduction in Ki67 labeling index observed for *PDE4D* knockdown cells was statistically significant ($p<0.01$ by T-test).

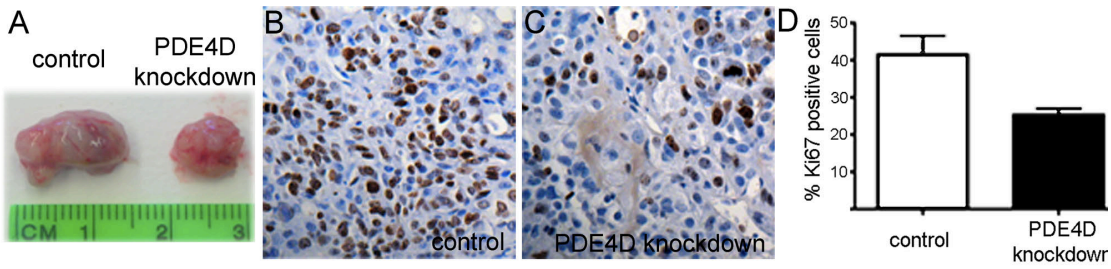
A
control
PDE4D knockdown
CM 1 2 3
B
control
C
PDE4D knockdown
D
% Ki67 positive cells
50
40
30
20
10
control
PDE4D knockdowr

**Supplemental Figure 5. *PDE4D* knockdown reduces the growth of DU145 cells *in vivo.*** Xenografts were made by injecting derivative DU145 cell lines expressing a *PDE4D*-targeting shRNA (n=7) or a scrambled sequence control shRNA (n=7) sub-cutaneously into CD-1 nu/nu male host mice ($10^6$ cells co-injected with matrigel). After 4 weeks of growth *in vivo*, the xenografts were harvested and weighed. (A) Wet weight of PDE4D knockdown xenografts was lower than control xenografts. The reduction in weight was statistically significant (P=0.027 by T-test). The xenograft tumors were processed for histology and tissue sections were stained with hematoxylin and eosin. (B) Low power view of xenograft tissue sections shows that both control xenografts (left) and knockdown xenografts (right) included significant cysts that were largely devoid of living tumor cells (indicated by the asterisks). These regions appeared to be more extensive in the PDE4D knockdown xenografts. (C) Higher magnification view of a control xenograft tissue section with a portion of the acellular cyst indicated by the asterisk. (D) Higher magnification view of a PDE4D knockdown xenograft tissue section with a portion of the acellular cyst indicated by the asterisk. A scale bar for C and D is shown in C.

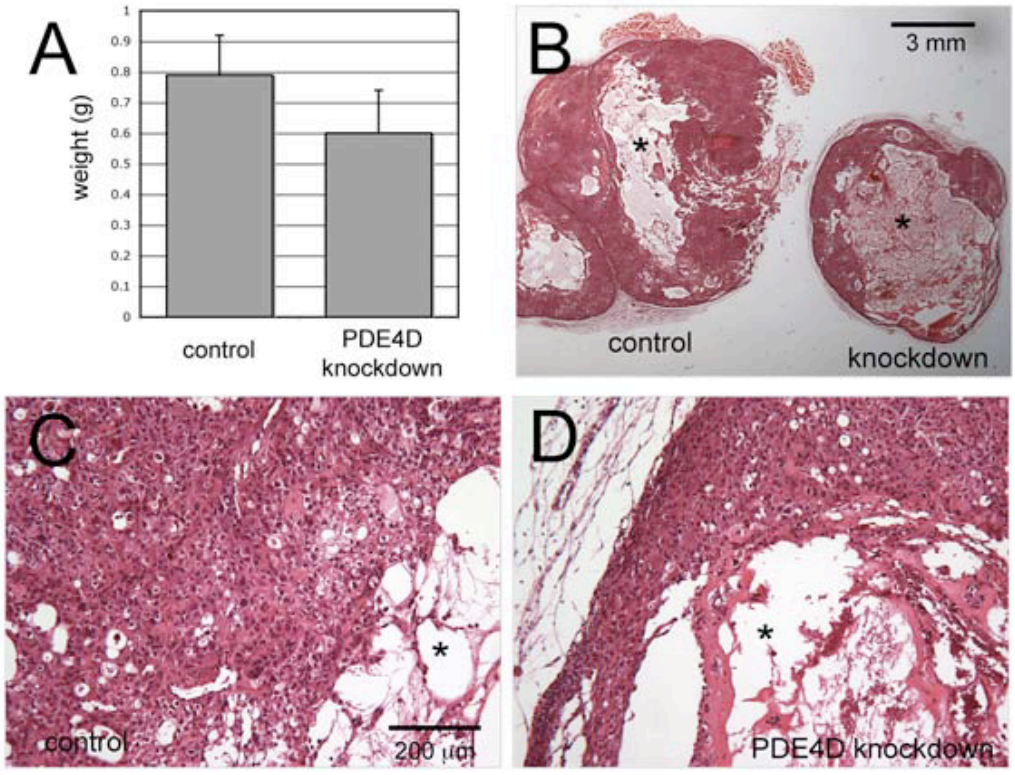
A
weight (g)
1
0.9
0.8
0.7
0.6
0.5
0.4
0.3
0.2
0.1
0
control
PDE4D knockdown
B
3 mm
*
*
control
knockdown
C
*
control
200 µm
D
*
PDE4D knockdown

# Chapter 3.

# A S*leeping Beauty* mutagenesis screen implicates *Braf* and *Nras* in prostate epithelial cell fate

Utilizing the *Sleeping Beauty* transposon system, we developed a transgenic mouse model to be used in forward and reverse genetic screens to further understand genetic pathways involved in prostate development and disease. The transgenic mouse contains a bicistronic transgene composed of the Sleeping Beauty transposase under the control of the prostatic epithelial cell specific promoter probasin (*AAR2Pb*) and a Luciferase reporter gene. Somatic mobilization of a mutagenic transposon induced a variety of phenotypes within the prostate epithelium, which included 1) increased proliferation in prostate glands reminiscent of a pubescent prostate 2) proliferative cell lesions of a diseased prostate and 3) altered epithelial cell fate. Cloning and sequencing of transposon integration sites from proliferating cell lesions identified *Braf* and *Nras* as common insertion sites. We also used transposon mobilization to ectopically express *Braf* in an *in vivo* urogenital sinus kidney capsule model. Ectopic expression of a C-terminal truncated form of *Braf* significantly increased proliferation in prostate epithelial cells, but did not cause histologic changes in the allografts. Automated quantitative analysis of BRAF in human prostate cancers showed that BRAF was over-expressed when compared to benign prostatic tissues, but over-expression was not indicative of survival or recurrence. These data indicate that the *Sleeping Beauty* transposon system is a useful tool in identifying and characterizing genetic pathways involved with prostate epithelial cell fate and prostate disease, and that studies with *BRAF* are warranted in prostate cancer.

## INTRODUCTION

The *Sleeping Beauty* transposon system is an unbiased bipartite forward genetic screen composed of an enzyme called a transposase, *Sleeping Beauty* (SB), and a mobilized piece of DNA called a transposon [Ivics,Z. 1997]. A unique feature of this system is that the transposon can contain virtually any cargo (DNA elements) with the only requirement being the cargo is flanked by inverted repeat direct repeat sequences for the transposase to bind. These features of the transposon have made the SB system amenable to many uses including gene therapy, germline studies, and cancer gene discovery screens [Belur, L.R. 2003; Ohlfest, J.R. 2005; Peng, PD 2009; Dupuy, A.J. 2002; Dupuy, A.J. 2001; Collier, L.S. 2009; Keng,V.W. 2009; Starr,T.K. 2009; Collier, L.S. 2005]. We previously used a Sleeping Beauty transposon screen to identify *Phosphodiesterase 4D* (*PDE4D*) as a novel proliferation-promoting factor that is important in prostate cancer, and were the first to show that prostate cancer genes can be discovered using the SB system [Rahrmann,E.P. 2009].

Prostate cancer is the most commonly diagnosed male cancer and leading cause of male cancer death [Gregorakis,A.K. 1998; McDavid, K. 2004]. Prostate cancer progression is thought to occur through histological and genetic alterations. One challenge to understanding the unique genetic alterations in prostate cancer is the genetic heterogeneity of prostate cancers. Prostate cancer initiation is characterized by changes in prostate epithelial cell proliferation called Prostate Intraepithelial Neoplasia (PIN) and progresses through a series of well-characterized histological alterations. However, genetic changes that occur during the development of prostate cancer are inadequately characterized.

In this study, we developed a transgenic mouse in which mobilization of a mutagenic transposon gave rise to foci of altered histology and proliferative cell lesions. We also utilized transposon mobilization to develop a system in which a candidate prostate cancer gene(s) can be characterized for the ability to induce histological or proliferative changes in the prostate. This bi-partite approach to modeling and characterizing genetic alterations using transposon mobilization provides key insights into candidate genes that may be important in prostatic disease.

## MATERIALS AND METHODS

**Vector Construction and Generation of PSIL Transgenic Mice.** A schematic of the transgene is shown in Figure 1. The vector, a bicistronic transgene created by cloning the transposase *SB10* cDNA behind the adult rat prostate epithelial cell specific promoter Probasin, *ARR2PB*. An internal ribosomal entry site (IRES) and a *luciferase* cDNA were cloned downstream of the *SB10* cDNA. Pro-nuclear injections were performed at the University of Minnesota Mouse Genetics Laboratory. Presence of the *AAR2PbSB10/IRESLuciferase* (PSIL) transgene was determined by Southern blot with a probe targeting SB10. In addition, DNA was isolated by adding 700ul a Triton-based digest buffer (1M Tris Chloride pH 8, 0.5 M EDTA, 5M NaCl, 1X Triton X-100) containing Proteinase K from tails of F1 offspring and subjected to PCR to amplify the transgene with the following conditions: PCR genotyping was performed using 1ul of Triton X digested Tail genomic DNA as template in a 25 µl PCR reaction volume. PCR primers used for *SB10* were forward 5'- GGACAACAAAGTCAAGGTAT-3' and reverse 5'- TAACTTGGGTCAAACGTTTC-3' (amplicon 215 bp); T2/Onc were forward 5'- CGCTTCTCGCTTCTGTTCGC-3' and reverse 5'- CCACCCCCAGCATTCTAGTT-3' (amplicons 250bp). PCR conditions for Clp Taq (1 x Clp buffer, 1 x sucrose Red, 0.25mM dNPTs, 3mM $MgCl_2$, 200nM both sense and anti-sense primers, 0.05 U/ul taq, 2ul of DNA solution) were used according to the manufacturer's instructions with an initial denaturing step of 94°C for 10 min; 30-cycles of denaturing at 94°C for 30 sec, annealing at 52°C (55°C for T2/Onc) for 30 sec and extension at 72°C for 1 min; followed by a final extension at 72°C for 5 min. PCR products were separated on a 1.5% agarose gel and genotype determined by the absence or presence of expected amplicons.

**Histology and Immunohistochemistry.** Tissues were fixed in 10% buffered formalin and embedded in paraffin blocks. Sections were cut at 5-µm thickness, and rehydrated through a series of graded ethanols. Slides underwent antigen retrieval by boiling for 30 minutes in antigen unmasking solution (Vector Laboratories). Endogenous peroxidases were quenched with 3% hydrogen peroxide solution for 10 minutes. For antibody

staining, a M.O.M. kit (Vector Laboratories) was used for blocking and antibody incubations. Primary antibodies used were mouse anti-Sleeping Beauty Transposase (1:100; R&D Systems), mouse anti-Ki67 (1:100; Novocastra), rabbit anti-Braf (1:100; Santa Cruz Biotechnology); rabbit anti-p21 (1:100; Thermo Scientific). Following a series of washes, slides were incubated with the corresponding anti-mouse biotinylated secondary antibody (1:10,000; Vector Laboratories). Slides were washed, incubated with the vectastain ABC kit (Vector Laboratories) for 30 minutes at room temperature, washed again, and stained using peroxidase substrate kit DAB (Vector Laboratories). Finally slides were counterstained with hematoxylin, dehydrated, and mounted with permount. TUNEL colorimetric staining was performed according to manufacturer's instructions (Promega). For Ki67 quantification in the SB; T2/Onc mice, one 20x field was captured for each of 8 single transgenic mice, 24 SB(E);T2/Onc mice, and 4 SB(D);T2/Onc mice. For calculating the percent labeling index in the empty vector control and T2-*Braf*; SB11 allografts, the number of positive cells for Ki67, TUNEL, or p21 staining were counted and divided by the total number of cells in each 20x field image in Photoshop. One 20x field was captured for each of 8 T2-*Braf*; SB11 and 8 empty vector control allografts.

**Xenogen Imaging.** Mice were injected with 100ul of a Ketamine cocktail (100mg/ml Ketamine, 20mg/ml Xylazine, 10mg/ml Acepromazine) for sedation (Sigma). Once sedated, mice underwent an intraperitoneal injection with 100ul of 31.25 mg/ml D-Luciferin (Pierce). After a 5 min incubation at room temperature, mice were imaged on the Xenogen IVIS Imaging System at 1 min exposure time.

**Linker Mediated PCR for Transposon Insertion Site Identification.** DNA was isolated from proliferative cell lesions. Briefly, tissue sections were stained with Ki67. Adjacent slides to those stained positive for Ki67 were scraped, digested, and DNA isolated using a QIAamp DNA FFPE Tissue kit (Qiagen) according to manufacturers instructions. Transposon-genomic DNA junctions were amplified as previously described [Keng, V.W. 2009; Starr, T.K. 2009]. Briefly, genomic DNA underwent linker mediated PCR (LM-PCR) to amplify genomic DNA-T2/Onc junctions as previously

described. LM-PCR products were purified using the MinElute 96 UF Plates (Qiagen), and submitted for high-through-put GS FLX Titanium sequencing (Fig. 4A). Unique genomic sequences were mapped to the mouse genome using the mouse genome maintained by the Wellcome Trust Sanger Institute at www.ensembl.org.

**Common Insertion Site Identification**. GS FLX Titanium reads were processed and analyzed using a custom semi-automated Perl processing pipeline first described in Starr et al., 2009 with additional modification described below [Starr,T.K. 2009]. Briefly, all sequence reads were assigned to tissue source libraries by matching a 10bp barcode present at the beginning of each sequence (allowing one mismatch). 96.5% of the initial 86545 sequence reads had a unique library assignment. All others were discarded. Raw sequences were scanned for IRDR using EMBOSS Vectorstrip with successively less stringent parameters (10%, 15%, and finally 20% mismatches allowed) until the maximum number of constructs were recognized and trimmed off. These trimmed insert sequences were mapped to the mouse genome (NCBIM37) using BLASN (DeCypher's TeraBLASTN, Active Motif, http://timelogic.com), requiring query sequences to align within 1bp of the start of right-IR/DR sequenced inserts or within 1bp of the end of left-IR/DR sequenced reads. Additionally the query sequence was required to match with at least 95% identity. 0.6% (~500) sequences could be uniquely mapped to the mouse genome. Redundant sequences from the same tissue sample that mapped to the same genomic position were coalesced into 223 nonredundant (NR) insertions. NR insertion positions were annotated using the EnsEMBL version 55 API with the name of the annotated gene. Because the insertions that appear in 2 or more donor mice at the same TA dinucleotide are mostly likely to be false-priming events, we eliminated all insertions containing insertions from two or more different mice to avoid the artifact [Keng,V.W. 2009; Starr,T.K. 2009]. 52 insertions that have two or more donor mice were removed, leaving 171 non-redundant, mapped sequences.

Unambiguously mapped non-redundant insertions were assigned to clusters if the local density of insertions in a given window size exceed that which would be expected by chance, as determined by exact Monte Carlo simulation [Keng,V.W. 2009; Starr,T.K.

2009]. For the combined dataset (171 non-redundant insertions), the significance thresholds obtained are ≥ 2 insertions within 90,000bp, For PIN dataset (160 non-redundant insertions), the value is ≥ 2 insertions within 95,000 bp.

**Urogenital Sinus Transfection and Kidney Capsule Surgery.** Male urogenital sinuses (UGSs) from embryonic day 16 mice were collected and transfected as described in Buresh et al [Buresh, R.A. 2010]. A transposon plasmid containing a mouse C-terminal truncated kinase domain *Braf* cDNA or an empty vector transposon plasmid (pT2/HB) at 8.5 ug/ul was co-transfected with Sleeping Beauty transposase 11 (SB11) at 0.85 ug/ul . UGSs were cultured with testosterone for 24 hours before being implanted under the kidney capsule of male CD-1 nu/nu mice [Buresh, R.A. 2010]. Allografts were grown *in vivo* for 8 weeks at which time the mice were sacrificed and allografts were excised and photographed. Half of the allograft was fixed in 10% buffered formalin and embedded in paraffin blocks while the other half was snap-frozen and RNA was extracted using a Macherey-Nagel RNA extraction kit according to manufacturer's instructions.

**PCR to Identify *Nras* Base Pair Changes.** DNA was extracted as above from the 2 independent proliferative prostate lesions in the mice identified as having insertions in *Nras*. PCR Primers for codons 12 and 13 were forward 5' ATGACTGAGTACAAACTGGT 3' and reverse 5' CTCTATGGTGGGATCATATT 3' (amplicon 112 bp). Primers for codons 59 and 61 were forward 5' GATTCTTACCGAAAGCAAGTGGTG 3' and reverse 5' ATTGATGGCAAATACACAGAGCAA 3' (amplicon 103 bp). Both primer sets were run at 94° for 3 min, 30 cycles of 94° 30 s, 60° 30 s, 72° 1 min, and 72° 5 min. PCR products were visualized and then cloned in TOPO TA vectors (Invitrogen) and sequenced by the University of Wisconsin Biotechnology Center.

**In situ PCR for Detection of Transposon/*Braf* transgene on Paraffin-fixed Slides.** Sections were cut at 5 micron thickness, and rehydrated through a series of graded ethanols. Slides underwent proteinase K digestion in PBS at 37°C for 30 minutes to

digest DNA binding proteins. Slides were heated in the microwave in 1X PBS for 60 seconds to ensure that no non-specific incorporation into damaged or nicked DNA occurred. For primary PCR, 150 ul of PCR master mix was added to the slide, a coverslip was applied, and the slide was sealed with clear nail polish. Master mix included 1X PCR buffer, 200 uM each of dATP, dCTP, dGTP, and dTTP, 4 mM $MgCl_2$, 6.4% BSA, 5 U/ul Amplitaq DNA polymerase, and 20 pM F and R primers. Primers for primary PCR were used to detect the inner splice donor of the transposon (5' CAGTCCTCCGATAGACTGCG 3') and *Braf* (5' GGAGGACAGAAGTCGGATGA 3'). Following the primary PCR reaction, slides were washed with 100% EtOH 3x 5 min each to remove coverslips and further washed with 1xPBT. In the secondary PCR reaction, 5 mM biotin-16-dUTP (Roche) was added to the Master mix. Primers for secondary PCR were used to detect a region of *Braf* amplified by the first PCR: 5' GGAGGACAGAGTCGGATGA 3' and 5' GTGTGGGTGCTGTCACATTC 3'. Slides were washed, incubated with the vectastain ABC kit (Vector Laboratories) for 30 minutes at room temperature, washed again, and stained using the peroxidase substrate kit DAB (Vector Laboratories). Finally slides were counterstained with hematoxylin, dehydrated, and mounted with permount.

**Quantitative RT-PCR for Detection of *Braf* in Allografts.** RNA was extracted from 3 samples for each treatment (empty vector control, T2-*Braf*; SB11) and was reverse transcribed according to previously published methods and subjected to RT-PCR on a StepOnePlus system (Applied Biosystems). PCR primers were forward 5' GGAGGACAGAAGTCGGATGA 3' and reverse 5' GTGTGGGTGCTGTCACATTC 3' (amplicon 179 bp).

**Automated Quantitative Analysis of BRAF expression on a Custom Tissue Microarray.** The Automated Quantitative Analysis (AQUA) was conducted on a prostate tissue microarray composed of 365 prostate cancer biopsies and 95 benign prostatic tissues with greater than 5 years of follow up data for all 210 patient cases using a protocol previously described [Rahrmann, E.P. 2009]. A BRAF antibody recognizing

the carboxy terminus was used (Santa Cruz Biotechnology) at 1:100. Low BRAF represents a normalized AQUA expression of 0-50 and high BRAF represents a normalized AQUA expression of 50 and above. Statistical significance for expression of BRAF in benign prostate tissue (95 samples) versus prostate cancer (365 samples) was examined by non-parametric T-test using the Mann-Whitney test. A Kaplan-Meier analysis was used to identify associations between BRAF protein expression and patient outcomes including death or biochemical recurrence for the prostate cancer samples.

## RESULTS

### Creating and validating the PSIL mouse model.

The transgenic mice contain a bicistronic transgene created by cloning the transposase (*SB10*) cDNA behind the adult rat prostate epithelial cell specific promoter *Probasin*, *ARR2PB*. Following confirmation of targeting, an internal ribosomal entry site (IRES) and a cDNA encoding luciferase were cloned downstream of the SB10 cDNA (Fig. 1A). Pro-nuclear injection of the transgene into embryonic stem cells generated nine founder mice, identified as SB(A) – SB(I). Founder mice were back-crossed to wild-type FVB/N mice, and F1 progeny were screened for germ-line transmission of the transgene by Southern blot analysis with a probe targeting the *AAR2PbSB10/IRESLuciferase* (PSIL) transgene and by genotyping with primers targeting SB10.

To confirm specificity of SB expression, a panel of tissues from the F1 offspring of each strain that contained the transgene by PCR analysis were harvested, processed, and evaluated by immunohistochemistry (IHC) with an antibody targeting SB10 (Fig. 1B). Of the nine strains of mice analyzed, only SB(E) demonstrated expression of the transposase by IHC. Moreover, SB expression was tightly regulated and only observed in the epithelial cells of the prostate and Purkinje cells in the cerebellum (Supplemental Fig. 1). In addition to IHC to confirm expression of the transgene, the luciferase expression of each mouse strain was also evaluated. Mice were injected with luciferin (substrate for luciferase enzyme) and imaged under the Xenogen Live imaging processor (Fig. 1C). Of the nine strains analyzed, only SB(D), which did not show SB expression by IHC, expressed luciferase in the correct anatomical position (Fig. 1C). Surprisingly, SB(E), which had robust expression of the transposase by IHC, did not express luciferase in the prostate. The differences in the SB expression and luciferase expression profiles can be reconciled by a few reasons. First, there may be fewer copies of the transgenes or it is expressed at very low level in the SB(D) mouse in which case IHC is not sensitive enough to detect transposase expression. As for luciferase expression, the IRES in the SB(E) may have been silenced preventing translation from the IRES. In light of these analyses, we chose to use SB(D) and SB(E) for further experiments.

**Altered epithelial cell fate in transposon mutagenized mice.**

To test our model for its ability to be used in prostate genetic screens, we chose to screen for new genes involved in prostate epithelial cell fate. SB(D) and SB(E) mice were bred to mice transgenic for the mutagenic transposon T2/Onc [Collier, L.S. 2005]. Briefly, T2/Onc contains DNA elements that can induce gain-of-function and loss-of-function mutations depending on which orientation the transposon inserted into the genome and where it inserted [Collier, L.S. 2005]. Mice that possess both transgenes (SB(D);T2/Onc or SB(E);T2/Onc) will mobilize T2/Onc specifically in the prostate epithelial cells. Single transgenic mice, mice that possess either the transposase or the transposon concatomer, served as controls. Mice were aged until 18 months at which point they were culled and their prostates harvested. We predicted that if T2/Onc inserted near/within a gene(s) and disrupted normal gene expression required to maintain adult prostate epithelial phenotypes we would be able to identify altered prostate phenotypes histologically.

Upon initial analysis of H&E stained prostate sections, we identified many mitotic figures in the transposon mutagenized mice prostates (data not shown). To confirm the findings, we specifically screened for proliferating epithelial cells in double and single transgenic mouse prostates by IHC using an antibody that targets proliferating cells, Ki67. The adult prostates of wild type mice are proliferatively quiescent and contain only a few Ki67 positive cells much like we observed in the single transgenic control prostates (SB(E) or T2/onc) (Fig. 2 A,D). In contrast, transposon mutagenized mice possessed many focal areas of Ki67 positive cells (Fig. 2B,C, E, F). When quantified, there was a significant increase in the number of proliferating cells in double transgenic mice versus single transgenic control mice (Fig. 2G).

Interestingly, the Ki67 staining patterns in transposon mutagenized mice resembled two distinct prostate epithelial phenotypes. The first Ki67 phenotype resembled a pubescent prostate, which contained many Ki67 positive cells within an organized prostate gland (Fig. 2B,E). The second Ki67 phenotype contained large, disorganized focal areas of Ki67 positive epithelial cells that resembled proliferative lesions found in the early stages of prostate disease (Fig. 2D/F). These unique phenotypes suggests that T2/Onc transposition may have mutated genetic pathways

involved in controlling the switch from a proliferating pubescent prostate to a growth quiescent adult prostate.

In addition to alterations in proliferation of prostate epithelial cells, transposon mutagenized prostates also had alterations in epithelial cell fate. Normal adult prostate glands are lined on the interior with columnar luminal secretory cells (Fig. 3A). In contrast, some prostate glands from transposon mutagenized mice contained goblet cell-like cells (Fig. 3B). Goblet cells are secretory glandular columnar epithelial cells normally found in the intestinal, urinary, and respiratory tracts. This epithelial cell alteration has been observed in other mouse models of prostate development; specifically over-expression of *H-RAS* under the *Probasin* promoter and in *p63*$^{-/-}$ prostates [Kurita, T. 2004; Scherl, A. 2004]. The presence of goblet cell-like cells in the prostates of transposon mutagenized mice suggests mutagenesis of genetic pathways involved in prostate epithelial cell differentiation.

**Identification of transposon insertion sites in prostatic hyperplasia.**

Histologically, we demonstrated that PSIL mice that mobilize the mutagenic transposon T2/Onc develop phenotypes that alter cell fate determination. To identify the gene(s) that have altered expression that gave rise to these phenotypes, DNA from 18 proliferating clusters of prostatic epithelial cells were isolated and one anterior lobe derived prostate tumor. The LM-PCR analysis identified 171 unique insertion events into the mouse genome from the 19 samples. The distribution of insertions appeared across most mouse chromosomes (Fig. 4B). Furthermore, the list of insertions was evaluated to identify common integration sites (CIS) by statistical analyses previously described [Starr,T.K. 2009; Keng,V.W. 2009]. The two genes at CIS in this experiment were *Braf* and *Nras* (Fig. 4C).

Insertions in *Braf* were observed in proliferative lesions from two independent mice. All the insertions occurred near/within exon 22 with the T2/Onc inserted in both orientations. The position of the T2/Onc suggests that *Braf* expression will be disrupted giving rise to an unregulated C-terminal kinase domain transcript. Immunohistochemistry in single or double transgenic mice with an antibody recognizing the C-terminus of *Braf*

showed that C-terminal *Braf* was over-expressed in the double transgenic mice (Supplemental fig. 2B). Insertions in *Nras* were observed in proliferative lesions from two independent mice. All insertions occurred within exon 2 in an orientation that predicts T2/Onc would drive over-expression of *Nras*. Sequencing of commonly mutated *Nras* codons 12, 13, 59, and 61 in the DNA of the proliferative lesions from the two independent mice did not identify any base pair changes that are commonly associated with *Nras* overexpression. Although both *BRAF* and *NRAS* genes are known to have a role in prostate development and have been implicated in prostate disease [Edwards, J. 2003; Jeong, JH 2008], we decided to focus our allograft experiment and TMA analyses on *BRAF* as less is known about *BRAF* in prostate cancer.

**Ectopic *Braf* expression altered epithelial cell fate.**

We developed a system in which candidate prostate cancer gene(s) are ectopically expressed via transposon mobilization in the UGS and grown under the kidney capsule of male nude mice for 8 weeks. This system was used to study the effect of ectopic expression of a C-terminal truncated form of *Braf* in the prostate. There was no significant difference in wet weight for the empty vector versus T2-*Braf*; SB11 allografts. However, quantitative RT-PCR showed a statistically significant increase in *Braf* transgene expression in T2-*Braf*; SB11 allografts when compared to empty vector control allografts (Supplemental fig. 2A). *In situ* PCR detection of *Braf* transgene expression in the allografts showed abundant Braf expression in the prostate epithelial cells (Fig. 5A). Immunohistochemistry with Ki67 showed increased proliferation of prostate epithelial cells (Fig, 5A). Few Ki67 positive cells were observed in the empty vector transfected allografts. Many of the proliferating cells were also positive for *Braf* transgene expression, as seen in the photomicrographs (Fig. 5A). However, there was no significant difference in TUNEL (apoptosis) or p21 (senescence) staining for the T2-Braf; SB11 versus empty vector allografts for (Fig. 5B). Also, no significant histologic changes were observed in the T2-Braf; SB11 allografts.

**BRAF is over-expressed in human prostate cancer.**

To extend our observations to a clinical data set, we performed AQUA analysis on a prostate cancer tissue microarray with extensive follow-up data. BRAF was significantly increased in prostate cancer tissue when compared to benign prostate tissue (Fig. 6A). However, there was no statistically significant difference in survival or recurrence for the low versus high BRAF expression data (Fig. 6B, 6C).

**DISCUSSION**

The PSIL mouse model is useful for identifying genes involved in different stages of prostate disease. We demonstrated that the PSIL mouse model can model a variety of prostate phenotypes including pubescent prostate development, a diseased state, and altered cell fate of prostate epithelium. In addition, we demonstrated that the PSIL model can identify genes involved in prostate pro-proliferative lesions. Because of the flexibility in the cargo that can be introduced into the transposon, the PSIL model is amenable for many uses including manipulation of known genetic pathways in mouse prostate epithelial cells by methods such as shRNA or cDNA delivery. The PSIL system will be a useful tool in unraveling and exploring the mechanisms that control the expression of genes involved in prostate development.

Additionally, candidate genes identified using the Sleeping Beauty screen were tested using the UGS-transfection approach described herein. Ectopic expression of C-terminal *Braf* by transposon mobilization in this system increased the number of Ki67-positive proliferating cells in the prostate epithelium, but did not alter the overall histology in the allografts. Although *BRAF* has been previously identified as a candidate prostate cancer gene, controversy still remains as to the mechanism that BRAF plays in prostate cancer. One such controversy is the prevalence of the $BRAF^{V600E}$ mutation in human prostate cancers. Only select cohorts of prostate cancer cases in the literature harbor the V600E mutation, such as was described for an Asian cohort with 10% prevalence (21 of 206 prostate adenocarcinomas) [Cho, N.Y. 2006]. However, others have screened different cohorts and did not find *V600E* mutations in cohorts of 93, 121, 79, 3, and 274, respectively [Liu, T. 2009; Burger, M. 2006; Kim, K.H. 2005]. In fact, Shen et al. screened a different Asian cohort and found no V600E mutations in 121 prostate adenocarcinomas [Shen, Y. 2010]. Jeong et al. used a doxycycline-inducible $BRAF^{V600E}$ activating mutation targeted to the prostate epithelium of mice on an Ink4a/Arf-/- background and found that the BRAF activating mutation was capable of initiating but not maintaining invasive prostate cancer [Jeong, JH 2008]. They also reported finding $BRAF^{V600E}$ mutations in 4 of 8 prostate adenocarcinoma samples studied.

However, to date, it is still unclear if the *BRAF* activating mutation is relevant for prostate cancer.

More recently, the potential role of *Braf* fusions in prostate cancer has emerged. Palanisamy et al. identified RAF-pathway rearrangement-positive prostate cancers (SLC45A3-BRAF and ESRP1-RAF), but they did not find activating mutations in these samples [Palanisamy, N. 2010]. The reported rearrangements are similar to an un-regulated active *Braf* kinase domain that was predicted from our insertional mutagenesis insertion site analysis. This un-regulated domain would lead to constitutive activation of Braf in the prostate epithelial cells.

Ectopic expression of a truncated form of *Braf* by transposon mobilization led to increased Ki67 positive epithelial cells in UGS allografts that correlated with increased Braf expression. However, no significant differences were found for apoptosis or senescence markers. Additionally, no significant histologic changes were found in the T2-*Braf*; SB11 allografts. Therefore, constitutive activation of *Braf* leads to increased proliferative potential of prostate epithelial cells, but additional genes may need to be altered to cause histologic changes associated with prostate disease. Finally, analysis of BRAF in a prostate cancer tissue microarray with detailed follow-up data showed that BRAF was over-expressed in prostate cancers as compared to benign prostatic tissues. More studies to further define the role of *BRAF* in human prostate cancer are needed, but there is likely a role for active BRAF signaling in human prostate epithelial proliferation and prostate disease.

**Figure 1. Characterization of the AAR2PbSB10/IRESLuciferase (PSIL) Transgenic Mouse.** A) Schematic of the PSIL transgene. B) Immunohistochemistry for SB10 expression in a prostate from a wild-type or PSIL SB(E) mouse. 40x magnification. C) Xenogen live imaging for luciferase expression after 1 minute of exposure. Luciferase expression was observed in 10 week old SB(D) but not SB(E) mice in the correct anatomical position (on the right) compared to wild-type littermate controls.

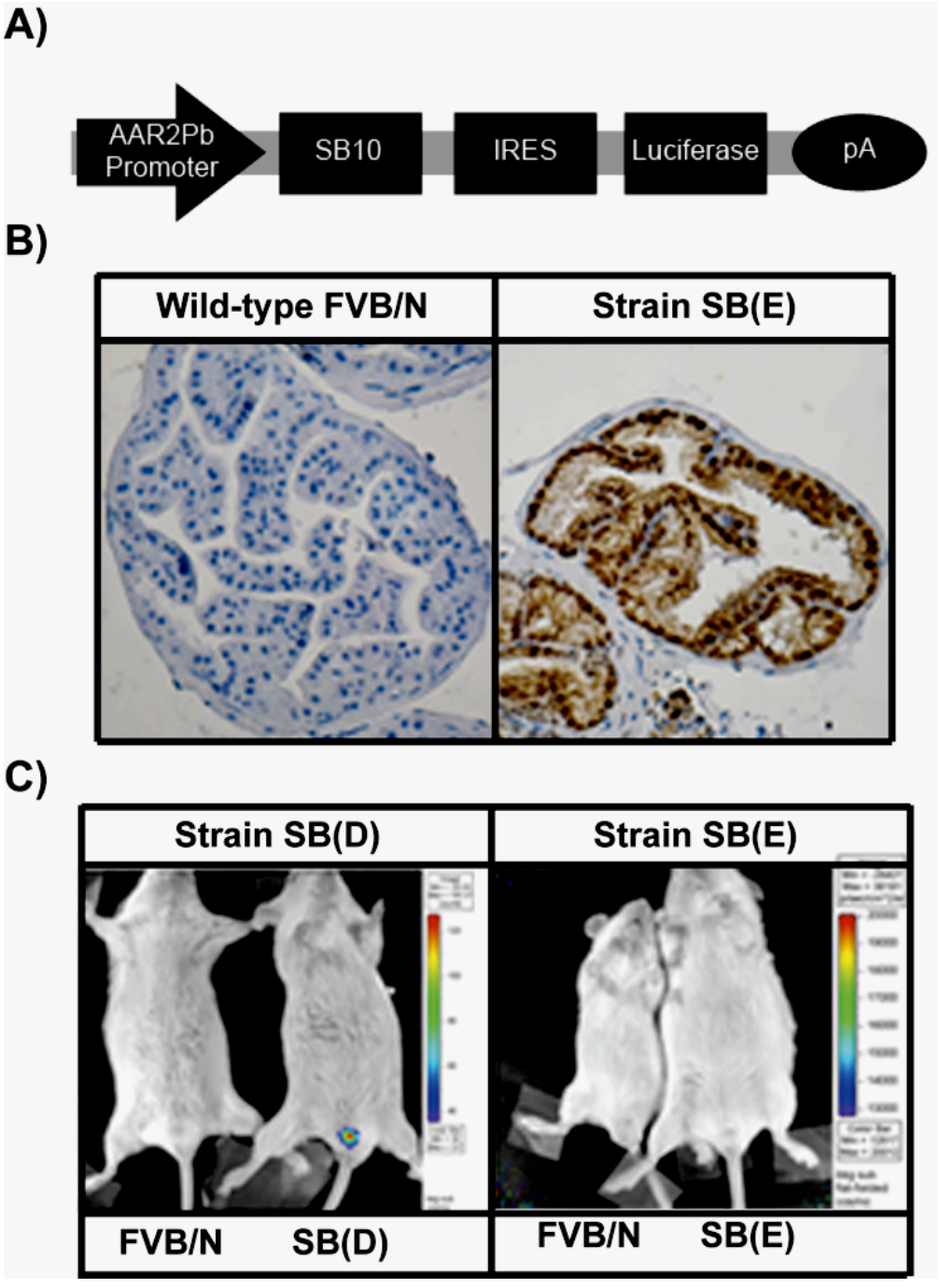
A)
AAR2Pb Promoter
SB10
IRES
Luciferase
pA
B)
Wild-type FVB/N
Strain SB(E)
C)
Strain SB(D)
Strain SB(E)
FVB/N SB(D)
FVB/N SB(E)

**Supplemental Figure 1. Immunohistochemistry for SB10 expression on tissues from strain SB(E).** Immunohistochemistry of various tissues from SB(E) mice. The tissues include prostate, cerebellum, heart, spleen, pancreas, kidney, liver, and lungs. Brown staining of nuclei represent SB expressing cells. Brown staining was observed only in the prostate epithelial cells and the Purkinje fibers of the cerebellum.

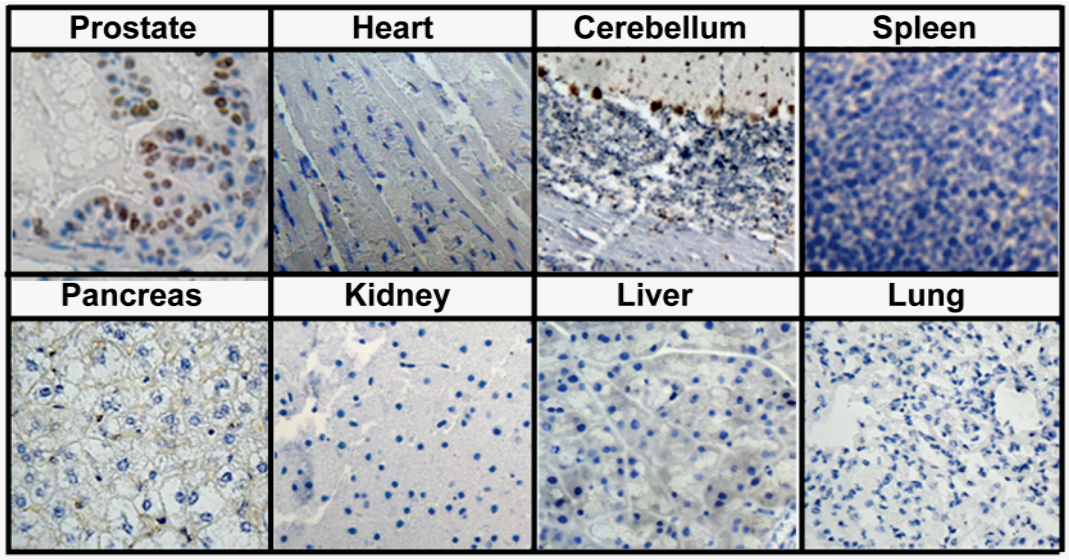
Prostate
Heart
Cerebellum
Spleen
Pancreas
Kidney
Liver
Lung

**Figure 2. Analysis of prostate phenotypes in transposon mutagenized mice.** Ki67 IHC of prostate sections from single transgenic control mice SB(D) and SB(E) (A, D) and double transgenic mice SB(D);T2/Onc and SB(E);T2/Onc (B,C,E,F). Some prostates have increased proliferation without loss of architecture resembling a developing prostate during puberty (B,E). Some prostates also develop disorganized proliferative lesions that resemble disease (C,F). Transposon mutagenized mice have a significant increase in Ki67 positive cells compared to single transgenic controls P=0.04 SB(E), P=0.01 SB(D) by student t-Test (G). Photographs were taken at 40X magnification.

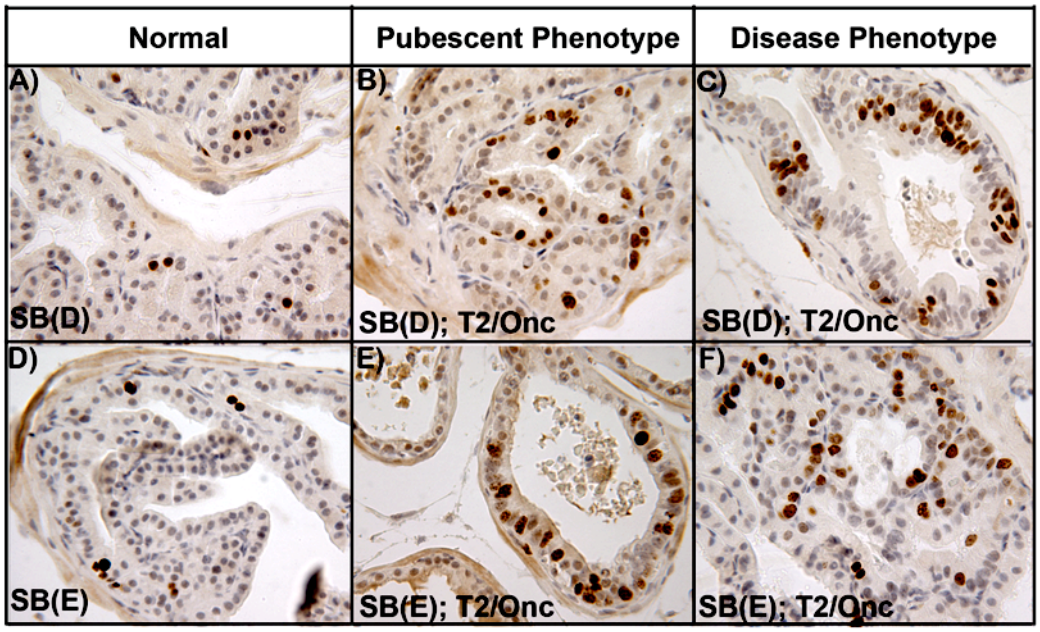
Normal
Pubescent Phenotype
Disease Phenotype
A)
SB(D)
B)
SB(D); T2/Onc
C)
SB(D); T2/Onc
D)
SB(E)
E)
SB(E); T2/Onc
F)
SB(E); T2/Onc

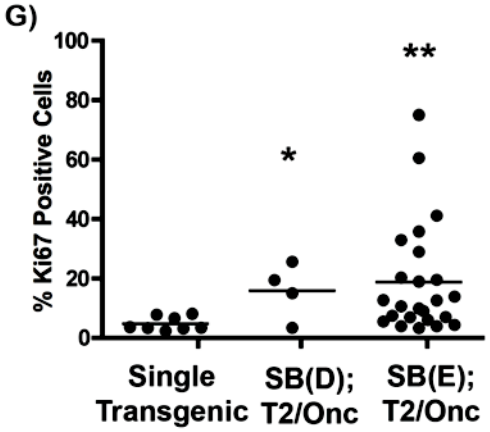
G)
% Ki67 Positive Cells
100
80
60
40
20
0
*
**
Single Transgenic
SB(D); T2/Onc
SB(E); T2/Onc

**Figure 3: Altered epithelial cell fate in transposon mutagenized mice.** H&E staining of prostates from control mice demonstrate normal architecture of luminal secretory cells in the prostate (A). Arrows represent normal columnar prostate epithelial cells. (B). Arrows represent goblet-like cells in the prostate glands of transposon mutagenized mice.

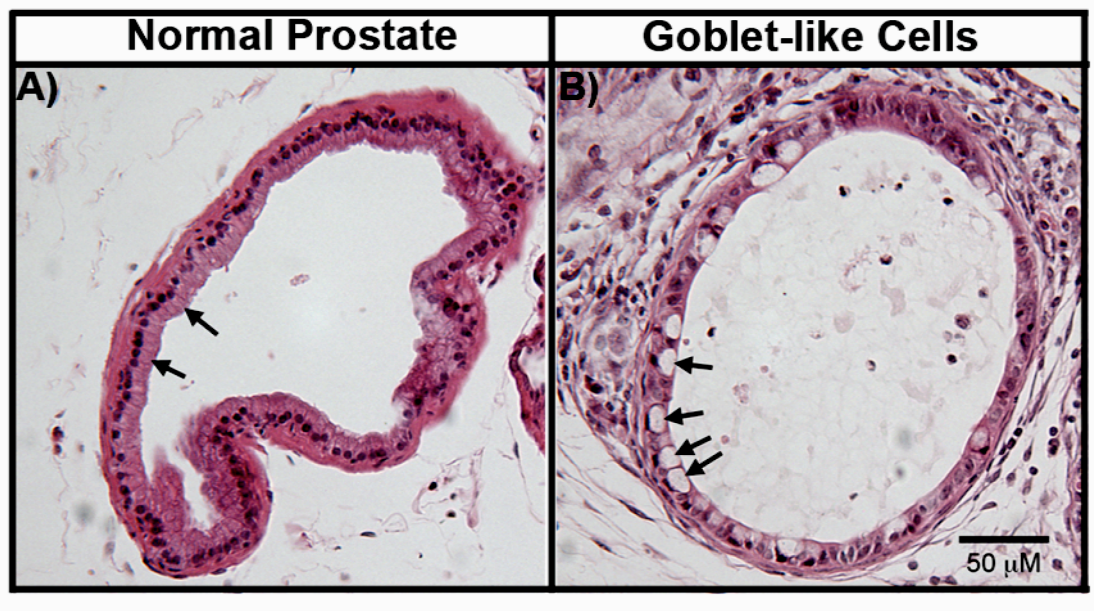
Normal Prostate
Goblet-like Cells
A)
B)
50 µM

**Figure 4: T2/onc insertion site analysis.** A) Agarose gel of LM-PCR products from proliferating epithelial cell clusters (1-5), a well characterized T2/onc derived sarcoma (+), and a no template control for (-). B) Histogram showing distribution of T2/Onc insertions in the mouse genome. C) Table of T2/Onc insertions into *Braf* and *Nras*

A)

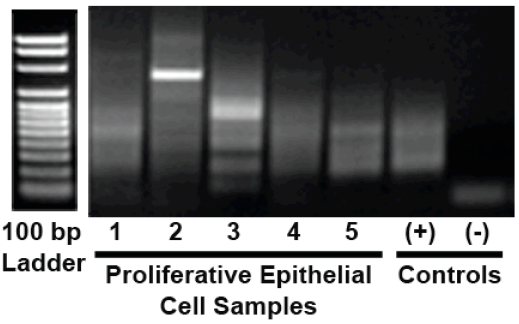


B)

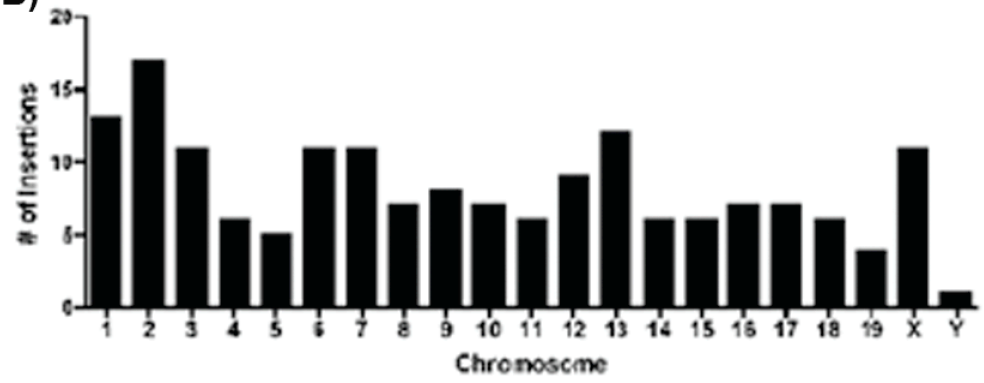


C)

**Common Insertion Sites**

| Gene | Chr. # Insertions | | Location | Predicted Effect |
|---|---|---|---|---|
| *Braf* | 6 | 5 | intronic | inactivate |
| *Nras* | 3 | 2 | intronic | c-term truncation |

**Supplemental Figure 2. *Braf* expression in allografts and in SB(E) and SB (E); T2/onc mice.** A) *Braf* transgene expression by qPCR in empty vector control versus T2-*Braf*; SB11 allografts. P=0.0008 by Student's T-test. B) Immunohistochemistry using an antibody recognizing the C-terminus of *Braf* in SB (E) and SB (E); T2/onc mice.

A)

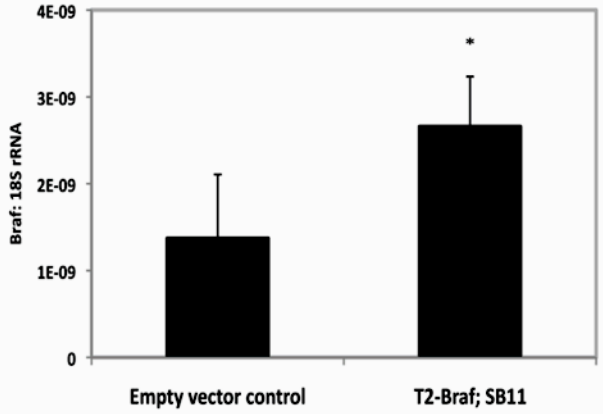
4E-09
3E-09
2E-09
1E-09
0
Braf: 18S rRNA
*
Empty vector control
T2-Braf; SB11

B)

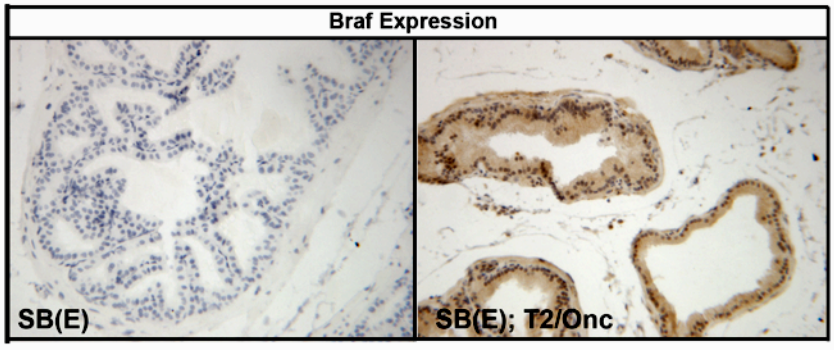
Braf Expression
SB(E)
SB(E); T2/Onc

**Figure 5. Ectopic expression of C-terminal *Braf* corresponds with increased Ki67 positive epithelial cells in UGS allografts.** A) *Braf* In situ PCR and Ki67 immunohistochemistry on adjacent sections from empty vector control or T2-*Braf*; SB11 allografts. 20x magnification. B) Labeling index for Ki67 (proliferation), TUNEL (apoptosis), and p21 (senescence) staining. T2-*Braf*; SB11 allografts have significantly increased Ki67 positive epithelial cells compared to empty vector control allografts. P=0.001 by ANOVA followed by Bonferroni's correction for multiple comparison. No significant differences were observed for TUNEL and p21 staining.

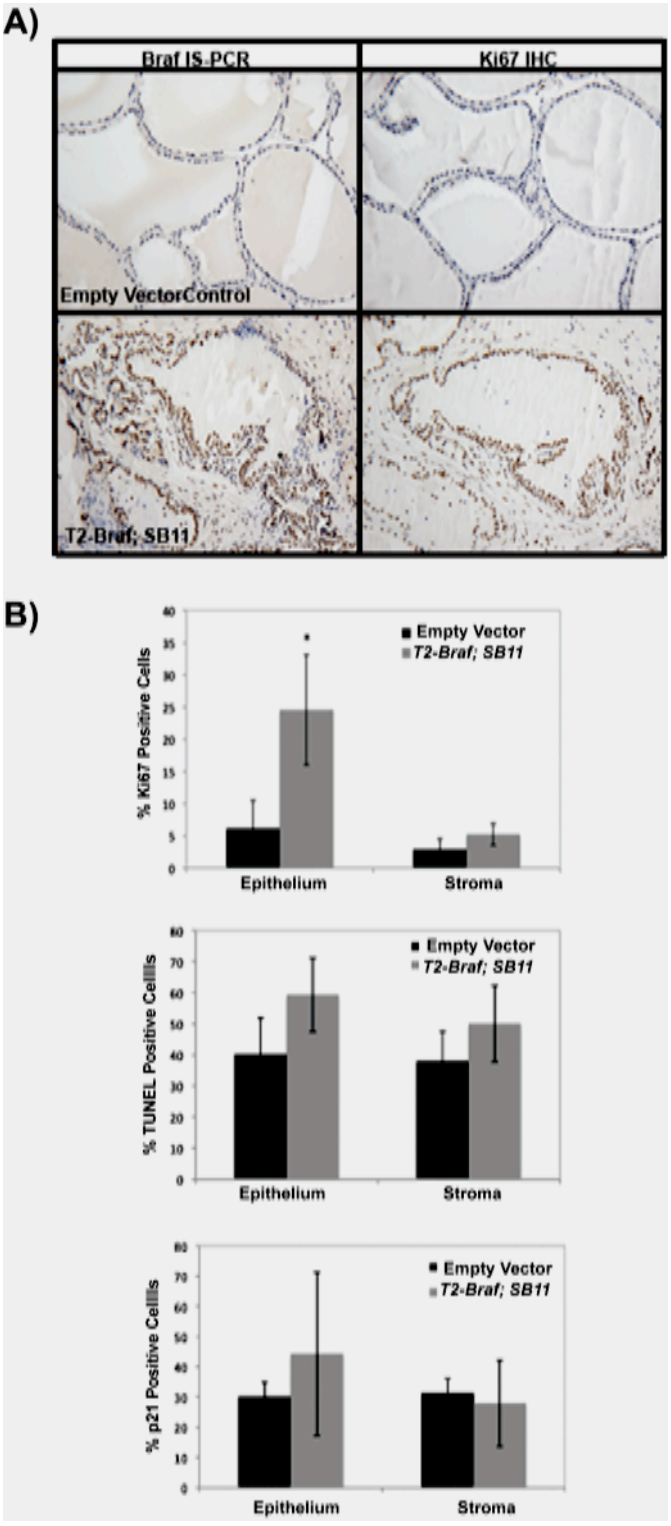
A)
Braf IS-PCR
Ki67 IHC
Empty VectorControl
T2-Braf; SB11
B)
% Ki67 Positive Cells
Empty Vector
T2-Braf; SB11
Epithelium
Stroma
% TUNEL Positive Cellls
Empty Vector
T2-Braf; SB11
Epithelium
Stroma
% p21 Positive Cellls
Empty Vector
T2-Braf; SB11
Epithelium
Stroma

**Figure 6. AQUA Analysis of BRAF in human prostate tissue microarrays.**
A) Normalized expression of BRAF (recognizing the C-terminus) in human benign versus prostate cancer samples from a tissue microarray. P= 0.0001 by non-parametric T-test using the Mann-Whitney test. B) Percent survival of low versus high BRAF expression by Kaplan-Meier analysis. Low BRAF expression represents a normalized value of 0-49.99 and high BRAF expression represents normalized values above 50. C) Percent recurrence-free survival by Kaplan-Meier analysis of low versus high BRAF expression.

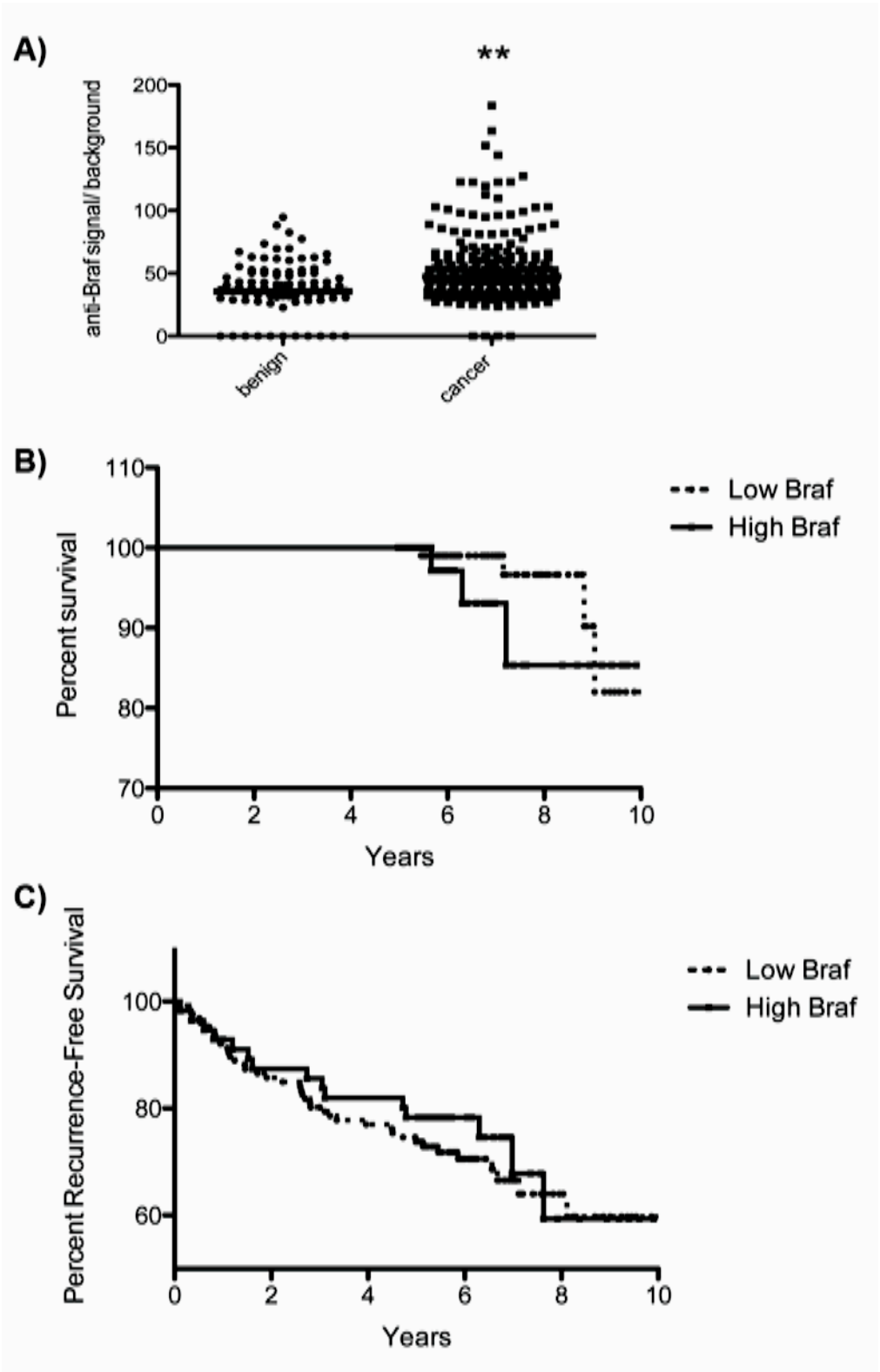
A)
**
anti-Braf signal/ background
200
150
100
50
0
benign
cancer
B)
Low Braf
High Braf
Percent survival
110
100
90
80
70
0
2
4
6
8
10
Years
C)
Low Braf
High Braf
Percent Recurrence-Free Survival
100
80
60
0
2
4
6
8
10
Years

# Chapter 4.

# *Trp53* loss of function cooperates with *EGFR* overexpression in Schwann cells to induce MPNST formation

Malignant peripheral nerve sheath tumors (MPNSTs) are genetically diverse, aggressive sarcomas in which current treatments for the disease are not adequate. Nearly 50% of human MPNSTs are associated with the loss of *Neurofibromin*, protein mutated in Neurofibromatosis Type 1 syndrome. The remaining incidences of MPNST are characterized as sporadic. Genetic analysis of human MPNSTs revealed that loss of TP53 function and/or overexpression of the epidermal growth factor receptor (*EGFR*) frequently occurs in MPNST formation. In this study, we developed a new sporadic model of MPNST formation using *Trp53* heterozygous mice that overexpress human *EGFR* in CNPase (3'-cyclic nucleotide 3'-phosphodiesterase) positive Schwann cells. *CNPase-hEGFR; Trp53*$^{+/-}$ mice developed Schwann cell tumors at a 64% penetrance. These mice predominately developed grade 1 neurofibromas of the dorsal root ganglion (~83%). The remaining tumors were predominantly grade 3 MPNSTs. Cell lines isolated from these tumors expressed Schwann cell markers and gave rise to tumors in immunecompromised mice. Genetic analysis of the cell lines by G-Banding and SKY demonstrated the cells were genetically unstable predominantly aneuploidy. In addition, the cell lines have a high frequency of loss of heterozygosity of the wild-type *Trp53* allele. Taken together, loss of Trp53 function cooperates with overexpression of *hEGFR* in CNPase positive Schwann cells to form MPNSTs in mice. Additionally, this system provides a new model for sporadic MPNST development that currently resembles the human disease.

## INTRODUCTION

Malignant peripheral nerve sheath tumors (MPNSTs) are aggressive, metastatic tumors originating from the Schwann cell lineage that comprise ~10% of diagnosed soft tissue sarcomas [Doorn,P.F. 1995; Ducatman,B.S. 1986; Zheng,H. 2008; Zou,C. 2009]. MPNSTs arise spontaneously or in association with Neurofibromatosis Type 1 Syndrome (NF1). Sporadic cases of MPNSTs have an incidence of 0.001% in the population while individuals with NF1 syndrome (1 in 3,500 people) have a ~10% lifetime risk of developing MPNSTs [Ducatman,B.S. 1986; Evans,D.G. 2002; McCaughan,J.A. 2007; Porter,D.E. 2009; Ferner,R.E. 2002]. MPNSTs are the most common malignancy in adults with NF1 and leading cause of NF1-related mortality. The primary treatment is surgical resection of the tumor, which is frequently not feasible due to the invasive nature and high incidence of metastasis of the tumors into surrounding tissues. Radiotherapy and chemotherapeutic treatments have proven to be ineffective for long-term treatment of MPNST, resulting in 5-year survival rates of only 20-50% [Ducatman,B.S. 1986; Zou,C. 2009; Ferner,R.E. 2002] . The severity and lack of adequate treatments for MPNSTs emphasizes the need for improved therapies and treatment.

Analysis of human MPNSTs has identified some of the common genetic drivers of this tumor type. One common event is the biallelic inactivation of the *NF1* gene, which encodes a small GTPase activating protein, Neurofibromin [Ballester,R. 1990; Xu,G.F. 1990; Kluwe,L. 1999; Kluwe,L. 1999; Rutkowski,J.L. 2000]. Loss of *NF1* can give rise to benign tumors called neurofibromas [Ballester,R. 1990; Xu,G.F. 1990; Kluwe,L. 1999; Kluwe,L. 1999; Rutkowski,J.L. 2000].. However, *NF1* loss alone likely is not sufficient for MPNST formation based on results from genetically engineered mouse models [Zhu, Y. 2002]. Instead, cooperating mutations such as inactivation of tumor suppressor genes in the TP53 pathway are frequently observed together with *NF1* gene mutations in human MPNSTs [Birindelli,S. 2001; Legius,E. 1994; Verdijk,R.M.]. Deletions and/or point mutations of *TP53* occur in ~75% of human MPNSTs [Holtkamp,N. 2007; Upadhyaya,M. 2008]. However, these mutations rarely inactive both alleles of *TP53* suggesting that loss of one allele is sufficient for MPNST formation

[Lothe,R.A. 2001]. Moreover, mouse models that have a deletion of one copy of the *Trp53* and *Nf1* locus in Cis on chromosome 11 (NPCis) rapidly develop sarcomas including MPNSTs [Cichowski, K. 1999; Vogel, K.S. 1999]. These data also show that cooperation between *Trp53* and *Nf1* loss can induce MPNST development. In addition to tumor suppressor gene losses in human MPNSTs, amplification of growth factor receptor genes commonly occurs.

*Epidermal Growth Factor Receptor* (*EGFR*) gene amplification occurs in human MPNSTs [Tawbi,H. 2008; Perry,A. 2002; Tabone-Eglinger,S. 2008]. Mouse models overexpressing human *EGFR* in Schwann cells show increased incidence of benign neurofibroma formation, but no MPNST formation [Ling,B.C. 2005]. However, experiments in which a mouse carrying a hypomorphic allele of EGFR was crossed onto the NPCis mouse lead to increased mouse survival [Ling,B.C. 2005]. Moreover, inhibition of EGFR kinase activity in cell culture based assays reduced migration of MPNST cells [Su,W. 2003]. These results suggest that EGFR at high levels can be involved MPNST progression but only in the context of other mutations. For example, a human cell line derived from an NF1 syndrome-associated MPNST was found to have both amplification of *EGFR* and deletion of exon 5-8 within the *TP53* gene [Hakozaki,M. 2009]. Moreover, in human esophageal cancers, *EGFR* overexpression and *TP53* mutations frequently co-occur [Esteve,A. 1993]. In addition, cell lines of human esophageal epithelia cells can be transformed with overexpression of *EGFR*, activation of *TERT*, and loss of *TP53* [Okawa,T. 2007]. We hypothesize that *EGFR* overexpression with loss of Trp53 function may cooperate to form MPNSTs.

Here, we describe a new mouse model of neurofibroma and MPNST formation. Mice that overexpress *EGFR* in CNPase expressing Schwann cells and were heterozygous for a *Trp53* loss of function allele developed Schwann cell tumors at a ~60% penetrance with median time of tumor harvest of 316 days (~10.5 months). Schwann cell tumors histologically resembled human grade 1 neurofibromas and grade 3 MPNSTs. Genetic analysis of tumor-derived cell lines demonstrated loss of the *Trp53* wildtype allele, and high incidence of aneuploidy characteristic of human MPNSTs [Wallace,M.R. 2000].

## MATERIALS & METHODS

**Generation of transgenic animals.** Generation of transgenic mice carrying the *3'-cyclic nucleotide 3'-phosphodiesterase* gene (*CNPase*) promoter driving the human *EGFR* cDNA (*CNPase-hEGFR)* has been previously described [Ling,B.C. 2005]. Transgenic mouse harboring a conditional *Trp53* allele possessing an R270H point mutation in exon 8 has been previously described [de Vries,A. 2002]. For our experiments, this was never bred to a Cre expressing mouse therefore the dominant negative allele was never expressed but used as a marker for the null allele essentially making every cell in the mouse heterozygous for *Trp53*. We refer to this allele as $Trp53^{+/-}$ to indicate it is not expressed due to the presence of a "floxed" stop cassette in intron 1 [de Vries,A. 2002]. Single transgenic mice were crossed to obtain double transgenic experimental mice possessing one allele of each transgene (as shown in Fig. 1A). All animal work was conducted under an institutionally approved animal welfare protocol.

**PCR genotyping.** Genotypes of transgenic mice were determined using a PCR based approach: Firstly, genomic DNA was isolated from tail clippings using standard proteinase K treatment, phenol-chloroform extraction and ethanol precipitation. Genomic DNA was resuspended in sterile TE {10mM tris-HCl (pH7.5), 1mM EDTA (pH 8)} and quantified using a Nanodrop spectrophotometer. PCR genotyping was performed using 100 ng of diluted genomic DNA as template in a 25 µl PCR reaction volume. PCR primers used for *CNPase-hEGFR* were forward 5'- TGACATCTCCTCCTCCCTTC'-3' and reverse 5'-TGCCCAACTGCGTGAGC-3' (amplicon 380 bp); $Trp53^{R270H}$ floxed allele were wild-type (WT) forward 5'- TTACACATCCAGCCTCTGTGG-3', WT reverse 5'- CTTGGAGACATAGCCACACTG -3' and flox forward 5'- AGCTAGCCACCATGGCTTGAGTAAGTCTGCA -3' (WT amplicon 170 bp and floxed allele amplicon 270 bp). PCR conditions for ReddyMix (Thermo Scientific) were used according to the manufacturer's instructions with an initial denaturing step of 95°C for 2 min; 30- to 35-cycles of denaturing at 95°C for 25 sec, annealing at 55°C for 35 sec and extension at 72°C for 65 sec; followed by a final extension at 72°C for 10 min. PCR

products were separated on a 1.5% agarose gel and genotype determined by the absence or presence of expected amplicons.

**Neurofibroma/MPNST analysis.** Neurofibromas and/or MPNSTs were carefully removed from the sacrificed animal under a dissecting microscope (Leica), washed and placed in cold phosphate buffered saline (PBS). These separated tumors were split into samples for DNA, RNA and protein extraction. Tissue samples for RNA were stored at -80°C in RNAlater (Sigma) to prevent RNase contamination and degradation. DNA extraction was done as previously described in the PCR genotyping section. Extraction of RNA was done using the Trizol reagent (Invitrogen) using protocols described by the manufacturer. Protein extraction was performed using standard isolation techniques. Histological sections were only taken for larger tumors (>2 mm in diameter). Formalin fixed-paraffin embedded sections from various tissues were sectioned at 5 microns using a standard microtome (Leica), mounted and heat-fixed onto glass slides. Tissue section slides were either processed and stained with hematoxylin-eosin (HE) using standard protocols, or used for immunohistochemistry (IHC) as described in the next section.

**Immunohistochemistry (IHC).** Tissues were fixed in 10% buffered formalin and embedded in paraffin blocks. Sections were cut at 5-μm thickness, and rehydrated through a series of graded ethanols. Slides underwent antigen retrieval by boiling for 30 minutes in antigen unmasking solution (Vector Laboratories). Endogenous peroxidases were quenched with 3% hydrogen peroxide solution for 10 minutes. For antibody staining, a M.O.M. kit (Vector Laboratories) was used for blocking and antibody incubations. Primary antibodies used were mouse anti-Ki67 (1:100; Novocastra), rabbit anti-S100 (1:100; Santa Cruz Biotechnology), rabbit anti-EGFR (1:100; Cell Signaling Technology), rabbit anti-phospho-EGFR (1:400; Cell Signaling Technology), mouse anti-p53 (1:100; Cell Signaling Technology), mouse anti-p21 (1:100; BD Pharmigen), rabbit anti-phospho-Erk (1:100; Cell Signaling Technology), rabbit anti-phospho-Akt (1:100; Cell Signaling Technology). Following a series of washes, slides were incubated with the corresponding anti-mouse biotinylated secondary antibody (1:10,000; Vector

Laboratories) or anti-rabbit biotinylated secondary antibody (1:10,000; Vector Laboratories). Slides were washed, incubated with the vectastain ABC kit (Vector Laboratories) for 30 minutes at room temperature, washed again, and stained using peroxidase substrate kit DAB (Vector Laboratories). Slides were counterstained with hematoxylin, dehydrated, cleared with citrosolv and mounted with permount (Fisher).

**Generation of MPNST cell lines**. MPNSTs were carefully dissected using aseptic techniques. The tumor was sliced into small pieces, placed into 1xDMEM containing (2 ug/ml) of Collagenase A. This solution was incubated at 37ºC in 5% $CO_2$ for 3 hours to allow dissociation of cells from the bulk tumor. Prior to plating, the solution was triterated and placed through a 33um filter. Cells were plated on 10cm dishes containing complete media (1xDMEM, 10% fetal bovine serum, 1x penicillin/streptomycin) and grown at 37ºC in 5% $CO_2$. These cell strains were transduced with a lentivirus containing a eGFP and luciferase reporter transgene. Successfully transduced cells as assessed by eGFP expression were cell sorted using a FACSAria. The top 5% of cells expressing eGFP were collected into 96-well plates as well as cells that were negative for eGFP. eGFP negative clones that grew from the cell sort were assessed by immunoflourescense with mouse anti-S-100 (1:100; Santa Cruz Biotechnology), rabbit anti-human EGFR (1:100; Cell Signaling Technology), rabbit anti-Olig2 (1:100; Abcam) to demonstrate Schwann cell origin and they express human EGFR.

**Quantitative RT-PCR.** RNA was isolated from cell lines using Tripure protocol (Roche). Isolated RNA underwent a TURBODNAse treatment (Ambion) to remove residual genomic DNA. 1ug of purified RNA was used in a reverse transcription reaction with Transcriptor first strand synthesis kit (Roche) following manufacturers protocol. The QRT-PCR reaction was performed on the eppendorf realplex$^2$ machine. It was a 20ul reaction consisting of 1xRoche Sybr Dye, 200nM of sense and anti-sense primers, 1ul of cDNA. Primers for the quantitative PCR: *Nf1* sense CCTTTGTCCATGGTGAAACTGA-3', antisense 5'CATGTGTGACTGAGGAACCAG T-3'; *Trp53* sense 5'-GGGAGGAGAGTACGTGCACATAA-3' antisense 5'-

CCCCTGTCATCTTTTGTCCCTT-3'; *hEGFR* sense 5'-ATGCCCG-CATTAGCTCTTAG-3' antisense 5'-GCAACTTCCCAAAATGTGCC-3'; *Gapdh* sense 5'-GTGTTCCTACCCCCAATGTGT-3' antisense 5'-GAGACAACCTGGTCCTCAGTGT-3'. PCR conditions for Roche Sybr Dye (Roche) were used according to the manufacturer's instructions with an initial denaturing step of 95°C for 15 min; 40-cycles of denaturing at 95°C for 15 sec, annealing at 55°C for 30 sec and extension at 72°C for 30 sec; followed by a final denaturation at 95°C for 15 sec then into a melting curve that went from 55°C for 15 sec to 95°C for 15 sec over the course of 20 min.

***Trp53* LOH Analysis.** The analysis was performed as previously described [Olive,K.P. 2004]. Briefly, genomic DNA isolated from tumor cell lines underwent PCR amplification for exon 8 of *Trp53*. Purified PCR products underwent a restriction enzyme digest with *Msl*1. The $Trp53^{R270H}$ allele possesses an *Msl*1 recognition sequence in exon 8 not observed in the wild-type allele. When separated on a 2% agarose gel containing $6x10^{-2}$ug/ml ethidium bromide, the two products represent the digested $Trp53^{R270H}$ allele.

**Cytogenetic analysis**. Spectral karyotyping analysis (SKY) was performed by the University of Minnesota Cytogenetics core. SKY was performed on cell lines derived from *CNPase-hEGFR;*$Trp53^{+/-}$ mouse tumor. Cells were treated for 3.25 hours with colcemid then harvested according to standard cytogenetic protocols. 11 metaphases were analyzed by G-banding. An additional eight metaphase cells were examined by multicolor FISH with Spectral Karyotyping. The G-band and FISH results were integrated for final karyotype interpretation.

**MPNST Allografts/Xenografts.** Cultured cells were trypsinzed, resuspended at $1x10^6$ in 1xPBS, and injected subcutaneously into SCID/BIEGE mice. After 1 month of growth, tumors were harvested, wet weights taken, and then fixed in 10% buffered formalin for histological analysis.

## RESULTS

### *CNPase-hEGFR; Trp53*$^{+/-}$ mice have increased neurofibroma and MPNST development.

*CNPase-hEGFR; Trp53*$^{+/-}$ mice were generated by breeding single transgenic mice together (Fig. 1A). These double transgenic mice developed tumors at many sites throughout the peripheral nervous system including the paraspinal dorsal root ganglion, trigeminal nerves, dermal nerves, and brachial plexus (Fig. 1B). The most frequently targeted site of tumor formation (~84% of tumors) was the dorsal root ganglion (Fig. 1C).

Histological analysis of tumors revealed that tumors of the dorsal root ganglion were predominantly grade 1 neurofibromas while tumors found in the periphery were grade 3 peripheral nerve sheath tumors (Fig. 2A). Using these criteria, we determined *CNPase-hEGFR; Trp53*$^{+/-}$ mice had a ~64% penetrance for all grades of Schwann cell tumors (Fig. 2B). Further analysis of the data demonstrated that ~31% of mice that developed tumors developed only neurofibromas, ~19% developed only MPNSTs, and the remaining ~14% developed both tumor types (Fig. 2B). Only 1 grade 2 Schwannoma was observed in the mouse cohort.

Comparing tumors incidence in the *CNPase-hEGFR; Trp53*$^{+/-}$ double transgenic mice to single transgenic controls, we observed that ~17% of *CNPase-hEGFR* mice developed neurofibromas with no MPNST formation, which has been previously reported [Ling,B.C. 2005]. Interestingly, the number of mice that developed grade 1 neurofibromas increased in the double transgenic mice, but the average number of neurofibromas observed per mouse (3.4±2.4) was not altered significantly compared to *CNPase-hEGFR* expressing mice only (5.1±2.1) (Table 1). In addition, the median time of neurofibroma only harvest was slightly decreased from 359 days to 328 days (Table 1).

*Trp53*$^{+/-}$ mice are functionally heterozygous for *Trp53* and demonstrated an ~8% incidence of Schwann cell tumor formation (~4% neurofibroma, ~4% MPNSTs). *Trp53*$^{+/-}$ mice produced far fewer tumors, but the average number of tumors per mouse (1.0 for both neurofibromas and MPNSTs) was comparable to the average number per

mouse observed in *CNPase-hEGFR; Trp53*$^{+/-}$ mice (3.4±2.4 neurofibromas and 1.0 MPNSTs). However, the median time of MPNST harvest was greatly decreased from 457 days to 284 days (Table 1). Taken together, these data suggest that *EGFR* overexpression and reduced *Trp53* expression cooperate for increased incidence and reduced latency of MPNST formation.

***CNPase-hEGFR; Trp53*$^{+/-}$ MPNSTs undergo divergent differentiation.**

In addition to the variety of tumor grades observed in the *CNPase-hEGFR; Trp53*$^{+/-}$ derived tumors, MPNSTs in this model were found to have divergent differentiation. The common histological appearance of human MPNSTs is the presence of spindle shaped cells with buckled or wavy nuclei within a tumor as observed in *CNPase-hEGFR; Trp53*$^{+/-}$ derived MPNSTs (Fig. 3A) [Magro,G.]. However, human MPNSTs can undergo divergent differentiation to other cell types within a tumor. These examples include epithelioid-like cell differentiation, a rare occurrence in human MPNSTs, (Fig. 3B), matrix producing cells (Fig. 3C), and wreath-like giant cells which occurs in ~5% of human MPNSTs (Fig. 3D) [Magro,G.; Pytel,P. 2005]. Divergent differentiation is thought to be a secondary event due to changes in the microenvironment from the primary tumor. These data suggest that *CNPase-hEGFR; Trp53*$^{+/-}$ derived tumors not only histologically resemble human MPNSTs, but also undergo histological alterations in tumor microenvironment similar to human MPNST development.

***CNPase-hEGFR; Trp53*$^{+/-}$ tumors activate signaling cascades.**

We performed immunohistochemistry for downstream markers of EGFR signaling (phosphorylation of Erk and Akt) as well as for loss of Trp53 function (p21 expression) to determine if *CNPase-hEGFR; Trp53*$^{+/-}$ derived tumors may be relying on these pathways (Figure 4). Overall, neurofibromas and MPNSTs express the human EGFR and the EGFR is phosphorylated suggesting the downstream signaling cascade is activated (Figure 4). IHC staining for phospho-Erk demonstrated that both neurofibromas and MPNSTs express phospho-Erk to varying degrees with more cells expressing phospho-Erk in the MPNSTs (Figure 4). IHC for phospho-Akt demonstrates that the pathway was

not activated in the neurofibromas, while there was variable expression in MPNSTs (Figure 4). IHC for Trp53 protein demonstrated that neurofibromas express Trp53 uniformly, while MPNST samples have variegated expression indicating some loss of heterozygosity may occur during tumor progression (Figure 4). To show that loss of Trp53 was altering downstream signaling, we performed IHC for p21 the downstream target of Trp53. When Trp53 is activated, p21 expression is upregulated and cell cycle arrest occurs [Agarwal,M.L. 1998; Levine,A.J. 1997]. Neurofibromas expressed little to no p21 while MPNSTs had a more robust p21 expression (Figure 4). Taken together, these data suggest that downstream signaling events of EGFR (phosphorylation of Erk and Akt) may activate Trp53 in some cells resulting in increased p21 expression. This situation may cause selective pressure for the loss of the wildtype *Trp53* allele in some cells of the MPNST.

**Characterization of *CNPase-hEGFR; Trp53*$^{+/-}$ MPNST derived cell lines.**

In order to further characterize the changes that are happening in cells that gave rise to the MPNSTs, single cell clones were isolated and expanded to create tumor-derived cell lines as described in the methods section. Each cell clone was analyzed by immunofluorescense for expression of Schwann cell markers S-100 and Olig2 to verify the cells of origin were Schwann cells (Fig. 5A). In addition, cells were analyzed for expression of hEGFR by immunofluorescense demonstrating that the cells still expressed hEGFR (Fig. 5A). Tumorigenicity of cell lines was evaluated by tumor formation abilities in SCID/BEIGE mice. All of the Schwann cell marker expressing cell lines formed tumors within ~3 weeks of subcutaneous injections as determined by the Xenogen Live Imaging system (Fig. 5B). Further characterization of the cell lines by QRT-PCR analysis for human *EGFR*, *Trp53,*and *Nf1* transcript levels indicated that the cells expressed human *EGFR* to varying degrees, generally have reduced *Trp53* expression, and *Nf1* transcript levels were not significantly altered compared to normal mouse Schwann cells (Fig. 5C). Together these data suggest that the cell lines reflect the phenotype of the primary tumors and provide a good model of sporadic MPNSTs.

***CNPase-hEGFR; Trp53$^{+/-}$* MPNST derived cell lines undergo L.O.H. for Trp53.**

As mentioned earlier, *TP53* is often deleted and mutated in human MPNST formation [Holtkamp,N. 2007; Upadhyaya,M. 2008]. However, biallelic loss of *TP53* is rare [Lothe,R.A. 2001]. In order to estimate the frequency of loss of heterozygosity (LOH) of *Trp53*, we utilized the *Msl*1 recognition site introduced into exon 8 of the *Trp53$^{R270H}$* allele but not present in the wild-type allele (Fig. 5D) [Olive,K.P. 2004]. This conditionally expressed allele was left unexposed to Cre in our experiments making each cell functionally heterozygous for *Trp53*. In this experiment, 80% of the tumor-derived cell lines underwent LOH for the wild-type *Trp53* allele within the first 3 passages after single cell sorting (Fig. 5D). Similar findings were previously reported by Vogel et al. and Cichowski et al. in which MPNST-derived cell lines from the NPCis mouse model underwent LOH for the wild-type *Trp53* allele [Cichowski, K. 1999; Vogel, K.S. 1999]. Overall, this suggests there is a selective pressure for the loss of the wild type *Trp53* allele in vivo and/or in cell culture.

***CNPase-hEGFR; Trp53$^{+/-}$* MPNST derived cell lines have chromosomal instability**

Human MPNSTs have highly variable chromosomal gains, losses, and rearrangements from patient-to-patient [Wallace,M.R. 2000]. Commonly, alterations include hypoploidy and near triploidy of karyotypes with gains observed specifically on chromosome 7, 8q, 15q and losses on chromosomal regions 1p, 9p, 11, 12p, 14q, 17q, 18, 22q, X, and Y [Forus,A. 1995; Lothe,R.A. 1996; Mechtersheimer,G. 1999; Mertens,F. 1995; Schmidt,H. 2001; Schmidt,H. 2000; Schmidt,H. 1999]. To identify specific chromosomal alterations, 5 tumor-derived cell lines from one MPNST were subjected to spectral karyotyping analysis. Results from this analysis demonstrated that clones from the same tumor were variable in the number of chromosomal changes (Supplemental Figure 1). Overall, the cell lines exhibited high levels of hyperploidy (Table 2). However, there was no specific entire chromosome amplification shared by all five lines. Interestingly, all five cell lines possessed translocations on chromosomes 16 and 19 and a small deletion on chromosome 13 (Table 2). These events may reflect the common mutations that cooperated with EGFR overexpression and reduced Trp53 expression that

gave rise MPNST formation, after which variable amounts of hyperploidy occurred in vivo and/or in cell culture.

## DISCUSSION

Mouse models of human cancers are important in understanding the underlying genetic alterations that give rise to cancer. They also provide important models for drug testing. There are few mouse models of MPNST formation. Current models reflect the development of this disease in a genetic subset of human patients, with NF1 syndrome. In this work, we have developed a model of sporadic MPNST and demonstrated cooperation between *EGFR* overexpression and loss of *Trp53*.

We demonstrated that EGFR overexpression and reduced Trp53 expression cooperate to give rise to Schwann cell tumors. *CNPase-hEGFR; Trp53*$^{+/-}$ double transgenic mice developed tumors at ~64% incidence and with an overall median time of tumor formation of ~309 days. Compared to single transgenic control mice, tumor formation was significantly increased and latency decreased. Moreover, these tumors histologically resemble human neurofibromas and MPNSTs. Genetically, tumor-derived cell lines undergo massive hyperploidy which is commonly found in human MPNSTs. Together, our data suggests that EGFR overexpression and reduced TP53 function strongly cooperate in Schwann cell tumor formation. However, these mutations were not sufficient to produce 100% penetrance of neurofibroma or MPNST development. This suggests that additional events are needed, such as loss of *Nf1* expression or alterations in other genes. Further genetic characterization of the MPNST-derived cell lines may provide insight into translocations, amplification, or deletions that are common among all the MPSNT cell lines and point to additional genetic alterations required for MPNST development in the context of *EGFR* overexpression and Trp53 loss of function.

Amplification of *EGFR* and mutations/deletions of the *TP53* locus are common events in human MPNST development [Holtkamp,N. 2007; Upadhyaya,M. 2008; Tawbi,H. 2008; Perry,A. 2002; Tabone-Eglinger,S. 2008]. However, there has not been a large-scale study correlating the expression of both of these events. Tabone-Eglinger et al., performed a large scale analysis of EGFR expression by immunohistochemistry on 52 MPNST samples (NF1 syndrome associated and sporadic) and found 86% of the samples to overexpress EGFR [Tabone-Eglinger,S. 2008]. From the 52 samples, they could only

assess 4 for co-expression of TP53 and found half of the samples overexpressing EGFR to be associated with loss of TP53 expression [Tabone-Eglinger,S. 2008]. Even with this low number of samples, their data as well as our functional data suggest that EGFR overexpression and reduced TP53 expression may co-occur frequently in human MPNST formation, where they strongly cooperate.

The reasons for this strong cooperation are unclear. It seems possible that EGFR activation by overexpression activates p53 limiting cell proliferation, perhaps by up-regulating p21. This provides strong selective pressure for loss of p53 function. Indeed, p53 loss and EGFR activation co-occur in other cell types such as in human esophageal cancer where there is a correlation between *EGFR* overexpression and p53 loss of function [Esteve,A. 1993; Itakura,Y. 1994; Parenti,A.R. 1995]. One example is in immortalized human esophageal epithelial cells. Okawa et al, demonstrated that overexpression of *EGFR*, activation of TERT, and reduction in *TP53* expression were capable of transforming esophageal epithelial cells [Okawa,T. 2007]. Ohashi et al., demonstrated that overexpression of *EGFR* in immortalized esophageal epithelial cells induced expression of cell cycle kinase inhibitors $p15^{INK4B}$, $p16^{INK4A}$, and *p21* [Ohashi,S.]. This senescent state was alleviated partially by introducing a mutant *TP53* leading to increased transformation of the immortalized esophageal cells. These studies suggest *EGFR* overexpression and loss of TP53 function may be a more common occurrence in human cancers than previously appreciated.

## SUMMARY

In summary, we have determined that *EGFR* overexpression and reduced *Trp53* expression cooperate potently for benign and malignant Schwann cell tumor development in mice. These new models provide important insight into the role of EGFR and TP53 function in development of aggressive MPNSTs. Currently, a clinical trial is ongoing for the use of Erlotinib, an EGFR inhibitor, for treatments of patients with MPNSTs (Erlotinib in Treating Patients With Unresectable or Metastatic Malignant Peripheral Nerve Sheath Tumor, NCT00068367). However, the initial results showed Erlotinib to be ineffective in the patient group assessed, but the status of *EGFR* expression was not assessed. Further studies using our models of sporadic MPNST development for evaluating EGFR inhibitors in combination with a small molecule that activates Trp53 to maintain expression in cells are warranted and may provide insight into the treatment of patients with cancers possessing these known mutations.

**Figure 1. Loss of Trp53 function and *EGFR* overexpression cooperate to form tumors.** (A) Breeding scheme to generate experimental animals. In addition to transgenes listed, mice also possessed transgenes for SB insertional mutagenesis. However, transposition did not occur in cohorts listed above (data not shown). (B) Necropsy images depict the many nerves targeted for tumor development. Arrows indicate the tumors location. (C) Graph illustrates the percentage of total tumors from each genotype that were targeted to each nerve.

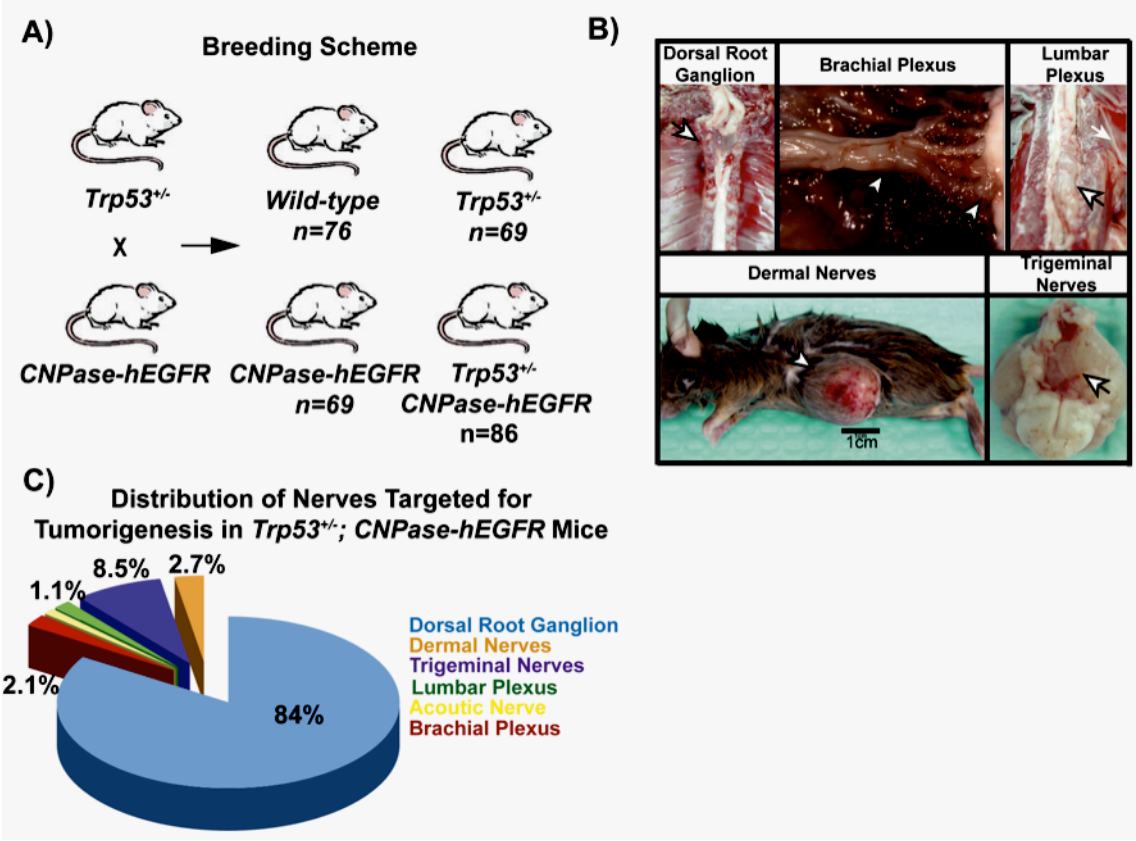
A)
Breeding Scheme
Trp53+/-
X
Wild-type
n=76
Trp53+/-
n=69
CNPase-hEGFR
CNPase-hEGFR
n=69
Trp53+/-
CNPase-hEGFR
n=86
B)
Dorsal Root Ganglion
Brachial Plexus
Lumbar Plexus
Dermal Nerves
Trigeminal Nerves
1cm
C)
Distribution of Nerves Targeted for Tumorigenesis in Trp53+/-; CNPase-hEGFR Mice
8.5%
2.7%
1.1%
2.1%
84%
Dorsal Root Ganglion
Dermal Nerves
Trigeminal Nerves
Lumbar Plexus
Acoutic Nerve
Brachial Plexus

**Figure 2. Nervous tissue tumors histologically resemble human neurofibromas and MPNSTs.** (A) Mice developed a variety of different tumor grades based on hematoxylin & Eosin staining (on left) and immunohistochemistry staining for Ki67 (proliferation marker) and S100 (Schwann cell marker) (B) Bar graph depicts the percent of mice that developed neurofibromas, MPNSTs, or both based on histological results.

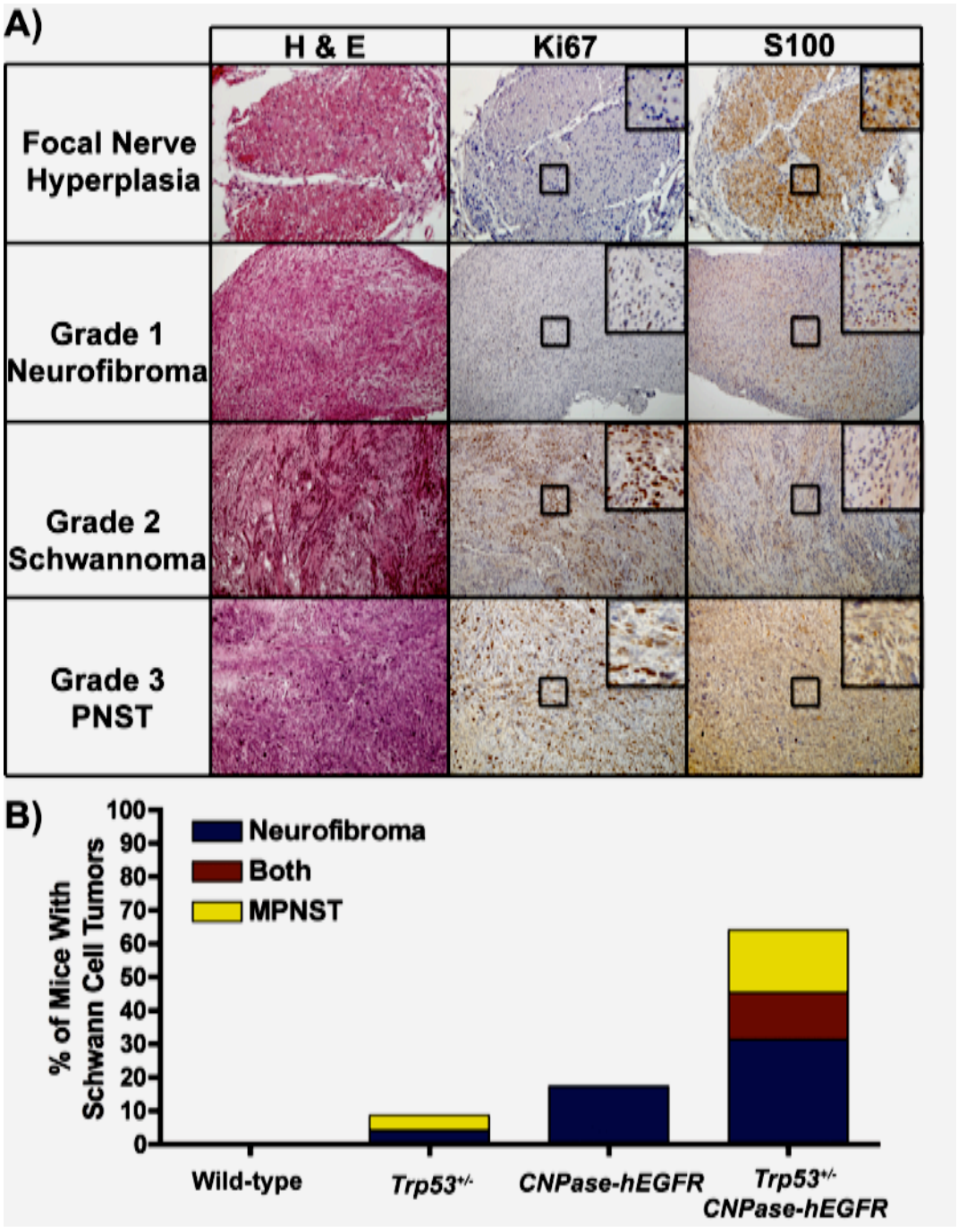
A)
H & E
Ki67
S100
Focal Nerve Hyperplasia
Grade 1 Neurofibroma
Grade 2 Schwannoma
Grade 3 PNST
B)
% of Mice With Schwann Cell Tumors
100
90
80
70
60
50
40
30
20
10
0
Neurofibroma
Both
MPNST
Wild-type
Trp53+/-
CNPase-hEGFR
Trp53+/- CNPase-hEGFR

**Table 1. Tumor number and harvest time.** This table indicates the number of mice with tumors, the average and standard deviation of tumors per mouse, and the median time of harvest for tumors from each mouse. This information is given for each genotype (far left column) and for each tumor type observed (3 main columns). Numbers in parentheses in the # mice with tumors column indicate total number of mice in each cohort while the other number represents the number of mice that developed tumors.

| | Neurofibroma Only | | | MPNST Only | | | Both | | |
|---|---|---|---|---|---|---|---|---|---|
| Genotype | # Mice with Tumors | # Tumors/ Mouse | Median Harvest Time (Days) | # Mice with Tumors | # Tumors/ Mouse | Median Harvest Time (Days) | # Mice with Tumors | # Tumors/ Mouse | Median Harvest Time (Days) |
| Control | 0 | 0 | N/A | 0 | 0 | N/A | 0 | 0 | N/A |
| *Trp53+/-* | 3 (69) | 1±0 | 310 | 3 (69) | 1±0 | 457 | 0 | 0 | 449 |
| *CNPase-hEGFR* | 12 (69) | 5.1±2.1 | 359 | 0 | 0 | N/A | 0 | 0 | 359 |
| *Trp53+/-; CNPase-hEGFR* | 27 (86) | 3.4±2.4 | 328 | 16 (86) | 1±0 | 284 | 12 (86) | 6.67±5.1 | 316 |

**Figure 3. MPNSTs demonstrate divergent differentiation.** (A) H&E stained section of the common spindle shaped, wavy nuclei morphology observed in human MPNSTs. (B) Arrows indicate epithelioid differentiated cells. (C) Arrows indicate matrix-producing cells. (D) Arrows indicate presence of wreath-like giant cells within MPNSTs.

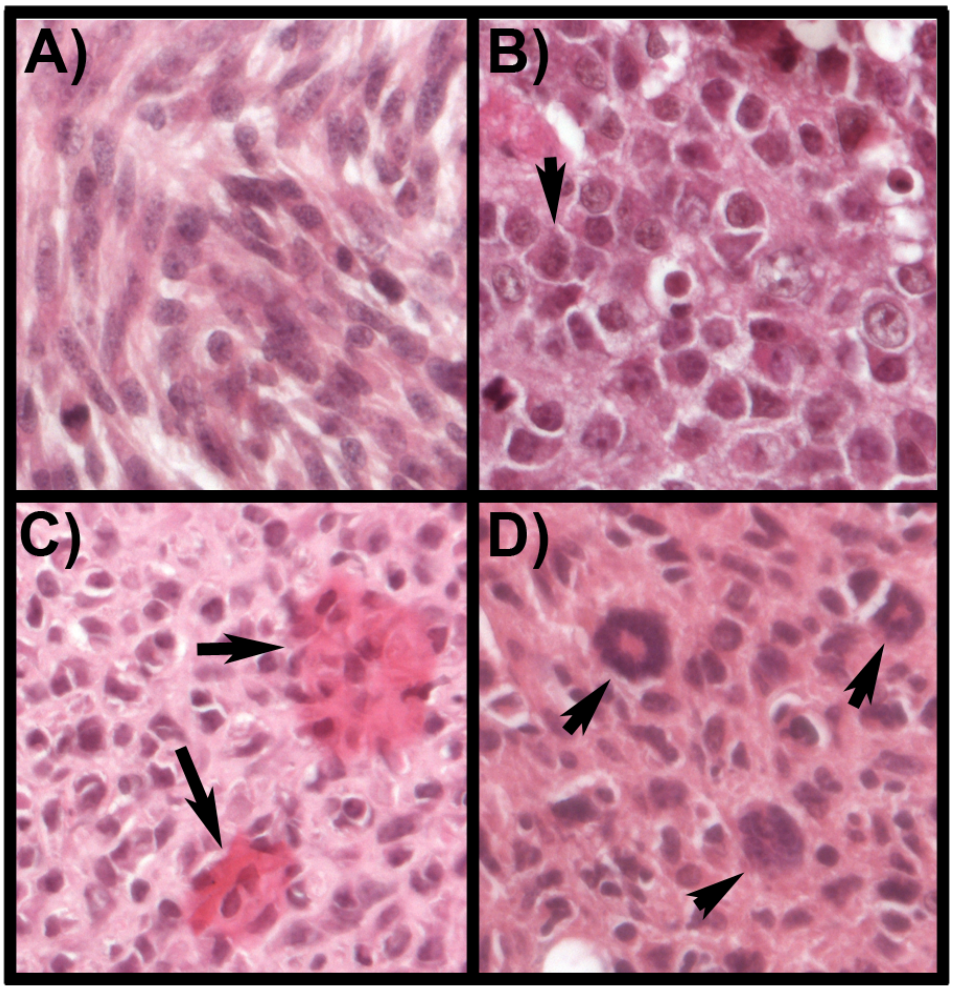
A)
B)
C)
D)

**Figure 4. Tumors activate downstream signaling pathways**. Immunohistochemistry of neurofibroma and MPNST tumors for EGFR and its downstream signaling targets: phospho-EGFR, phospho-Erk, phospho-Akt, and Trp53 and its downstream target p21.

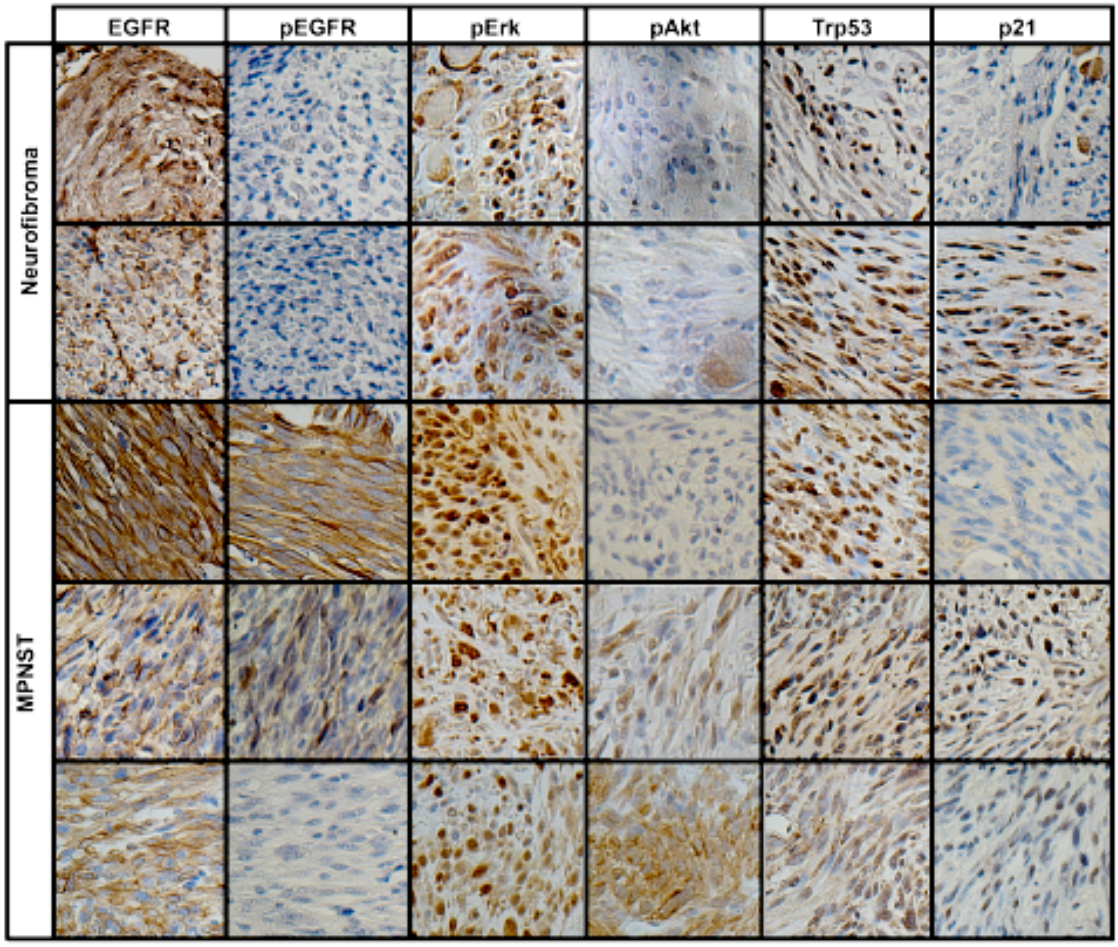
EGFR
pEGFR
pErk
pAkt
Trp53
p21
Neurofibroma
MPNST

**Figure 5**. **Characterization of tumor cell lines** (A) Immunofluorescent analysis of tumor cell lines for Schwann cell markers S100 and Olig2 and for expression of the human EGFR transgenes. (B) Luciferase live imaging of cell strains injected into SCIDBIEGE mice demonstrating they still have capacity for tumor formation. (C) Quantitative PCR analysis of *Trp53*, *Nf1*, and human *EGFR* mRNA expression. (D) Agarose gel electrophoresis of PCR products from a *Trp53* Loss Of Heterozygosity experiment. A band at 600bp represents the wildtype *Trp53* allele while the double smaller bands represent the digested $Trp53^{R270H}$ allele.

A)

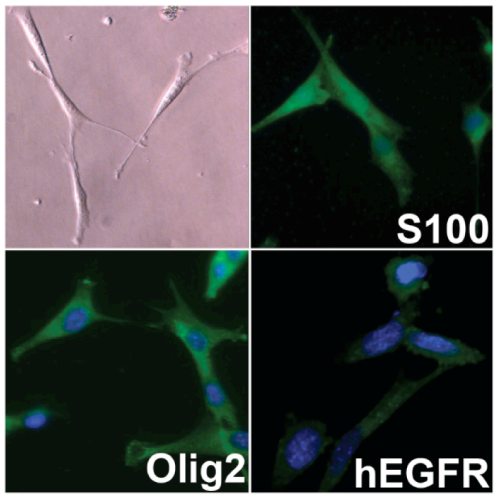


B)

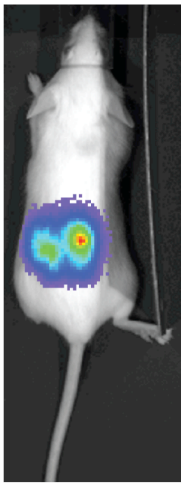

C)

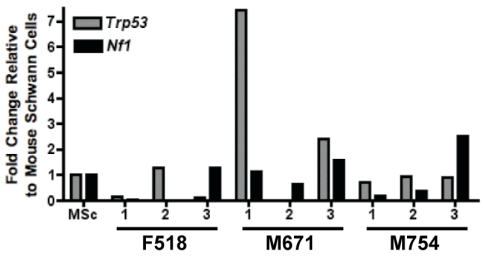


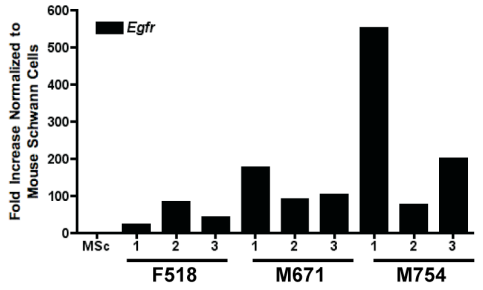


D)

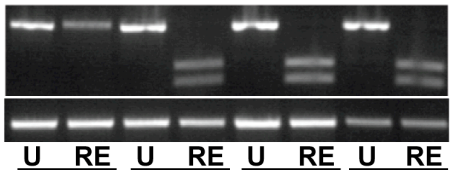


| Cell Source | n= | % with LOH |
|---|---|---|
| Bulk Tumor | 5 | 40 |
| Cell Strain | 5 | 80 |
| Cell Line | 15 | 80 |

**Supplemental Figure 1**. **Spectral karyotyping analysis of MPNST-derived cell lines** (A) 1 clone from F518 MPNST with the closest normal looking karyotype. (B) 2$^{nd}$ clone from F518 MPNST that has the most complex karyotype with diverse whole chromosomal amplifications and translocations.

A)

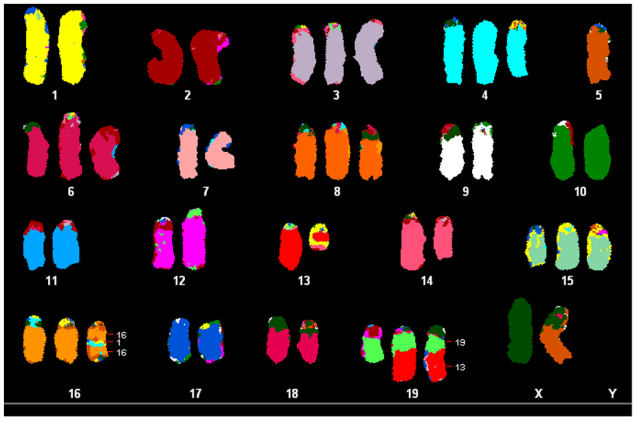
1
2
3
4
5
6
7
8
9
10
11
12
13
14
15
16
17
18
19
X
Y

B)

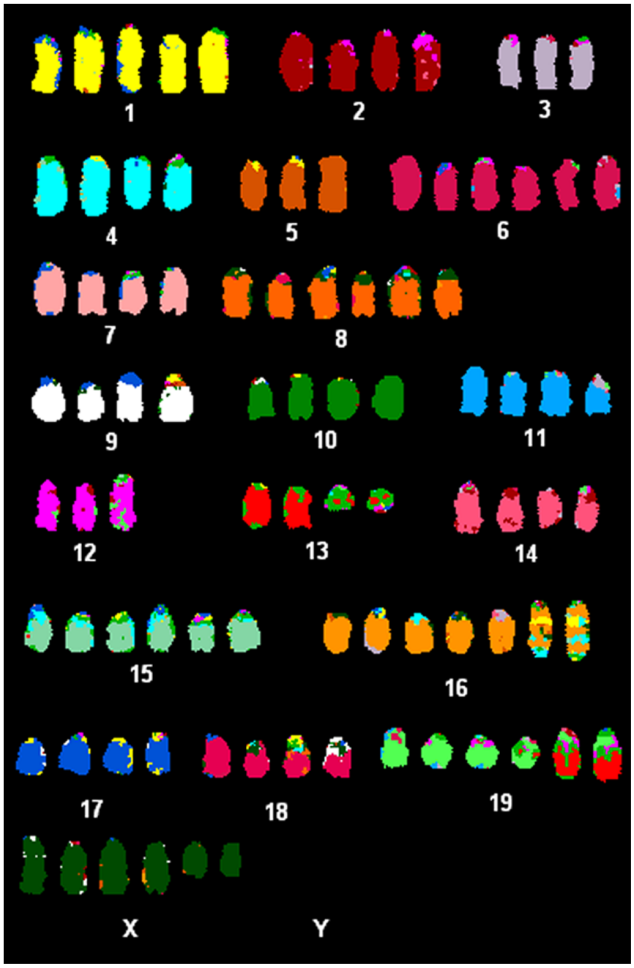
1
2
3
4
5
6
7
8
9
10
11
12
13
14
15
16
17
18
19
X
Y

**Table 2. Spectral karyotyping analysis of tumor-derived cell lines.** Five tumor-derived cell lines from the same tumor were assessed by SKY analysis to determine genomic stability. Each of the five cell lines was assessed for the chromosomal numbers, as well as for translocations and deletions.

| Chromosome # | Line 1 | Line 2 | Line 3 | Line 4 | Line 5 |
|---|---|---|---|---|---|
| Monosomy | 1 | 0 | 0 | 0 | 0 |
| Disomy | 11 | 1 | 2 | 1 | 0 |
| Trisomy | 8 | 6 | 7 | 0 | 3 |
| Tetrasomy | 0 | 9 | 6 | 11 | 10 |
| Pentasomy | 0 | 1 | 5 | 1 | 1 |
| Hexasomy | 0 | 2 | 0 | 5 | 5 |
| Septasomy | 0 | 0 | 0 | 2 | 1 |
| Octasomy | 0 | 1 | 0 | 0 | 0 |
| Alterations | | | | | |
| Translocations | 2 (16,19) | 4 (13,16,19,X) | 3 (16,18,19) | 2 (16,19) | 2 (16,19) |
| Deletions | 2 (13,14) | 1 (13) | 1 (13) | 2 (13, X) | 2 (13, X) |

# Chapter 5.

# An insertional mutagenesis screen implicates *Cav1* in MPNST formation.

## INTRODUCTION

Malignant peripheral nerve sheath tumors (MPNSTs) are aggressive, metastatic sarcomas of Schwann cell origin, which occur sporadically (~50% cases) or in association with inherited tumor pre-disposition syndromes such as Neurofibromatosis types 1 and Neurofibromatosis type 2 [Ducatman,B.S. 1986; Evans,D.G. 2002; Ferner,R.E. 2002; McCaughan,J.A. 2007; Porter,D.E. 2009]. The lifetime risk of developing an MPNST is 0.001% in the case of sporadic origin, while individuals afflicted with NF1 syndrome (1:3,500 people) have a 5-13% lifetime risk of developing an MPNST [Ducatman,B.S. 1986; Evans,D.G. 2002; Ferner,R.E. 2002; McCaughan,J.A. 2007; Porter,D.E. 2009; Gutmann, D.H. 2001]. Sporadic MPNSTs generally afflict individuals between 40-50 years of age while NF1 associated MPNSTs occur in the first decade of life [Porter,D.E. 2009]. Moreover, NF1 associated MPNSTs tend to be more aggressive and have a poorer outcome compared to sporadic MPNSTs [Hagel, C. 2007; Porter,D.E. 2009]. Primary treatment of MPNSTs is resection of the tumor followed by non-specific chemotherapeutic agents. However, MPNSTs are aggressive and invasive. Surgical resection is not always successful in eliminating tumors. The lack of specific targeted therapies and knowledge of genetic pathways altered in MPNST development have lead to 5-year survival rates of less than 25% [Ducatman,B.S. 1986; Porter,D.E. 2009]. Identification of genetic pathways altered in MPNST development may provide new novel drug targets for improved treatment of MPNST.

The cell of origin for MPNSTs is thought to be the Schwann cell [Urich, H. 1998]. Schwann cells are glial cells of the peripheral nervous system. Mature Schwann cells function as support cells for the axons of nerves in the peripheral nervous system. They encompass axons providing protection from physical damage and regulate the surrounding chemical environment. In addition, Schwann cells facilitate action potentials generated along axons of nerves to maintain signaling along axons. Importantly, these cells are targets of tumorigenesis in Neurofibromatosis type 1 and 2 syndromes [Gutmann, D.H. 2001]. The hallmark of NF1 syndrome is the development of benign tumors called neurofibromas. These tumors are heterogeneous in that they are composed of a variety of cell types: Schwann cells, perineurial cells, fibroblasts, mast cells, and

axons [Friedman, J.M. 1999; Huson, SM 1994]. Neurofibromas can manifest in two forms. They can grow around and encapsulate the subcutaneous dermal nerves, creating many dermal masses that can be removed surgically with ease and are not prone to MPNST transformation, or as a plexiform neurofibroma that grows within the body often to the nerve roots and embeds itself into the surrounding tissue. Plexiform neurofibromas are prone to malignant transformation (~10% of tumors) into MPNSTs .

Genetic analysis of human tumors to identify genetic alterations that give rise to benign neurofibromas and then further progression into the aggressive and invasive MPNST has revealed only a handful of genes. The most commonly mutated gene is *NF1, Neurofibromin*, the hallmark gene of Neurofibromatosis Type 1 syndrome [Messiaen, L.M. 2000]. *NF1* is a RAS-GTPase activating protein [Ballester,R. 1990; Xu,G.F. 1990]. Deletion or mutation of this gene in cells causes increased and aberrant signaling through the RAS/MAPK pathway in human neurofibromas and MPNST derived cell lines [Sherman, L.S. 2000; Basu, T.N. 1992]. Deregulation of this pathway leads to increased signals for growth and proliferation. Additional signaling pathways altered include increased signaling through PI3K/AKT/mTor/S6Kinase and cAMP signaling [Johannessen, C.M. 2008; Johannessen, C.M. 2005]. In addition to loss of Neurofibromin function, expression of growth factor receptors such as the *EGFR* and growth factor receptor ligands such as *Neuregulin*, *PDGF*, *HGF*, *SCF*, and *TGFß1* are increased stimulating growth and proliferation of normally growth quiescent Schwann cells to form benign neurofibromas [DeClue, J.E. 2000; Stonecypher, M.S. 2005; Kadono, T. 2000; Kadono, T. 1994; Fukuda, T. 1998; Rao, U.N.M. 1997; Watanabe, T. 2001]. As tumors grow, the cells are prone to acquiring additional mutations to transform the benign tumor into an aggressive MPNST. In humans, loss of cell cycle regulators such as *TP53*, *RB1*, and *CDKN2A* in combinations with amplifications or mutations of growth factor receptors such as *ErbB2, EGFR, cKIT, c-Met, PDGFR, HGFR* drive formation of MPNSTs [Birindelli,S. 2001; Legius,E. 1994;22 Perry,A. 2002; Menon, AG 1990; Kourea, H.P. 1999; Nielsen, G.P. 1999; Mantripragada, K.K. 2008; Mawrin, C. 2002; Holtkamp, N. 2006; Storlazzi, CT 2006; Badache, A. 1998; Badache,A. 1998] . In addition to specific gene mutations, MPNSTs tend to have hypodiploid or near-triploid

whole chromosomal amplification and losses; namely gains on chromosome 7, 8q, 15q and losses on 1p, 9p, 11, 12p, 14q, 17q, 18, 22q, X, and Y [Forus,A. 1995; Lothe,R.A. 1996; Mechtersheimer,G. 1999; Mertens,F. 1995; Plaat,B.E. 1999; Schmidt,H. 2001; Schmidt,H. 2000; Schmidt,H. 1999]. Interestingly, microarray comparisons between NF1 associated versus sporadic MPNSTs have not identified any specific molecular signature associated with either tumor but found many similar alterations [Watson, M.A. 2004; Holtkamp, N. 2004; Miller, S.J. 2006]. Taken together, though some genes and genetic pathways have been identified as altered in both NF1 associated and sporadic MPNST development, there are still many left to uncover in order to create effective therapies for treatment of MPNSTs in humans.

Much work as been done to use known genetic alterations in human MPNST development to model this disease in mice. Initial mouse models to study NF1 focused on creating *Nf1* knockout mice. *Nf1*$^{+/-}$ mice developed pheochromocytomas and leukemias but no evidence of neurofibroma or MPNST development [Jacks, T. 1994]. *Nf1*$^{-/-}$ mice died *in utero* due to many developmental abnormalities [Brannan, C.I. 1994; Lakkis, M.M. 1998]. Chimeras of *Nf1*$^{-/-}$ embryos and wild-type mice, *Nf1* is not inactivated in all cell types, developed neurofibromas [Cichowski, K. 1999]. Conditional inactivation of the *Nf1* gene has shown mixed results depending on the Cre-recombinase. Experiments utilizing *Krox20-Erg2-Cre* required body-wide *Nf1* haploinsufficiency to cooperate with *Nf1* null Schwann cells to form neurofibromas [Zhu,Y. 2002]. This model reflects closely the development of neurofibromas in the context of people with NF1 syndrome as every cell in the body is haploinsufficient for *NF1*. The use of *Dhh-Cre* to inactivate *Nf1* specifically in Schwann cells in mice with wild-type *Nf1* in all other cells is sufficient to generate dermal neurofibromas and plexiform neurofibromas [Wu, J. 2008]. This model may reflect a scenario observed in sporadic MPNST development as majority of cells have intact *NF1* genes in the tumor environment. Besides alterations in *Nf1* expression, there are few other models of neurofibroma and MPNST formation.

Transgenic mouse models overexpressing *EGFR* in Schwann cells predominantly develop nerve hyperplasia with very low incidence of neurofibroma formation [Ling, B.C. 2005]. However, transgenic mice overexpressing *neuregulin-1* developed dermal

neurofibromas, plexiform neurofibromas, and reported cases of MPNST formation with accumulation of various tumor suppressor mutations observed in human MPNSTs [Huijbregts, R.P.H. 2003]. In addition to transgenic mice with single gene alterations to give rise to Schwann cell tumorigenesis, gene combinations have also been utilized. *Nf1* and *Trp53* are commonly mutated in human MPNSTs and genetically linked in mice. Based on these facts, two labs independently developed the NPCis mouse model (deletion of *Nf1* and *Trp53* on the same chromosome) in which MPNST formation occurred and was associated with high incidence of Loss of Heterozygosity of the wild-type chromosome [Cichowski, K. 1999; Vogel, K.S. 1999]. Recently, *Pten* has been implicated in MPNST formation in humans and in mouse models. Conditional inactivation of *Nf1* and *Pten* expression and overexpression of a *Kras* mutant using *GFAP-Cre* lead to high MPNST penetrance [Gregorian,C. 2009]. Mutations in either one of these alleles alone were not sufficient for MPSNT formation. Taken together, the current mouse models of MPNST formation suggest that multiple mutations are required for MPNST formation and that *Nf1* can cooperate with multiple mutations to give rise to MPNST formation. Therefore, we hypothesize that other novel genetic driver mutations likely exist.

To elucidate the genetic mechanisms of MPNST development, we performed a forward genetic screen in mice targeting the *Sleeping Beauty* (*SB*) transposon-based somatic mutagenesis system to the Schwann cells. In addition to identifying novel genes involved in MPNST development we also focused on identifying genes that cooperate with known mutations involved in human MPSNT formation; specifically *EGFR* overexpression and reduced TP53 function. We used the *CNPase-hEGFR* transgenic mice to overexpress *EGFR* in the Schwann cell lineage [Ling, B.C. 2005]. These mice overexpress the human EGFR cDNA behind the human CNP promoter. Overtime, *CNPase-hEGFR* mice develop nerve hyperplasia and ~5% incidence of benign neurofibroma formation. However, no MPNST formation has been observed. In order to identify TP53 cooperating mutations, we used the conditional dominant negative $Trp53^{R270H}$ allele [de Vries,A. 2002]. We used the dominant negative allele because in human MPNSTs, deletions and point mutations occur in ~75% of cases but biallelic loss

of *TP53* is rare [Holtkamp,N. 2007; Lothe,R.A. 2001; Upadhyaya,M. 2008].The expression of the allele was limited to the Schwann cells by breeding to mice that possess the *Cnp-Cre* allele [Lappe-Siefke,C. 2003]. The incidence of MPNST formation in *Cnp-Cre*; *Trp53*$^{R270H}$ has not been previously reported. However, mutagenesis alone, or in concert with these cancer predisposing alleles, provided informative models for the development of MPNST.

Here, we describe new mouse models of neurofibroma and MPNST formation. ~72% of *Cnp-Cre*; *Trp53*$^{R270H}$*; CNPase-hEGFR* mice developed MPNSTs with a median time of tumor harvest 362 days. Layering SB-mutagenesis with the *Cnp-Cre*; *Trp53*$^{R270H}$*; CNPase-hEGFR* alleles increases the incidence to ~82% with a median time of tumor harvest 299 days. Bioinformatic analysis of the cloned transposon insertion sites identified many genes previously implicated in MPSNT development including *Nf1*, *Nf2*, and *Pten*. Moreover we identified many genes involved in a variety of genetic pathways such as TGF-ß and Wnt/ß-Catenin signaling pathways. One gene, *Caveolin-1*, was repeatedly mutagenized in our screens. Cell lines from SB-derived tumors with T2/Onc insertions into *Cav1* lead to increased ß-Catenin levels. shRNA knockdown of *Cav1* in immortalized rat Schwann cells increased the levels of ß-Catenin. Moreover, *Cav1*$^{+/-}$*; CNPase-hEGFR* mice develop high incidence of neurofibromas and grade 2 PNSTs compared to single transgenic control mice. Together, these data suggest that using the *Sleeping Beauty* mutagenesis system we identified genes and genetic pathways that may provide new therapeutic targets for MPNST treatment.

## MATERIALS & METHODS

**Generation of transgenic animals.** To specifically target *Sleeping Beauty* mediated mutagenesis to Schwann cells, three transgenes were introduced into mice. The first transgene conditionally expresses the *Sleeping Beauty* (SB11) transposase enzyme (*R26-lsl-SB11*) when Cre recombinase is also present within the cell [Dupuy,A.J. 2009; Keng, V.W. 2009; Starr, T.K. 2009]. The second transgene is an oligodendritic and Schwann cell specific Cre-recombinase controlled by the CNP promoter (*CNPase-Cre*) [Lappe-Siefke,C. 2003]. The third transgene is a concatomer of oncogenic transposons capable of activating and/or disrupting endogenous gene expression (*T2/Onc15*) [Collier, L.S. 2005]. Mice possessing all three transgenes (*CNPase-Cre; R26-lsl-SB11; T2/Onc15*) undergo insertional mutagenesis in oligodendritic and Schwann cell lineage cells. In addition, we used predisposing alleles for MPNST development. Overexpression of the human EGFR cDNA was done using the *CNPase-hEGFR* mouse [Ling,B.C. 2005]. Loss of Trp53 function was achieved using the conditional $Trp53^{R270H}$ allele mouse [de Vries,A. 2002]. These mice were bred together to form experimental and control cohorts (shown in Figure 1A). $Cav1^{-/-}$ mice were purchased from Charles River laboratories.

**PCR genotyping.** Genotypes of transgenic mice were determined using a PCR based approach: Firstly, genomic DNA was isolated from tail clippings using standard proteinase K treatment, phenol-chloroform extraction and ethanol precipitation. Genomic DNA was resuspended in sterile TE {10mM tris-HCl (pH7.5), 1mM EDTA (pH 8)} and quantified using a Nanodrop spectrophotometer. PCR genotyping was performed using 100 ng of diluted genomic DNA as template in a 25µl PCR reaction volume. PCR primers used for *CNPase-Cre* were sense 5'-CATAGCCTGAAGAACGAGA-3' and antisense 5'-GATGGGGCTTACTCTTGC-3' (amplicon 894 bp); *R26-lsl-SB11* were *SB* sense 5'- CTAAAAGGCCTATCACAAAC-3', *Rosa26* wildtype sense 5'-CTGTTTTGGAGGCAGGAA-3' and Rosa26 wildtype antisense 5'-CCCCAGATGACTACCTATCCTCCC-3' (wildtype amplicon 420 bp and floxed allele amplicons 266bp); *T2/Onc15* were sense 5'- CGCTTCTCGCTTCTGTTCGC-3' and

antisense 5'-CCACCCCCAGCATTCTAGTT-3' (amplicon 250 bp); *CNPase-hEGFR* were sense 5'- TGACATCTCCTCCTCCCTTC'-3' and antisense 5'-TGCCCAACTGCGTGAGC-3' (amplicon 380 bp); *Trp53*$^{R270H}$ floxed allele were wildtype sense 5'- TTACACATCCAGCCTCTGTGG-3', wildtype antisense 5'-CTTGGAGACATAGCCACACTG -3' and flox forward 5'-AGCTAGCCACCATGGCTTGAGTAAGTCTGCA -3' (WT amplicon 170 bp and floxed allele amplicon 270 bp); Cav1 exon 2 sense 5'-GTGTATGACGCGCACACCAAG-3'; Neo sense 5'-CTAGTGAGACGTGCTACTTCC-3'; intron 2 antisense 5'-CTAAAAGGCCTATCACAAAC-3' (WT amplicon 650bp and knockout allele 330bp). PCR conditions for ReddyMix (Thermo Scientific) were used according to the manufacturer's instructions with an initial denaturing step of 95°C for 2 min; 30- to 35-cycles of denaturing at 95°C for 25 sec, annealing at 55°C for 35 sec and extension at 72°C for 65 sec; followed by a final extension at 72°C for 10 min. PCR products were separated on a 1.5% agarose gel and genotype determined by the absence or presence of expected amplicons.

**Neurofibroma/MPNST analysis.** Neurofibromas and/or MPNSTs were carefully removed from the sacrificed animal under a dissecting microscope (Leica), washed and placed in cold phosphate buffered saline (PBS). These separated tumors were split into samples for DNA, RNA and protein extraction. Tissue samples for RNA were stored at -80°C in RNAlater (Sigma) to prevent RNase contamination and degradation. DNA extraction was done as previously described in the PCR genotyping section. Extraction of RNA was done using the Trizol reagent (Invitrogen) using protocols described by the manufacturer. Protein extraction was performed using standard isolation techniques. Histological sections were only taken for larger tumors (>2 mm in diameter). Formalin fixed-paraffin embedded sections from various tissues were sectioned at 5 microns using a standard microtome (Leica), mounted and heat-fixed onto glass slides. Tissue section slides were either processed and stained with hematoxylin-eosin (HE) using standard

protocols, Toluidine Blue using standard protocols, or used for immunohistochemistry (IHC) as described in the next section in order to determine tumor type and grade.

**Immunohistochemistry (IHC).** Tissues were fixed in 10% buffered formalin and embedded in paraffin blocks. Sections were cut at 5-μm thickness, and rehydrated through a series of graded ethanols. Slides underwent antigen retrieval by boiling for 30 minutes in antigen unmasking solution (Vector Laboratories). Endogenous peroxidases were quenched with 3% hydrogen peroxide solution for 10 minutes. For antibody staining, a M.O.M. kit (Vector Laboratories) was used for blocking and antibody incubations. Primary antibodies used were mouse anti-Ki67 (1:100; Novocastra), rabbit anti-S100 (1:100; Sant Cruz Biotechnology), rabbit anti-phospho Erk (1:100; Cell Signaling Technology), rabbit anti-phospho EGFR (1:100; Cell Signaling Technology), rabbit anti-EGFR (1:200; Cell Signaling Technology), rabbit anti-phospho Akt (1:50; Cell Signaling Technology), mouse anti-ß-Catenin (1:100; Santa Cruz Biotechnology), mouse anti-activated ß-Catenin (1:100; Millipore), rabbit anti-Cav1 (1:100; Cell Signaling Technology). Following a series of washes, slides were incubated with the corresponding anti-mouse or anti-rabbit biotinylated secondary antibody (1:10,000; Vector Laboratories). Slides were washed, incubated with the vectastain ABC kit (Vector Laboratories) for 30 minutes at room temperature, washed again, and stained using peroxidase substrate kit DAB (Vector Laboratories). Finally slides were counterstained with hematoxylin, dehydrated, cleared with citrosolv and mounted with permount (Fisher). Slides were analyzed and assessed for tumor grade by pathologist Dr. Margaret Collins.

**Linker Mediated PCR .** DNA was isolated using methods described in genotyping section from neurofibromas and MPNSTs. Transposon-genomic DNA junctions were amplified as previously described [Keng, V.W. 2009; Starr, T.K. 2009]. LM-PCR products were purified using the MinElute 96 UF Plates (Qiagen), and sequenced on Illumina sequencing platform.

**Transposon Insertion Site Analysis.** For each lane of Illumina data, sequences are loaded into a database table. Barcodes, IRDR, and linker sequences are identified in the sequences using mysql queries. Sequences without genomic data (derived from the vector), sequences to short to map, and sequences that do not began with TA artifactual sequences are identified and sequentially removed. For each library, the remaining sequences are then condensed to remove duplicate sequences retaining information regarding the total count. Sequence information is then mapped to the genome using the bowtie algorithm to identify uniquely mappable regions and these mappings are combined for each of the Illumina lanes of data. Mapped sequences are then condensed to 100 bp genomic regions to minimize potential over-counting of specific insertion events that are in close proximity. Based on the number of mappings relative to the total number of mappings obtained for each library, sets of insertion regions are generated at various thresholds. The first set contains all regions found to map to a library with sequence counts greater than 1% of the total per library, which are not found on the chromosome hosting the transposon prior to mobilization. Regions greater than 0.1% 0.01% and all mappings are also calculated. These lists of regions are then used for Conserved Integration Site (CIS) calculation. Additional lists of regions for CIS calculation are generated based on different groupings of the data for example CIS lists can be calculated using groups of libraries from animals with common genotypes or phenotypes. Inserts found on the SB donor chromosome are also removed to eliminate bias from local hopping in the CIS analyses. CIS calculation Conserved Integration Sites (CIS) are calculated by analyses of a given set of insertions to identify regions that show more insertions than would be expected by random chance within specific window sizes (200000,100000,50000,25000,12500 bases) The window sizes were chosen to search a wide range of windows and to avoid biasing towards insertions found at single sites. For each potential window examined a peak finding algorithm is run iteratively to return the maximum number of inserts and the maximum number of libraries present within each potential window for each window size. The likelihood of a given number of insertions being obtained within a window of a given size is calculated using Poisson distribution statistics. Given the size of the genome, the total number of inserts used to

look for CIS, and the window size an estimate of the likelihood of randomly observing a specific number of insertions assuming a random distribution is directly calculated. These windows are then combined to determine non-overlapping windows with the lowest p-values and these are defined as CIS.

**Microarray Analysis.** Human nerve, neurofibroma, plexiform neurofibroma and MPNST microarray data was previously reported in Hummel et al. and Subramanian et al. [Hummel,T.R.; Subramanian,S.]. Briefly, this data was used to compare the changes in gene expression of our CIS list genes to identify candidate genes that are substantially altered in human MPNST compared to neurofibroma.

**Generation of MPNST cell lines**. MPNSTs were carefully dissected using aseptic techniques. The tumor was sliced into small pieces, placed into 1xDMEM containing (2 ug/ml) of Collagenase A. This solution was incubated at 37ºC in 5% $CO_2$ for 3 hours to allow dissociation of cells from the bulk tumor. Prior to plating, the solution was triterated and placed through a 33um filter. Cells were plated on 10cm dishes containing complete media (1xDMEM, 10% fetal bovine serum, 1x penicillin/streptomycin) and grown at 37ºC in 5% $CO_2$. These cell strains were transduced with a lentivirus containing an eGFP and luciferase reporter transgene. Successfully transduced cells as assessed by eGFP expression were cell sorted using a FACSAria. The top 5% of cells expressing eGFP were collected into 96-well plates as well as cells that were negative for eGFP. eGFP negative clones that grew from the cell sort were assessed by immunoflourescense with mouse anti-S-100 (1:100; Santa Cruz Biotechnology), rabbit anti-human EGFR (1:100; Cell Signaling Technology), rabbit anti-Olig2 (1:100; Abcam) to demonstrate Schwann cell origin and they express human EGFR.

**Cell lines.** Rat immortalized Schwann cells were acquired from ACTT. The cell lines CRL2941 and CRL2942 were used for subsequent experiments for identify the role of Cav1 in Schwann cell tumorigenesis. . Cells were plated on 10cm dishes containing complete media (1xDMEM (CellGro), 10% fetal bovine serum, 1x

penicillin/streptomycin (CellGro)) and grown at 37ºC in 5% $CO_2$. Cells were assessed for expression of ß-Catenin by immunoflourescense (1:100; Santa Cruz Biotechnology). pTRIPZ shRNAs targeting *Cav1* were purchased from OpenBiosystems. shRNA expression was induced with 2ug/ml of Doxycycline for 3 days. Analysis of Cav1 knockdown was done by western blot using standard protocols. Alterations in proliferation were assessed using an MTS assay following the manufacturers protocol.

## RESULTS

### SB mutagenesis accelerated MPNST formation.

We targeted SB transposon mutagenesis to Schwann cells and their precursors using the Schwann cell specific Cre-recombinase transgene, *CNPase-Cre,* and a conditional SB mutagenesis system [Lappe-Siefke,C. 2003; Dupuy,A.J. 2009; Keng, V.W. 2009; Starr, T.K. 2009]. In addition, we intended to discover cooperating mutations with genetic alterations already identified in human MPNST development; namely EGFR overexpression and TP53 loss of function [Tabone-Eglinger,S. 2008; Verdijk,R.M.]. To address this, we included a *CNPase-hEGFR* transgene to overexpress the human EGFR cDNA in Schwann cells and a conditional dominant negative $Trp53^{R270H}$ allele in which its expression is limited to the Schwann cells [Ling, B.C. 2005; de Vries,A. 2002]. Together, we developed four experimental cohorts to identify genes involved in MPSNT development (Figure 1A)**.**

The four cohorts were comprised of mice undergoing transposition alone, transposition in the context of loss of function of Trp53 by expressing the $Trp53^{R270H}$ allele, transposition in the context of *EGFR* overexpression, and lastly transposition in the context of loss of Trp53 function ($Trp53^{R270H}$) and *EGFR* overexpression (Figure 1A). Mice that possessed the pre-disposed alleles but did not posses components for transposition were used as controls. Overall, mice that undergo transposition either alone or in the context of loss of Trp53 function or EGFR expression developed few Schwann cell tumors. However, Schwann cell tumors were observed at various nerve locations throughout mice undergoing transposition in the context of Trp53 loss of function and *EGFR* overexpression as well as in the control mice that possessed the predisposed alleles but transposition did not occur. The majority of the tumors originated at the paraspinal dorsal root ganglion (DRG) (Figure 1B). Histological analysis of Schwann cell tumors from all four cohorts using H&E staining and antibodies against the proliferative marker Ki67 and the Schwann cell marker S100 demonstrated that mice developed different grades of tumors from benign grade 1 neurofibromas, grade 2 plexiform-neurofibromas, and aggressive grade 3 MPNSTs (Figure 1C). Moreover, these

tumors expressed the Sleeping Beauty transposase by immunohistochemistry and were undergoing transposition as demonstrated by a PCR-excision assay (Figure 1E).

We determined that transposition alone was not efficient at generating MPNSTs as only ~2% of mice developed an MPNST by 450 days (Figure 1D). Mice that undergo transposition on the *Trp53*$^{R270H}$ background also did not have increased incidence of MPNST formation (~5%) compared to the *Trp53*$^{R270H}$ control mice (~7%). Transposition on an EGFR overexpression background increased neurofibroma formation from 17% observed in the control mice to 35% and induced MPNST formation (~7% of mice). Interestingly, expression of *CNPase-hEGFR* and *Cnp-Cre*; *Trp53*$^{R270H}$ alleles cooperated to increase neurofibroma (~58% of mice) and MPNST (~24% of mice) formation with a median time of tumor harvest of 401 and 362 days respectively. Importantly, mice that also underwent SB mutagenesis on both of the pre-disposed alleles developed neurofibromas (~45%) and increased frequency of MPNST development (~63%) with reduced latency (301 and 299 days respectively) (Figure 1D). Tumor penetrance and frequency for each genotype is summarized in Supplemental Table 1.

**SB-derived MPNSTs undergo divergent differentiation.**

In addition to the variety of tumor grades observed in the control and SB-derived tumors, we also observed cases of divergent MPNST differentiation, which has been shown to occur in some patients. The common histological appearance of human MPNSTs is the presence of spindle shaped cells with buckled or wavy nuclei within a tumor (Figure 1C) [Pytel,P. 2005]. However, human MPNSTs can undergo divergent differentiation to other cell types within a tumor such as epithelioid-like cell differentiation, a rare occurrence in human MPNSTs, osteoid differentiation, palisaded nuclei, pseudorosettes, and wreath-like giant cells (Supplemental Figure 1A) [Pytel,P. 2005; Magro,G.]. Divergent differentiation is thought to be a secondary event due to changes in the microenvironment from the primary tumor. Moreover, when comparing the events of tumor formation and divergent differentiation to genotype (*CNPase-Cre; Trp53*$^{R270H}$*; CNPase-hEGFR* vs. both alleles in concert with transposition), we observed increased incidence of divergent differentiation with SB-derived tumors in both plexiform-

neurofibromas and MPNSTs compared to tumor derived from just the predisposing tumor alleles (Supplemental Figure 1B). No divergent differentiation was observed in neurofibromas. Taken together, these data suggest our model of MPNST development mimics all stages and types of MPNSTs observed in humans.

**CIS Analysis of SB-derived Tumors.**

To identify mutated genes that cooperated to form Schwann cells tumors, we analyzed transposon insertion sites from 269 SB-derived neurofibromas and 105 SB-derived MPNSTs from 100 mice to identify CISs. Criteria for determining CISs are described in the methods section. For this screen, we chose the minimum number of mice that must possess T2/Onc insertions in a CIS to be 4 mice for neurofibromas and 3 mice for MPNSTs. Using these criteria, we identified 215 CISs associated with neurofibroma formation and 109 CISs associated with MPNST formation (Supplemental Table 2).

Analysis of the CIS-associated genes found in SB-derived neurofibromas and MPNSTs demonstrated that the known Schwann cell tumor suppressor gene, *Nf1*, was repeatedly mutated which validated the screen (Table 1) . In addition, the tumor suppressor *Pten*, which has recently been implicated in MPNST formation, was frequently mutated by transposon insertions [Gregorian,C. 2009]. Interestingly, analysis of the top 10 CISs found in MPNSTs identified many of the genes to be repeatedly mutated together suggesting that mutating these genes may cooperate for MPNST formation (Figure 2A). Specifically, insertions in *Nf1* and *Pten* co-occurred in tumors from 13/62 mice ($p<7.94E-05$), suggesting these genes in our model cooperated to form MPNSTs (Figure 2B). Microarray data from either purified Schwann cells or bulk human tissues from nerve, dermal neurofibroma, plexiform-neurofibromas, and MPNSTs demonstrated reduction in *NF1* and *PTEN* expression as disease progression occurred (Figure 2C). In addition, when *Nf1* and *Pten* were biallelically inactivated *in Dhh-Cre* positive Schwann cells, mice developed rapid and aggressive grade 2 PNSTs compared to control littermates by 21 days of age (unpublished results, communication with Dr. Vincent Keng). Moreover, both NF1 and PTEN are apart of the PI3K/AKT/mTOR pathway, which has been implicated as a genetic pathway highly altered in human

MPNSTs, and been a focus for therapeutic targeting using PI3K and mTOR inhibitors [Johannessen, C.M. 2008; Johannessen, C.M. 2005]. We therefore conclude that loss of *NF1* expression does not relieve strong selective pressure to inactivate *PTEN* during progression to MPNST.

In addition to known genes and genetic pathways altered in MPNST formation, we focused on identifying new genetic pathways altered in MPNST formation that may provide new therapeutic targets. Using Ingenuity Pathway Analysis (IPA) on the 83/109 MPNST CISs that are associated with a known gene, we identified 3 networks highly enriched for in our data set: gene expression in cardiovascular development (30 CISs), neurological cancer (27 CISs), and cell morphology/cell cycle molecules (22 CISs) (Supplemental Figure 2). In addition to this analysis, we specifically assessed signaling pathways that were enriched in our data set using IPA (Supplemental Figure 3). The most significantly enriched signaling pathway with CIS-associated genes was TGF-ß signaling ($p<4.31e-6$, 6/83 molecules). CIS-associated genes within this pathway included *Acvr1*, *Acvr1B*, *Acvr1C*, *Bmpr2*, *Cbp*, and *Runx2*. It has been previously implicated that neurofibromas respond to and overexpress TGFß-1 as a progrowth factor for tumorigenesis [257 Kadono, T. 1994]. However, this mechanism is still unclear. Another pathway of interest enriched for CIS-associated genes was the Wnt/ß-catenin pathway ($p<3.93e-4$, 6/83 molecules). CIS-associated genes with this pathway included *Acvr1, Acvr1B, Acvr1C, Bmpr2, Cbp, Mark2*, and *Trp53* (not a CIS, but included because used as pre-disposing background). Together, these pathways have not been previously implicated in MPNST development directly. Further studies analyzing specifically how these pathways are altered in human cancers may provide insight into new drug targets.

**Reduced Cav1 expression leads to increased ß-catenin expression.**

One gene recurrently mutated in our screen was *Caveolin*-1 (*Cav1*). Cav1 is an essential component of caveolae, which are used in the endocytic pathway to internalize receptors and other transmembrane proteins at the plasma membrane into the cell for predominantly degradation and recycling [Anderson,R.G. 1998; Galbiati,F. 2001; Scherer, P.E. 1995]. In mice, 6 isoforms of *Cav1* are translated (Figure 4A). In our

screen, *Cav1* was mutated in 3 different tumors all within intron 7 of *Cav1*. The direction of the T2/Onc insertions predicts a truncated c-terminal transcript of *Cav1* (Figure 4A). Moreover, this intronic region is conserved in all 6 isoforms suggesting that the T2/Onc insertions could downregulate *Cav1* expression. Analysis of microarray expression of *Cav1/CAV1* in neurofibromas, plexiform neurofibromas, and MPNSTs from mouse models of these diseases and human tumor samples demonstrated reduced mRNA expression as disease progression occurred (Figure 4B). This data suggests a tumor-suppressive role for *Cav1*.

To assess whether T2/Onc insertions within *Cav1* have a functional impact, cell lines were isolated from SB-derived tumors. Tumors that possessed a T2/Onc insertion within *Cav1* expressed very low levels of *Cav1* compared to control tumor cell lines without *Cav1* insertions (Figure 4C). Previous studies on Cav1 have demonstrated that Cav1 binds directly/compartmentalized with growth factor receptors such as Neur/Erb-B2, EGFR, eNOS, H-Ras, c-Neu, Src and signaling pathway molecules such as Ras, Raf-1, MEK-1/2 and ERK-1/2 and reduces signaling through these pathways [Couet,J. 1997; Garcia-Cardea, G. 1997; Engelman, J.A. 1998; Engelman, J.A. 1997; Li, S. 1996]. Reduction of *CAV1* in human lung, renal, and epidermoid carcinoma cell lines have demonstrated increased signaling through the EGFR pathway, specifically via activation of ß-Catenin [Agelaki,S. 2009; Lu,Z. 2003]. To identify functionally how reduction of *Cav1* expression may provide a selective advantage for Schwann cell tumor growth, we assessed alterations in ß-Catenin expression. Immunofluorescent imaging of SB-derived cell lines with reduced Cav1 not only showed increased ß-Catenin expression but also showed increased ß-Catenin levels in the nucleus indicative of transcriptionally active ß-Catenin (Figure 4C).

To determine if loss of Cav1 alone was sufficient for inducing increased levels of ß-Catenin, we transduced immortalized Rat Schwann cells with an inducible shRNA construct targeting *Cav1*. Non-silencing sequences were used as a control (Figure 4D). Immunofluorescent analysis of cells targeted with *Cav1-shRNAs* demonstrated that cells expressing the *shRNA* (expressing RFP) had an increased staining of ß-Catenin compared to non-targeted cells (Figure 4E). Moreover, we observed increased ß-Catenin

expression in the nuclei of cells targeted with the shRNA against *Cav1,* suggesting there was increased in ß-Catenin-dependent transcriptional activity (Figure 4E). Overall, our data suggests that reduction of *Cav1* expression in Schwann cells gives rise to increased signaling through ß-Catenin that provides a proliferative advantage.

**Loss of Cav1 expression cooperated with EGFR overexpression for PNST formation *in vivo.***

Previous studies demonstrated reduced expression of *Cav1* potentiated EGFR signaling [Lu,Z. 2003; Agelaki,S. 2009]. To determine if loss of *Cav1* can increase EGFR signaling and lead to increased tumor formation, we crossed $Cav1^{-/-}$ mice to *CNP-hEGFR* transgenic mice. *CNP-hEGFR;* $Cav1^{+/-}$ mice with corresponding single transgenic control littermates were aged to 2, 4, and 7 months. At 2 and 4 months, there was a slight increase in the hyperplastic phenotype associated with the *CNP-hEGFR* mouse, specifically increased widths of sciatic nerves (data not shown). However, by 7 months there was a significant increase in the size of the paraspinal dorsal root ganglion (DRG) of *CNP-hEGFR;* $Cav1^{+/-}$ mice compared to the littermate controls (Figure 5A and 5B). Histological analysis of the tissues demonstrated that DRG from $Cav1^{+/-}$ mice appeared normal, DRG from *CNP-hEGFR* mice have peripheral nerve hyperplasia, and the DRG from *CNP-hEGFR;* $Cav1^{+/-}$ mice were a mix of grade 1 neurofibromas and grade 2 PNSTs (Figure 5A). Analysis of downstream signaling pathways of EGFR demonstrated that there was an increase in pErk and ß-Catenin expression (Figure 5C). Moreover, there was a substantial increase in activated ß-Catenin in *CNP-hEGFR;* $Cav1^{+/-}$ DRGs compared to control littermates (Figure 5C). The increase in pErk may be partially attributed to specific reduction in Cav1, as Cav1 is a negative regulator of Erk1/2 activation and that Cav1-/- mice demonstrate increase expression of *Erk1/2* [Williams,T.M. 2004; Engelman, J.A. 1998; Galbiati, F. 1998]. Interestingly, there was no apparent increase in pAkt levels in these same mice (Figure 5C). Previous reports have shown *Cav1* overexpression to sustain AKT signaling and increase cell survival in prostate cancer cells [ Li, L. 2003] This may suggest that reduced *Cav1* expression may

lead to reduced Akt activity and cause a preference in signaling through pERK and ß-Catenin in the context of increased EGFR signaling in Schwann cell tumorigenesis.

**DISCUSSION**

Using a *Sleeping Beauty* forward genetic screen, we identified hundreds of genes that likely cooperate with *EGFR* overexpression and *Trp53* loss of function for benign neurofibroma and MPNST formation. The most frequently mutated genes in our screen were *Nf1* and *Pten*. Mutations that lead to loss of the *NF1* gene, which encodes a RAS GTPase activating protein, gives rise to Neurofibromatosis type 1 syndrome. Individuals with this syndrome develop benign Schwann cell tumors called neurofibromas and have a lifetime risk of ~10% of developing an MPNST. However, loss of *NF1* is likely not sufficient for MPNST formation based on genetically engineered mouse models of *Nf1* loss [Zhu, Y. 2002; Wu, J. 2008]. In addition to *Nf1* mutation in our SB-screen, *Pten* was highly mutated and the mutations co-occurred with a significant frequency. Recently, Gregorian et al. demonstrated that inactivation of one allele of *Pten* in Schwann cells with overexpression of a mutated activated form of $KRas^{G12D}$ gave rise to robust MPNST formation [Gregorian,C. 2009]. However, neither mutation alone was sufficient for generating MPNSTs. This data suggests that, like *Nf1*, *Pten* mutations alone are not sufficient for MPSNT formation. Recent efforts in our lab have demonstrated that biallelic inactivation of *Nf1* and *Pten* in a mouse model gives rise to robust neurofibroma and PNST formation (Dr. Vincent Keng, unpublished results). Therefore, our screen not only identified genes implicated in MPNST formation, but identified potential interacting genetic pathways, that when placed together in a mouse model gave rise to a robust MPNST phenotype. Continued analysis of the data set to find CISs that co-occur in a significant number of mice may provide additional mouse models of MPNST formation that may be useful in testing therapeutics for a variety of targeted pathways.

In addition to finding new drug targets, we were also interested in identifying mutations that cooperate with genes known to have a role in MPNST, namely EGFR overexpression. From the list of CISs, we found *Cav1* to be repeatedly mutated. Cav1 is the major constituent of Caveolae, a special type of lipid raft, which are involved in signal transduction and endocytosis [Anderson,R.G. 1998; Galbiati,F. 2001; Okamoto,T. 1998]. Previous studies on *Cav1* identified a direct interaction with EGFR, and that Cav1 expression attenuated EGFR signaling [Khan,E.M. 2006; Lajoie,P. 2007; Pike,L.J. 2005].

This direct interaction leads to decreased ability of EGFR to autophosphorylate, in turn leading to reduced signaling through downstream signal transduction pathways [Couet,J. 1997; Park,W.Y. 2000]. The role of CAV1 in human tumorigenesis is not clear. Down-regulation of *CAV1* expression occurs in osteosarcomas and Ewings sarcoma in addition tumor suppressive roles of CAV1 have been identified in breast carcinomas, and squamous cell carcinoma cell [Fiucci,G. 2002; Lee,S.W. 1998; Cantiani,L. 2007; Razani,B. 2000; Tirado,O.M. 2006]. Moreover, the *Cav1*$^{-/-}$ mouse creates a sensitized background to tumor formation, such as squamous cell carcinoma and breast cancer with increased incidence of metastatic lung tumors [Capozza,F. 2003; Williams,T.M. 2004; Williams,T.M. 2003; Williams,T.M. 2004]. However, CAV1 overexpression has also been associated with metastatic breast and prostate cancers in humans as having a pro-metastatic function [Ho,C.C. 2002; Li,L. 2001; Tahir,S.A. 2001; Jones,C. 2004; Pinto,A.E. 2006]. This biphasic role of CAV1 in human tumors may be associated with alterations in signal transduction pathways needed for growth versus migration.

*CAV1* is expressed in normal Schwann cells and Schwann-cell derived cell lines from rats [Mikol,D.D. 1999]. Our data suggests that Cav1 has a tumor suppressive function in MPNST formation. Microarray data from human tumors demonstrated that as disease progression occurred from the benign neurofibroma to an MPNST, there was loss of *CAV1* expression. A microarray study of 25 vestibular Schwannomas, tumor common in Neurofibromatosis Type 2 syndrome, identified *CAV1* has significantly downregulated [Aarhus,M.]. Moreover, immunohistochemical analysis of these tumors demonstrated reduced expression of CAV1 compared to normal nerve controls [Aarhus,M.]. Our *in vivo* mouse model with reduced *Cav1* expression cooperated with *EGFR* overexpression in Schwann cells to form grade 1 neurofibromas and grade 2 PNSTs. Moreover, tumor formation was associated with increased expression of not only ß-Catenin, but ß-Catenin levels were elevated in the nuclei of the tumors suggesting ß-Catenin-dependent transcription is active. This data proposes a new role of ß-Catenin activity not previously appreciated for MPSNT formation. Targeting of the Wnt/ß-Catenin pathway with small molecule inhibitors or activators, that lead to reduced ß-Catenin signaling, may be warranted in the treatment of human MPNSTs.

Another gene repeatedly mutated and highly ranked on both the neurofibroma and MPNST CIS list was *Creb Binding Protein* (*Crebbp* or *CBP*). *CBP* is a transcriptional coactivator that tethers transcription factors to RNA polymerase II [Gu,W. 1997]. *CBP* also possesses protein acetyltransferase activities that functions on both histones and specific transcription factors such as TP53, which leads increased binding affinity to DNA [Gu,W. 1997; Kee,B.L. 1996; Nakajima,T. 1997; Ogryzko,V.V. 1996]. Humans born with mutations in *CBP* develop Rubinstein-Taybi syndrome [Petrij,F. 1995]. Individuals with this syndrome develop craniofacial defects, heart defects, and have a higher incidence of mental retardation and tumor formation at a young age [Petrij,F. 1995]. *CBP* is also a target of alteration by chromosomal translocations in human leukemias and functions as a transcriptional coactivator for known fusion genes *NUP98-HOXA9* and *MOZ-TIF2* [Blobel,G.A. 2000; Deguchi,K. 2003; Kasper,L.H. 1999]. Moreover, mouse models that conditionally inactivate *CBP* in T-cells gives rise to lymphomagenesis in synergy with $p27^{Kip1}$ loss [Kang-Decker,N. 2004]. Taken together, the data suggest that CBP predominantly acts as a tumor suppressor. CBP is expressed in Schwann cells [Fonte,C. 2007; Fonte,C. 2005]. However, its role as a coactivator is still unclear in Schwann cell development. Microarray analysis of human tumors illustrates reduction in *CBP* expression as tumor progression occurs from a benign neurofibroma to a MPNST (data not shown). In addition, *CBP* was repeatedly mutated in both neurofibromas and MPNSTs in our screen and mutations in MPNSTs were often found in the context of *Nf1, Pten, Taok1,* or *Stag2* mutations. This may suggest a cooperative role for *CBP* with these genes in the formation of MPNSTs. Further studies understanding the role(s), *CBP* has with these other genes for Schwann cell tumorigenesis are warranted.

**SUMMARY**

In summary, using a Sleeping Beauty forward genetic screen we have identified hundreds of new candidate cancer genes that may cooperate with overexpression of EGFR and/or loss of TP53 function to give rise to MPNST formation. Moreover, the majority of these genes have not been implicated in Schwann cell tumorigenesis previously. Further testing of these candidate cancer genes may unravel new genetic pathways to target for treatment of human MPNSTs. One such case may be the targeting of the WNT/ß-Catenin pathway in humans as our genetic data suggests that loss of Caveolin-1 and overexpression of EGFR cooperate in vitro and in vivo to increase expression of ß-Catenin in Schwann cells.

**Figure 1. SB mutagenesis increased MPNST formation.** (A) List of the 4 animal cohorts assessed to identify cooperating genes for MPNST formation. (B) Necropsy images depicting the many nerves targeted for tumor development. (C) Histological analysis of the tumors indicated that mice developed various grades of Schwann cell tumors including neurofibromas, plexiform-neurofibroma, and MPNSTs. (D) Bar graph depicting the percent of mice that developed each tumor type based on genotype. Neurofibromas and plexiform-neurofibromas were pooled together. (E) Immunohistochemistry demonstrating tumors derived from mice undergoing transposition express Sleeping Beauty. The Excision assay is a PCR based showing the transposon donor concatemer (* 2.2kb band) and the footprint where transposons have been mobilized out of the concatemer (*220bp band).

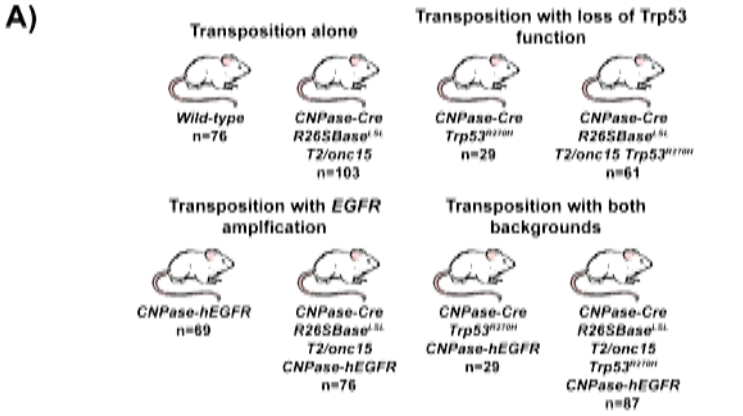
A)
Transposition alone
Transposition with loss of Trp53 function
Wild-type
n=76
CNPase-Cre
R26SBase
T2/onc15
n=103
CNPase-Cre
Trp53
n=29
CNPase-Cre
R26SBase
T2/onc15 Trp53
n=61
Transposition with EGFR amplification
Transposition with both backgrounds
CNPase-hEGFR
n=69
CNPase-Cre
R26SBase
T2/onc15
CNPase-hEGFR
n=76
CNPase-Cre
Trp53
CNPase-hEGFR
n=29
CNPase-Cre
R26SBase
T2/onc15
Trp53
CNPase-hEGFR
n=87

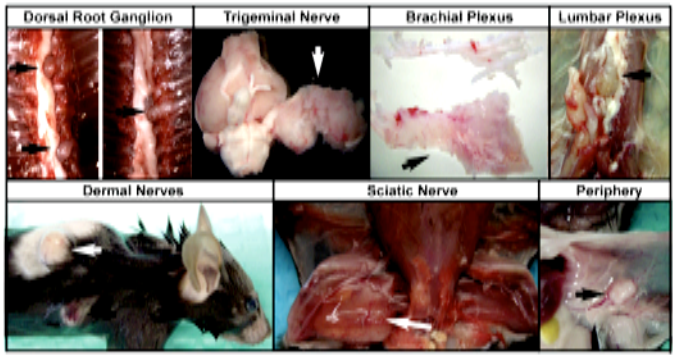
B)
Dorsal Root Ganglion
Trigeminal Nerve
Brachial Plexus
Lumbar Plexus
Dermal Nerves
Sciatic Nerve
Periphery

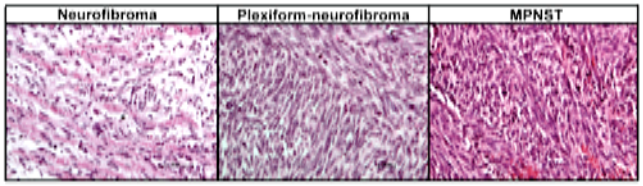
C)
Neurofibroma
Plexiform-neurofibroma
MPNST

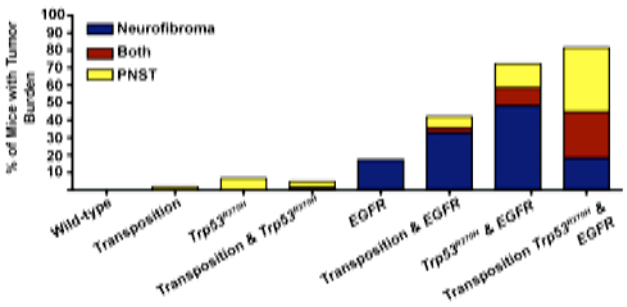
D)
% of Mice with Tumor Burden
Neurofibroma
Both
PNST
Wild-type
Transposition
Trp53
Transposition & Trp53
EGFR
Transposition & EGFR
Trp53 & EGFR
Transposition Trp53 & EGFR


E)
No Primary
Sleeping Beauty
Excision Assay

**Supplemental Table 1. Tumor penetrance, frequency, and latency for each genotype.** For each genotype representing all the animal cohorts, listed are the number of animals that developed a tumor (number in parenthesis represents total number in cohort), the average number of tumors with standard deviation per mouse, and the median time of tumor harvest with standard deviation per mouse. Since the mice often developed more than one type of tumor, the statistics were separated into 6 groups. The first three groups separated animals if they and one of the tumor types or both: animals that developed only neurofibromas (includes plexiform), animals that developed only MPNSTs, animals that developed only both tumor types. The last three groups separated animals that developed a specific tumor type regardless if another tumor type was present: animals with neurofibromas, animals with MPNSTs, and lastly any animal that had a Schwann cell tumor.

| | Neurofibroma Only | | | MPNST Only | | | Both Only | | | All MPNSTs | | | All Neurofibromas | | | All Tumors | | |
|---|---|---|---|---|---|---|---|---|---|---|---|---|---|---|---|---|---|---|
| Genotype | # Mice with Tumors | # Tumors/ Mouse | Median Harvest Time (Days) | # Mice with Tumors | # Tumors/ Mouse | Median Harvest Time (Days) | # Mice with Tumors | # Tumors/ Mouse | Median Harvest Time (Days) | # Mice with Tumors | # Tumors/ Mouse | Median Harvest Time (Days) | # Mice with Tumors | # Tumors/ Mouse | Median Harvest Time (Days) | # Mice with Tumors | # Tumors/ Mouse | Median Harvest Time (Days) |
| Control | 0 (76) | 0 | 0 | 0 (76) | 0 | 0 | 0 (76) | 0 | 0 | 0 (76) | 0 | 0 | 0 (76) | 0 | 0 | 0 (76) | 0 | 0 |
| Transposition | 1 (103) | 10±0 | 317 | 2 (103) | 1±0 | 319.5±135.1 | 0(103) | 0 | 0 | 2 (103) | 1±0 | 319.5±135.1 | 1 (103) | 10±0 | 317 | 3 (103) | 4±5.2 | 318±95.5 |
| *Trp53R270H* | 0 (29) | 0 | 0 | 2 (29) | 1±0 | 381±121.6 | 0 (29) | 0 | 449 | 2 (29) | 1±0 | 381±121.6 | 0 (29) | 0 | 0 | 2 (29) | 1±0 | 381±121.6 |
| *Trp53R270H* with Transposition | 1(61) | 7±0 | 385 | 2 (61) | 1±0 | 344.5±31.8 | 0 (61) | 0 | 0 | 2 (61) | 1±0 | 344.5±31.8 | 1(61) | 7±0 | 385 | 3 (61) | 3±3,5 | 364.5±29 |
| *CNPase-hEGFR* | 12 (69) | 5.1±2.1 | 358.5±53.3 | 0 (69) | 0 | 0 | 0 (69) | 0 | 0 | 0 (69) | 0 | 0 | 12 (69) | 5.1±2.1 | 358.5±53.3 | 12 (69) | 5.1±2.1 | 358.5±53.3 |
| *CNPase-hEGFR* with Transposition | 25 (76) | 6.2±4.1 | 419±74 | 5 (76) | 1±0 | 369±19.8 | 2 (76) | 9.5±3.5 | 397±71.4 | 7(76) | 1±0 | 369±36.1 | 27 (76) | 6.3±4.1± | 419±72.5 | 32 (76) | 5.4±4.3 | 403±78.6 |
| *Trp53R270H; CNPase-hEGFR* | 14 (29) | 6.6±3.5 | 401±61 | 4 (29) | 1.25±.5 | 253±140.1 | 3 (29) | 8.3±2.1 | 401±40.6 | 7 (29) | 1.3±.5 | 362±126.8 | 17 (29) | 6.7±3.3 | 401±59.0 | 21 (29) | 5.9±3.8 | 400±87.2 |
| *Trp53R270H; CNPase-hEGFR* with Transposition | 16 (87) | 5.1±3.9 | 279±79 | 32 (87) | 1.6±.9 | 292±74.4 | 23 (87) | 7.9±3.8 | 303±61.9 | 55 (87) | 1.7±.9 | 299±69.2 | 39 (87) | 5.6±3.9 | 301±68.6 | 71 (87) | 4.5±4 | 299±71 |

**Supplemental Figure 1. SB-derived MPNSTs undergo divergent differentiation.** (A) H&E staining of various SB-derived MPNSTs demonstrating the different types of divergent differentiation present that also occur in human MPNSTs. (B) Bar depicting the frequency that divergent differentiation occurred in plexiform-neurofibromas versus MPNSTs. No divergent differentiation was observed in neurofibromas.

A)

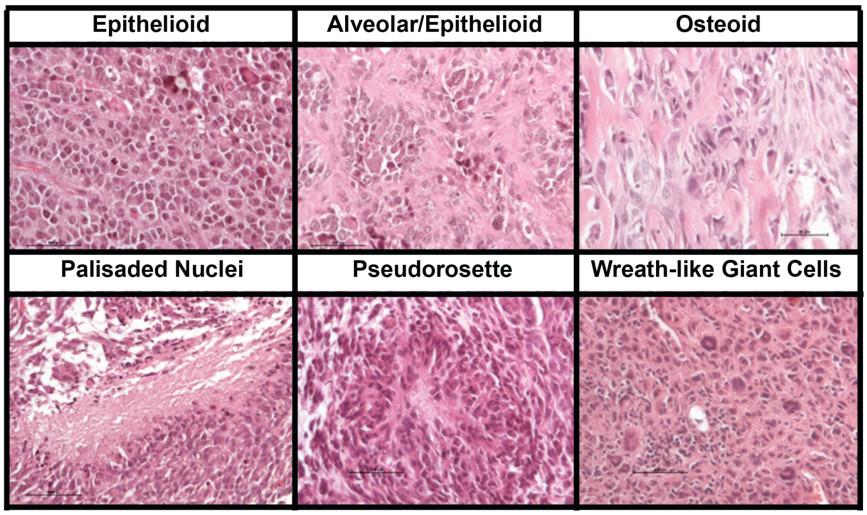
Epithelioid
Alveolar/Epithelioid
Osteoid
Palisaded Nuclei
Pseudorosette
Wreath-like Giant Cells

B)

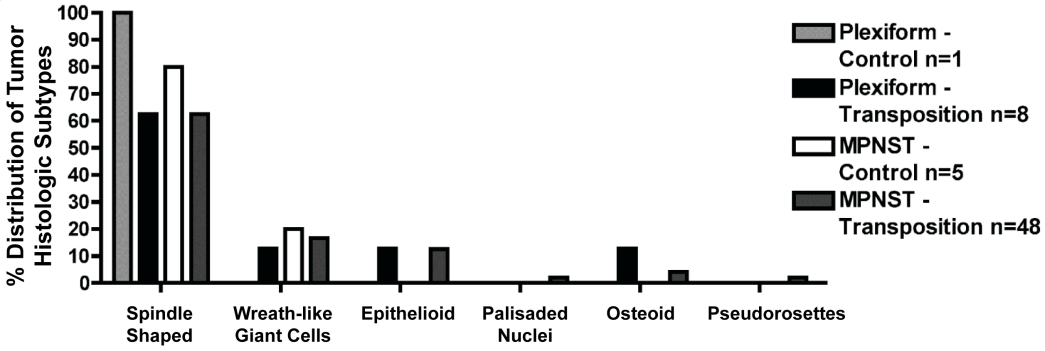
% Distribution of Tumor Histologic Subtypes
100
90
80
70
60
50
40
30
20
10
0
Spindle Shaped
Wreath-like Giant Cells
Epithelioid
Palisaded Nuclei
Osteoid
Pseudorosettes
Plexiform - Control n=1
Plexiform - Transposition n=8
MPNST - Control n=5
MPNST - Transposition n=48

**Supplemental Table 2. Full list of CIS-associated genes.** Tables listing all the CIS-associated genes/regions of the genomes for both neurofibromas (left) and MPNSTs (right). Each tumor type was divided into 3 columns. The first column lists the name of the CIS-associated gene or in the cases where no genes were present within 1MB, no predicted gene was listed. The second column lists the number of mice that possessed T2/On insertions that contributed to forming the CIS. The last column lists the genomic region the CISs span within the mouse genome build NCBI/mm9.

| Neurofibroma Associated CISs | | |
|---|---|---|
| CIS-associated Gene | Number Mice with Insertion | Chromosomal Location |
| *Nf1* | 18 | chr11:79180900-79380900 |
| *Mll5* | 14 | chr5:22835400-23035400 |
| *Csmd1* | 13 | chr8:16534200-16734200 |
| *Crebbp* | 13 | chr16:4046900-4246900 |
| *Rbm26* | 12 | chr14:105499300-105699300 |
| *Rbm16* | 11 | chr17:3134300-3234300 |
| *Ankrd17* | 11 | chr5:90623700-90823700 |
| *AK039113* | 11 | chr3:28173600-28373600 |
| *Arhgap12* | 11 | chr18:6034100-6234100 |
| *Ptpn13* | 11 | chr5:103820900-104020900 |
| *1700081L11Rik* | 11 | chr11:104197800-104297800 |
| *Plce1* | 11 | chr19:38627900-38827900 |
| *Cyp2j8* | 10 | chr4:96180000-96192500 |
| *Stag2* | 10 | chrX:39578300-39628300 |
| *Tnks* | 10 | chr8:35964600-36014600 |
| *no gene* | 10 | chrY:2850500-2900500 |
| *Qk* | 10 | chr17:10407500-10507500 |
| *Scn7a* | 10 | chr2:66461100-66661100 |
| *Srgap2* | 10 | chr1:133188900-133388900 |
| *Strn3* | 10 | chr12:52709400-52909400 |
| *Creb5* | 9 | chr6:53243100-53255600 |
| *AC131780* | 9 | chr9:3004800-3054800 |
| *Ccny* | 9 | chr18:9344800-9444800 |
| *Brd4* | 9 | chr17:32383800-32483800 |
| *Nedd4* | 9 | chr9:72406300-72606300 |
| *Whsc1* | 9 | chr5:34095600-34295600 |
| *Zfand3* | 9 | chr17:30146100-30346100 |
| *Sgcd* | 9 | chr11:46930800-47130800 |
| *Ankrd44* | 9 | chr1:54705100-54905100 |
| *Odz3* | 9 | chr8:49450800-49650800 |
| *Cadm2* | 9 | chr16:67159400-67359400 |
| *Ahsa2* | 9 | chr11:23209500-23409500 |
| *Lama4* | 9 | chr10:38694300-38894300 |
| *Utrn* | 9 | chr10:12367600-12567600 |
| *Taok1* | 8 | chr11:77356100-77406100 |
| *Pum2* | 8 | chr12:8699900-8749900 |
| *Wac* | 8 | chr18:7874500-7924500 |
| *Ube2g1* | 8 | chr11:72403500-72453500 |
| *Mllt10* | 8 | chr2:18060700-18160700 |
| *Grlf1* | 8 | chr7:17110700-17210700 |
| *Ehbp1* | 8 | chr11:22069200-22169200 |
| *Cxxc5* | 8 | chr18:35949700-36049700 |
| *Cadm1* | 8 | chr9:47413000-47613000 |

| MPNST Associated CISs | | |
|---|---|---|
| CIS-associated Gene | Number Mice with Insertion | Chromosomal Location |
| *Nf1* | 29 | chr11:79155400-79355400 |
| *Pten* | 23 | chr19:32851300-32901300 |
| *Stag2* | 9 | chrX:39423200-39623200 |
| *Eras* | 8 | chrX:7503900-7516400 |
| *Crebbp* | 8 | chr16:4086300-4286300 |
| *AC131780* | 6 | chr9:3005600-3030600 |
| *Foxr2* | 6 | chrX:149538600-149563600 |
| *Taok1* | 6 | chr11:77384400-77409400 |
| *Rasa3* | 6 | chr8:13605500-13705500 |
| *Zfand6* | 6 | chr7:91589700-91789700 |
| *Smc1a* | 5 | chrX:148444700-148494700 |
| *Fmnl2* | 5 | chr2:52884800-53084800 |
| *Rabgap1* | 5 | chr2:37190300-37390300 |
| *Thada* | 5 | chr17:84628000-84828000 |
| *Nox3* | 5 | chr17:3582400-3782400 |
| *Gpc5* | 5 | chr14:116078100-116278100 |
| *1700081L11Rik* | 5 | chr11:104205400-104405400 |
| *Cdc27* | 5 | chr11:104205400-104405400 |
| *Spag9* | 5 | chr11:93861800-94061800 |
| *Fbxw11* | 5 | chr11:32405700-32605700 |
| *Lrp4* | 5 | chr2:91213800-91413800 |
| *Atp10b* | 5 | chr11:42688600-42888600 |
| *Ppp3cb* | 4 | chr14:21347400-21359900 |
| *Slc16a12* | 4 | chr19:34737100-34749600 |
| *Gdi2* | 4 | chr13:3563200-3588200 |
| *Itpr3* | 4 | chr17:27222800-27247800 |
| *AC144860.1* | 4 | chr17:95231400-95256400 |
| *no gene* | 4 | chr4:5049600-5074600 |
| *no gene* | 4 | chrY:2868000-2918000 |
| *Igf1r* | 4 | chr7:75284800-75334800 |
| *Chl1* | 4 | chr6:103552800-103652800 |
| *Slc13a1* | 4 | chr6:24043200-24143200 |
| *Bet1* | 4 | chr6:3977500-4077500 |
| *Trip12* | 4 | chr1:84721500-84821500 |
| *Bmpr2* | 4 | chr1:59807200-59907200 |
| *Ralgapa1* | 4 | chr12:56782600-56882600 |
| *Nr6a1* | 4 | chr2:38626900-38726900 |
| *mmu-mir-181a-2* | 4 | chr2:38626900-38726900 |
| *mmu-mir-181b-2* | 4 | chr2:38626900-38726900 |
| *Epc2* | 4 | chr2:49320300-49420300 |
| *Tbc1d20* | 4 | chr2:152022600-152122600 |
| *Zfp217* | 4 | chr2:169903300-170003300 |
| *Gria3* | 4 | chrX:38784500-38884500 |

| | | | | | |
|---|---|---|---|---|---|
| *Cnot6l* | 8 | chr5:96438800-96638800 | *Lsm14a* | 4 | chr7:35110300-35210300 |
| *Birc6* | 8 | chr17:74897900-75097900 | *Prr8* | 4 | chr5:28646800-28746800 |
| *Tcba1* | 8 | chr10:32297300-32497300 | *AK139823* | 4 | chr12:26656900-26756900 |
| *Herc2* | 8 | chr7:63370300-63570300 | *Txndc11* | 4 | chr16:11074500-11174500 |
| *Psmd14* | 8 | chr2:61441100-61641100 | *Runx2* | 4 | chr17:44765000-44865000 |
| *Ndufs4* | 8 | chr13:115008500-115208500 | *Cugbp2* | 4 | chr2:6626700-6726700 |
| *Traf3* | 8 | chr12:112288500-112488500 | *Pak7* | 4 | chr2:135839900-135939900 |
| *Tcba1* | 8 | chr10:32003400-32203400 | *Cav1* | 4 | chr3:1724`065-17415317 |
| *Cul2* | 7 | chr18:3365200-3415200 | *Pard3* | 3 | chr8:129605700-129618200 |
| *Pias1* | 7 | chr9:62731000-62831000 | *Ptbp2* | 3 | chr3:119452300-119464800 |
| *Creb3l2* | 7 | chr6:37274500-37374500 | *Mark2* | 3 | chr19:7356000-7368500 |
| *Rfwd2* | 7 | chr1:161196100-161296100 | *Nf2* | 3 | chr11:4686600-4699100 |
| *Lama2* | 7 | chr10:27144500-27244500 | *Fgfr2* | 3 | chr7:137307900-137320400 |
| *Phip* | 7 | chr9:82796300-82896300 | *Coro1c* | 3 | chr5:114339000-114351500 |
| *Zfml* | 7 | chr6:83851400-83951400 | *Eri3* | 3 | chr4:117258600-117271100 |
| *Mll3* | 7 | chr5:24896100-24996100 | *Nfkb1* | 3 | chr3:135345600-135358100 |
| *Tnrc15* | 7 | chr1:89253600-89353600 | *Acvr1* | 3 | chr2:58285600-58298100 |
| *Cdc215* | 7 | chr13:17748300-17848300 | *Zswim6* | 3 | chr13:108598000-108610500 |
| *Nup153* | 7 | chr13:46766100-46866100 | *Rasa1* | 3 | chr13:85371700-85384200 |
| *Dmd* | 7 | chrX:82020300-82220300 | *0610007P08Rik* | 3 | chr13:63982000-63994500 |
| *Ncam1* | 7 | chr9:49408000-49608000 | *Ptch1* | 3 | chr13:63636900-63661900 |
| *Odz3* | 7 | chr8:49726300-49926300 | *Adipor2* | 3 | chr6:119318200-119343200 |
| *Sox6* | 7 | chr7:122963200-123163200 | *Picalm* | 3 | chr7:97295000-97320000 |
| *Sox6* | 7 | chr7:122710700-122910700 | *AK042944* | 3 | chr8:111048600-111073600 |
| *Plekha5* | 7 | chr6:140290100-140490100 | *Rasgrf1* | 3 | chr9:89856300-89881300 |
| *Atp8a1* | 7 | chr5:68045400-68245400 | *Ccdc93* | 3 | chr1:123361400-123386400 |
| *Mpdz* | 7 | chr4:80919200-81119200 | *Nek7* | 3 | chr1:140487700-140512700 |
| *Tox* | 7 | chr4:6611500-6811500 | *Dennd1b* | 3 | chr1:140930600-140955600 |
| *Ccdc85a* | 7 | chr11:28301200-28501200 | *Ube2e1* | 3 | chr14:19125600-19150600 |
| *Lims1* | 7 | chr10:57783300-57983300 | *Nde1* | 3 | chr16:14170100-14195100 |
| *Csmd1* | 7 | chr8:16931400-17131400 | *Fbxo34* | 3 | chr14:48096100-48121100 |
| *Nfib* | 7 | chr4:81931400-82131400 | *Zfp521* | 3 | chr18:14094000-14119000 |
| *Eml5* | 7 | chr12:99954600-100154600 | *Faf1* | 3 | chr4:109490400-109515400 |
| *Ube2w* | 7 | chr1:16455400-16655400 | *Sppl3* | 3 | chr5:115487700-115512700 |
| *Ddx10* | 6 | chr9:52994600-53007100 | *Zfp868* | 3 | chr8:72062600-72087600 |
| *Ggnbp2* | 6 | chr11:84670400-84682900 | *RP23-326E10.1* | 3 | chrX:109874800-109899800 |
| *Galnt13* | 6 | chr2:54470600-54483100 | *AL929540.1* | 3 | chrX:88471200-88521200 |
| *mmu-mir-30a* | 6 | chr1:23268000-23293000 | *Tnks* | 3 | chr8:36023900-36073900 |
| *D17Wsu92e* | 6 | chr17:27907500-27957500 | *no gene* | 3 | chr5:56237100-56287100 |
| *Col5a1* | 6 | chr2:27774100-27824100 | *no gene* | 3 | chr17:61993300-62043300 |
| *Sbf2* | 6 | chr7:117498700-117598700 | *Pvrl3* | 3 | chr16:46492000-46542000 |
| *Cutl1* | 6 | chr5:136880100-136980100 | *Tbc1d5* | 3 | chr17:50967600-51017600 |
| *Med13l* | 6 | chr5:119096900-119196900 | *Cpsf6* | 3 | chr10:116774300-116824300 |
| *Spata6* | 6 | chr4:111396400-111496400 | *Sec63* | 3 | chr10:42510400-42560400 |
| *AA536749* | 6 | chr11:59503700- | *Arid4a* | 3 | chr12:72091900- |

| | | | | | |
|---|---|---|---|---|---|
| | | 59603700 | | | 72141900 |
| *mmu-mir-744* | 6 | chr11:65516500-65616500 | *Wdr20a* | 3 | chr12:111984100-112034100 |
| *Rock2* | 6 | chr12:16907600-17007600 | *Gmds* | 3 | chr13:32014400-32064400 |
| *Diap2* | 6 | chrX:126315300-126415300 | *Gcap14* | 3 | chr14:37773100-37823100 |
| *Nfatc3* | 6 | chr8:108587400-108687400 | *Kif22* | 3 | chr7:134182500-134232500 |
| *Csmd1* | 6 | chr8:17371200-17471200 | *Insc* | 3 | chr7:121893100-121943100 |
| *Csmd1* | 6 | chr8:16024000-16124000 | *AC113955.2* | 3 | chr7:46820700-46870700 |
| *Dock1* | 6 | chr7:142237000-142337000 | *Setd5* | 3 | chr6:113048800-113098800 |
| *Dock1* | 6 | chr7:142050300-142150300 | *Ahcyl1* | 3 | chr3:107461800-107511800 |
| *Schip1* | 6 | chr3:68332300-68432300 | *Arnt* | 3 | chr3:95277500-95327500 |
| *Map4k4* | 6 | chr1:39963300-40063300 | *SH3d19* | 3 | chr3:85800800-85850800 |
| *Slc35f1* | 6 | chr10:52676800-52776800 | *Fstl5* | 3 | chr3:76426200-76476200 |
| *March3* | 6 | chr18:56916900-57016900 | *Kpna4* | 3 | chr3:68889100-68939100 |
| *Macrod2* | 5 | chr2:141350800-141363300 | *AC123747.1* | 3 | chr3:14793400-14843400 |
| *Sesn3* | 5 | chr9:14089100-14101600 | *Agps* | 3 | chr2:75704200-75754200 |
| *Ptbp2* | 5 | chr3:119435200-119460200 | *Keg1* | 3 | chr19:12764400-12814400 |
| *Mbnl1* | 5 | chr3:60321900-60346900 | *D18Ertd653e* | 3 | chr18:68293100-68343100 |
| *5730446C15Rik* | 5 | chr19:21745100-21770100 | *Plxna2* | 3 | chr1:196584100-196634100 |
| *2310035C23Rik* | 5 | chr1:107613000-107638000 | *Spred2* | 3 | chr11:19862400-19912400 |
| *Smg7* | 5 | chr1:154701800-154726800 | *Tom1l2* | 3 | chr11:60086900-60136900 |
| *BC016423* | 5 | chr13:3548300-3573300 | *Hlf* | 3 | chr11:90221300-90271300 |
| *Ppp2r2a* | 5 | chr14:67645300-67670300 | *Ayt12* | 3 | chr13:73622200-73672200 |
| *Pten* | 5 | chr19:32835200-32860200 | | | |
| *Rcor3* | 5 | chr1:193928300-193953300 | | | |
| *Serinc5* | 5 | chr13:93455000-93480000 | | | |
| *Herc1* | 5 | chr9:66223100-66273100 | | | |
| *Bbs9* | 5 | chr9:22470500-22520500 | | | |
| *no gene* | 5 | chr9:31844000-31894000 | | | |
| *Myo9b* | 5 | chr8:73835600-73885600 | | | |
| *Cntn4* | 5 | chr6:105917300-105967300 | | | |
| *Cyth3* | 5 | chr5:144384400-144434400 | | | |
| *Orc3l* | 5 | chr4:34513300-34563300 | | | |
| *Tmtc2* | 5 | chr10:104632900-104682900 | | | |
| *Eml5* | 5 | chr12:100031700-100081700 | | | |
| *Papd4* | 5 | chr13:93924800-93974800 | | | |
| *Cog3* | 5 | chr14:76116800-76166800 | | | |
| *BC003993* | 5 | chr2:77759700-77809700 | | | |
| *Btbd3* | 5 | chr2:138091400-138141400 | | | |
| *Stxbp6* | 5 | chr12:46150400-46200400 | | | |
| *Erg* | 5 | chr16:95609100-95659100 | | | |
| *Arid1b* | 5 | chr17:5094900-5144900 | | | |
| *Prkg1* | 5 | chr19:31447100-31497100 | | | |
| *A930041I02Rik* | 5 | chr2:38999000-39049000 | | | |
| *G63001rF10Rik* | 5 | chrX:68323200-68423200 | | | |
| *Zfp553* | 5 | chr7:134647400-134747400 | | | |
| *Kcnip4* | 5 | chr5:49411400- | | | |

| | | |
|---|---|---|
| | | 49511400 |
| *Cacna2d1* | 5 | chr5:15476600-15576600 |
| *Pdlim5* | 5 | chr3:141979500-142079500 |
| *Rbms1* | 5 | chr2:60701600-60801600 |
| *Lrp1b* | 5 | chr2:41499500-41599500 |
| *Cacnb2* | 5 | chr2:14593700-14693700 |
| *Phlpp1* | 5 | chr1:108122900-108222900 |
| *Nav3* | 5 | chr10:109317500-109417500 |
| *Ube2g1* | 5 | chr11:72464300-72564300 |
| *Tlk2* | 5 | chr11:105031500-105131500 |
| *Epc1* | 5 | chr18:6433700-6533700 |
| *Kcnn2* | 5 | chr18:45819400-45919400 |
| *Prkg1* | 5 | chr19:30980600-31080600 |
| *Sorbs2* | 5 | chr8:46534800-46634800 |
| *Csmd1* | 5 | chr8:16207700-16307700 |
| *Faf1* | 5 | chr4:109379300-109479300 |
| *Zfhx4* | 5 | chr3:5277600-5377600 |
| *Ranbp29* | 5 | chr13:43504900-43604900 |
| *Map4k3* | 5 | chr17:80993000-81093000 |
| *Vti1b* | 4 | chr12:80262300-80274800 |
| *Jmjd1b* | 4 | chr18:34942900-34955400 |
| *Zfp608* | 4 | chr18:55123900-55136400 |
| *Raly* | 4 | chr2:154678400-154690900 |
| *AI314180* | 4 | chr4:58811700-58824200 |
| *Ppp1cb* | 4 | chr5:32793500-32806000 |
| *Stim2* | 4 | chr5:54494100-54506600 |
| *Usp47* | 4 | chr7:119226600-119239100 |
| *9430010O03Rik* | 4 | chr8:8665500-8678000 |
| *Ptprg* | 4 | chr14:12755900-12768400 |
| *Ppp1r12b* | 4 | chr1:136827700-136840200 |
| *Adam23* | 4 | chr1:63552400-63564900 |
| *Prdm5* | 4 | chr6:65759000-65784000 |
| *Sbno1* | 4 | chr5:124819700-124844700 |
| *BC031434* | 4 | chr4:144768900-144793900 |
| *Setd7* | 4 | chr3:51344300-51369300 |
| *Smad4* | 4 | chr18:73801900-73826900 |
| *Ppm1b* | 4 | chr17:85380800-85405800 |
| *Vapa* | 4 | chr17:65944900-65969900 |
| *Cd2ap* | 4 | chr17:42972400-42997400 |
| *no gene* | 4 | chr10:8769500-8794500 |
| *Ube2g2* | 4 | chr10:77076700-77101700 |
| *Snx13* | 4 | chr12:35727300-35752300 |
| *Pcnx* | 4 | chr12:82976500-83001500 |
| *Cyp7b1* | 4 | chr3:18034000-18059000 |
| *Bptf* | 4 | chr11:106951400-106976400 |
| *Adamts17* | 4 | chr7:74069000-74094000 |
| *Insr* | 4 | chr8:3214500-3239500 |

| | | |
|---|---|---|
| *Myst3* | 4 | chr8:24012200-24037200 |
| *4732435N0Rik* | 4 | chr8:71003700-71028700 |
| *2400003C14Rik* | 4 | chr8:112199800-112224800 |
| *Zbtb44* | 4 | chr9:30843700-30868700 |
| *AK084170* | 4 | chr9:41348500-41373500 |
| *Tmod3* | 4 | chr9:75384300-75409300 |
| *Ptchd1* | 4 | chrX:152001700-152051700 |
| *Utx* | 4 | chrX:17772000-17822000 |
| *Sept7* | 4 | chr9:25063000-25113000 |
| *Xpo6* | 4 | chr7:133284900-133334900 |
| *Picalm* | 4 | chr7:97312500-97362500 |
| *Ntrk3* | 4 | chr7:85494900-85544900 |
| *Ube3a* | 4 | chr7:66488400-66538400 |
| *Wnk1* | 4 | chr6:119913700-119963700 |
| *Creb5* | 4 | chr6:53515500-53565500 |
| *Wasl* | 4 | chr6:24567500-24617500 |
| *Snd1* | 4 | chr6:28538300-28588300 |
| *Gnai1* | 4 | chr5:17824600-17874600 |
| *Reln* | 4 | chr5:21462200-21512200 |
| *Cadps2* | 4 | chr6:23716600-23766600 |
| *Txndc4* | 4 | chr4:48255600-48305600 |
| *Zcchc7* | 4 | chr4:44812200-44862200 |
| *Gulp1* | 4 | chr1:44632000-44682000 |
| *Vps41* | 4 | chr13:18841900-18891900 |
| *Dach1* | 4 | chr14:98232800-98282800 |
| *Zfp407* | 4 | chr18:84619300-84669300 |
| *Spire1* | 4 | chr18:67716800-67766800 |
| *Rnf13* | 4 | chr3:57542000-57592000 |
| *Cnksr2* | 4 | chrX:154314500-154364500 |
| *Mtap4* | 4 | chr9:109885000-109935000 |
| *Arhgef12* | 4 | chr9:42766800-42816800 |
| *Map3k7ip2* | 4 | chr10:7632200-7682200 |
| *Nf2* | 4 | chr11:4663300-4713300 |
| *Lpp* | 4 | chr16:24893100-24943100 |
| *Fvr13* | 4 | chr16:46451300-46501300 |
| *Pag1* | 4 | chr3:9764900-9814900 |

**Table 1. Top 10 CIS-associated genes for SB-derived neurofibromas and MPNSTs.** Table listing the top 10 CISs for each tumor type observed. Each tumor type was divided into 3 columns. The first column lists the name of the CIS-associated gene. The second column lists the number of mice that possessed T2/Onc insertions that contributed to forming the CIS. The last column lists the genomic region the CISs span within the mouse genome build NCBI/mm9 on ensembl.org

| Top 10 Neurofibroma Associated CISs | | | Top 10 MPNST Associated CISs | | |
|---|---|---|---|---|---|
| CIS-associated Gene | Number Mice with Insertion | Chromosomal Location | CIS-associated Gene | Number Mice with Insertion | Chromosomal Location |
| *Nf1* | 18 | chr11:79180900-79380900 | *Nf1* | 29 | chr11:79155400-79355400 |
| *Mll5* | 14 | chr5:22835400-23035400 | *Pten* | 23 | chr19:32851300-32901300 |
| *Csmd1* | 13 | chr8:16534200-16734200 | *Stag2* | 9 | chrX:39423200-39623200 |
| *Crebbp* | 13 | chr16:4046900-4246900 | *Eras* | 8 | chrX:7503900-7516400 |
| *Rbm26* | 12 | chr14:105499300-105699300 | *Crebbp* | 8 | chr16:4086300-4286300 |
| *Rbm16* | 11 | chr17:3134300-3234300 | *AC131780* | 6 | chr9:3005600-3030600 |
| *Ankrd17* | 11 | chr5:90623700-90823700 | *Foxr2* | 6 | chrX:149538600-149563600 |
| *Arhgap12* | 11 | chr18:6034100-6234100 | *Taok1* | 6 | chr11:77384400-77409400 |
| *Ptpn13* | 11 | chr5:103820900-104020900 | *Rasa3* | 6 | chr8:13605500-13705500 |
| *Plce1* | 11 | chr19:38627900-38827900 | *Zfand6* | 6 | chr7:91589700-91789700 |

**Figure 2. *Nf1* and *Pten* identified as cooperating mutations.** (A) Heat map illustrating how often T2/Onc insertions in genes from the Top-10 CIS list co-occurred with one another in MPNST tumors. (B) Heat map illustrating the number of tumors that had insertions in *Pten* (red lines on top row) and *Nf1* (red lines on middle row) within MPNSTs (bottom row red) and neurofibromas (bottom row open black space). 13/62 animals that had MPNSTs had insertions in both *Nf1* and *Pten* $p<7.94e-05$ (C) Heat map of human microarray data of Schwann cell tumor development. The top heat map illustrates microarray data of purified Schwann cells from human tissues, the bottom heat map is microarray data from bulk human tissues. Normal human nerve (NH), dermal neurofibromas (dNF), plexiform-neurofibromas (pNF), and MPNSTs.

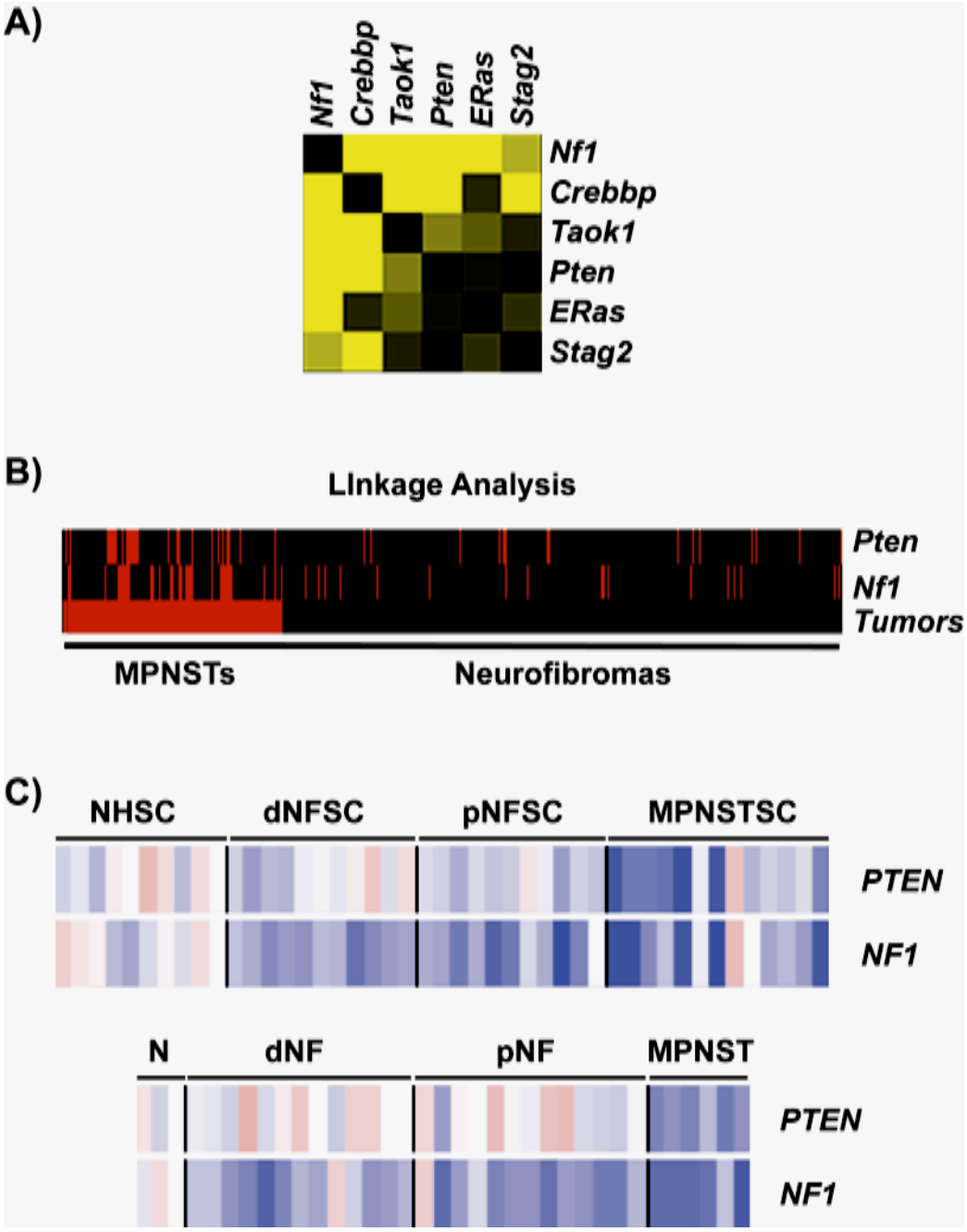
A)
Nf1
Crebbp
Taok1
Pten
ERas
Stag2
Nf1
Crebbp
Taok1
Pten
ERas
Stag2
B)
LInkage Analysis
Pten
Nf1
Tumors
MPNSTs
Neurofibromas
C)
NHSC
dNFSC
pNFSC
MPNSTSC
PTEN
NF1
N
dNF
pNF
MPNST
PTEN
NF1

**Supplemental Figure 2. Ingenuity pathway analysis of MPNST CISs gene networks.** 83 CIS-associated genes were analyzed using IPA software. From this analysis, 3 networks were enriched for the MPNST CIS-associated genes, shaded in grey on the network maps. The first network was the gene expression in cardiac development in which 30 CISs contributed to the total 54 genes in the network. For the neurological cancer network, 27 CISs contributed to the total 48 genes in the network. For the cell morphology network, 22 CISs contributed to the total 42 genes in the network.

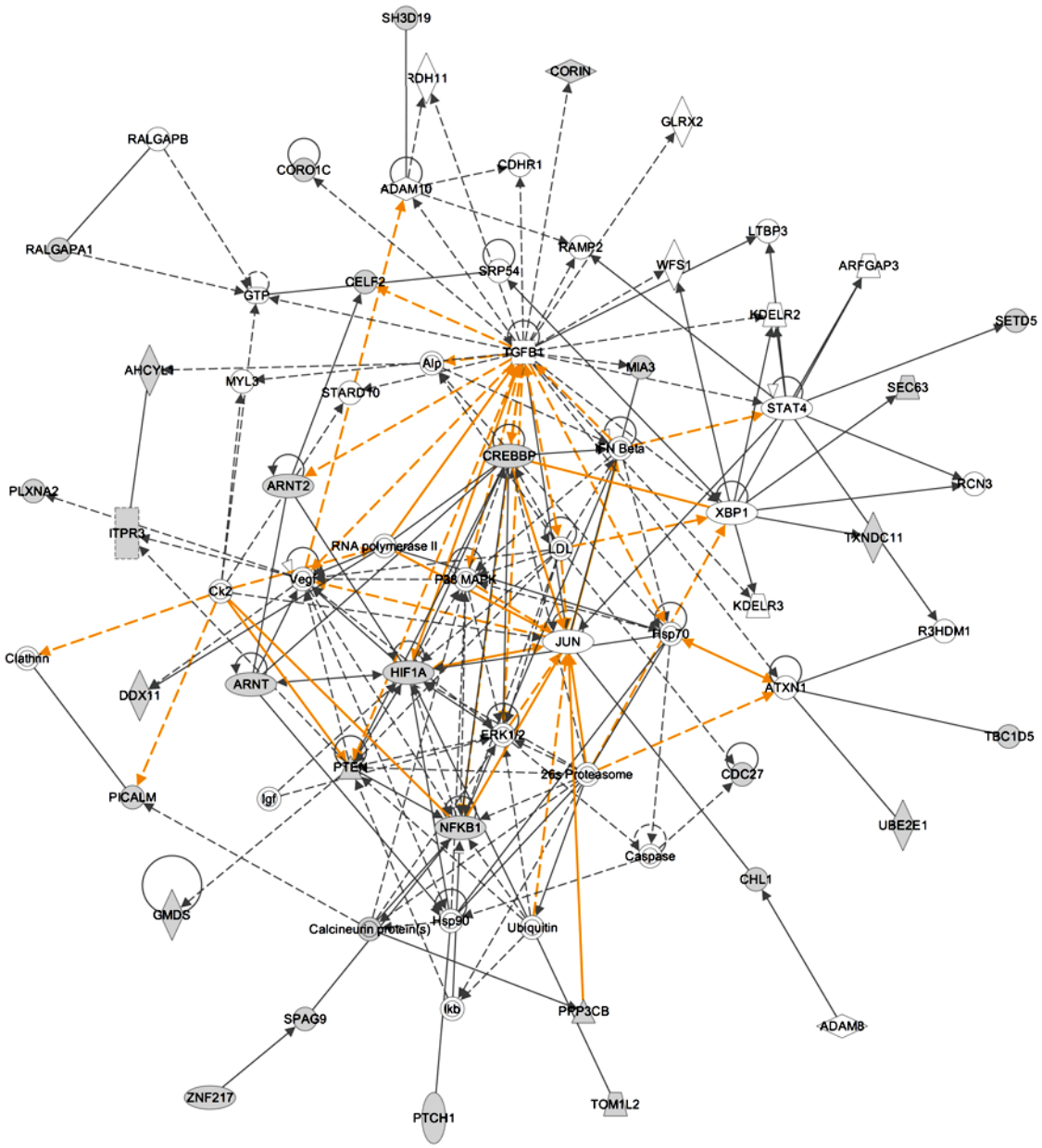
SH3D19
RDH11
CORIN
GLRX2
RALGAPB
CORO1C
CDHR1
ADAM10
RALGAPA1
RAMP2
LTBP3
WFS1
ARFGAP3
GTP
CELF2
SRP54
KDELR2
SETD5
TGFB1
AHCYL1
Alp
MIA3
MYL3
STARD10
SEC63
STAT4
CREBBP
IFN Beta
PLXNA2
ARNT2
RCN3
XBP1
ITPR3
TXNDC11
RNA polymerase II
LDL
Vegf
P38 MAPK
Ck2
KDELR3
Hsp70
R3HDM1
Clathrin
JUN
HIF1A
ARNT
ATXN1
DDX11
TBC1D5
ERK1/2
PTEN
26s Proteasome
CDC27
PICALM
Igf
NFKB1
UBE2E1
Caspase
CHL1
GMDS
Hsp90
Calcineurin protein(s)
Ubiquitin
Ikb
SPAG9
PPP3CB
ADAM8
ZNF217
PTCH1
TOM1L2

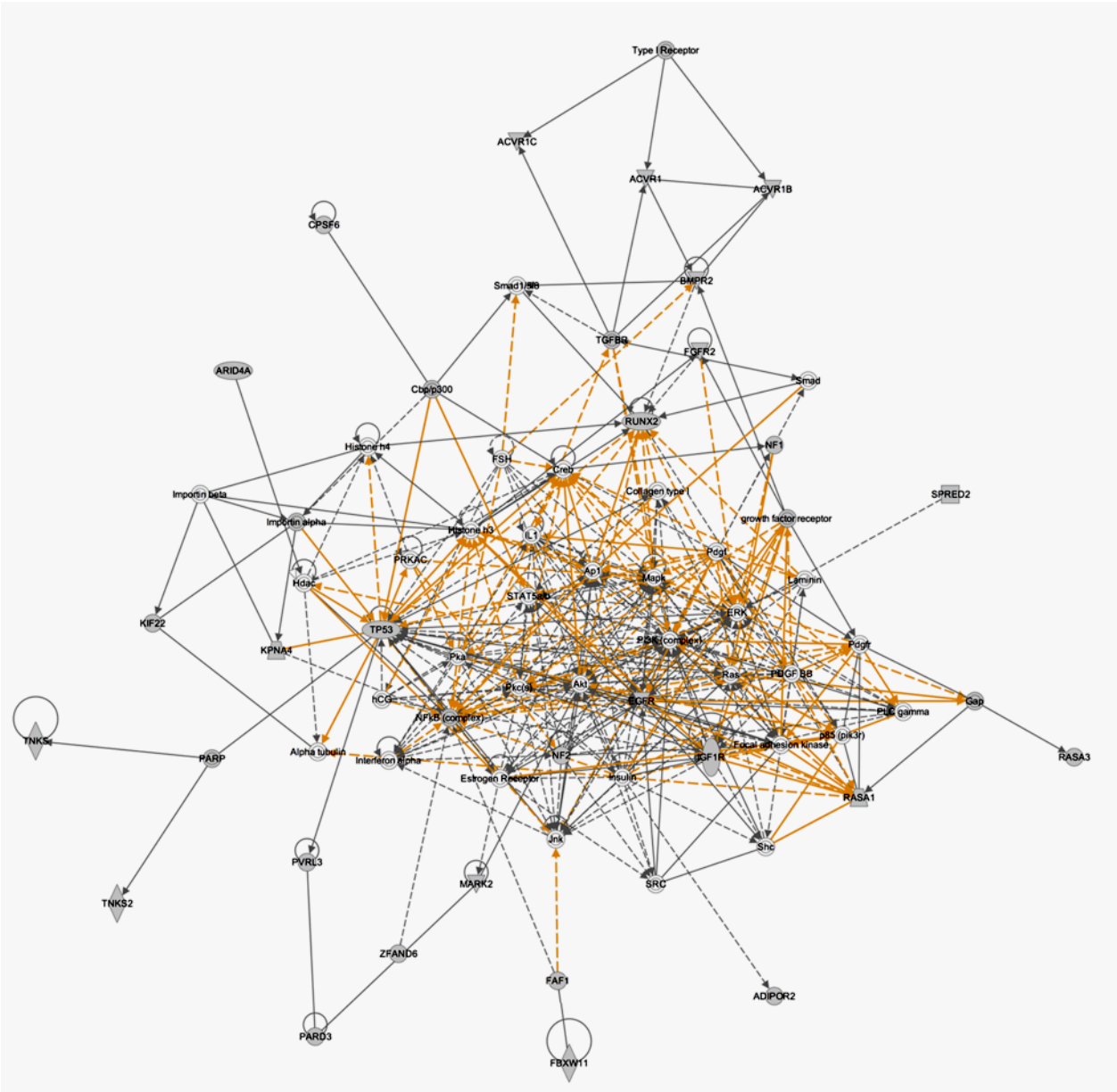
Type I Receptor
ACVR1C
ACVR1
ACVR1B
CPSF6
Smad1/5/8
BMPR2
TGFBR
FGFR2
ARID4A
Cbp/p300
Smad
RUNX2
Histone h4
NF1
FSH
Creb
Importin beta
Collagen type I
SPRED2
Importin alpha
Histone h3
IL1
growth factor receptor
PRKAC
Pdgf
Hdac
Ap1
Mapk
Laminin
STAT5a/b
ERK
KIF22
TP53
PI3K (complex)
Pdgf
KPNA4
Pka
Ras
PDGF BB
hCG
Pkc(s)
Akt
EGFR
Gap
PLC gamma
NFkB (complex)
p85 (pik3r)
TNKS
Focal adhesion kinase
RASA3
PARP
Alpha tubulin
Interferon alpha
NF2
IGF1R
Estrogen Receptor
Insulin
RASA1
Jnk
Shc
PVRL3
MARK2
SRC
TNKS2
ZFAND6
FAF1
ADIPOR2
PARD3
FBXW11

**Supplemental Figure 3. Ingenuity pathway analysis of MPNST CISs signaling pathways.** 83 CIS-associated genes were analyzed using IPA software. From this analysis, 55 signaling pathways were significantly enriched with a p-value<0.05 (listed on the left). The p-values for each signaling pathway are depicted in the bar graph on the right. The vertical red line depicts the significance threshold.

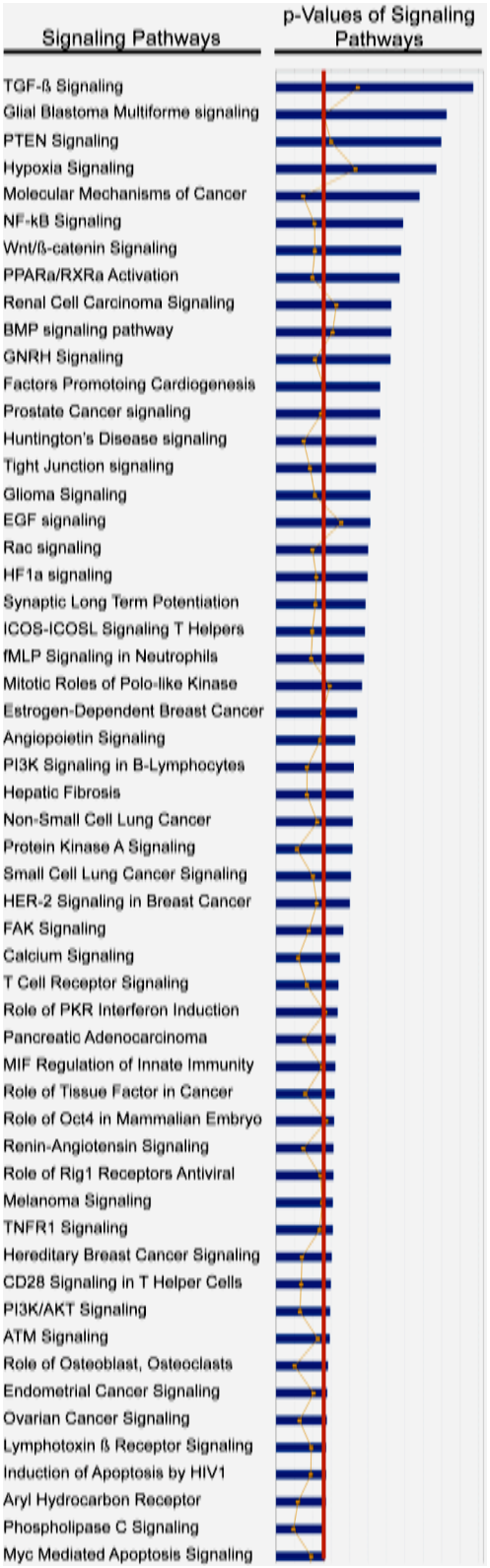
Signaling Pathways
p-Values of Signaling Pathways
TGF-ß Signaling
Glial Blastoma Multiforme signaling
PTEN Signaling
Hypoxia Signaling
Molecular Mechanisms of Cancer
NF-kB Signaling
Wnt/ß-catenin Signaling
PPARa/RXRa Activation
Renal Cell Carcinoma Signaling
BMP signaling pathway
GNRH Signaling
Factors Promotoing Cardiogenesis
Prostate Cancer signaling
Huntington's Disease signaling
Tight Junction signaling
Glioma Signaling
EGF signaling
Rac signaling
HF1a signaling
Synaptic Long Term Potentiation
ICOS-ICOSL Signaling T Helpers
fMLP Signaling in Neutrophils
Mitotic Roles of Polo-like Kinase
Estrogen-Dependent Breast Cancer
Angiopoietin Signaling
PI3K Signaling in B-Lymphocytes
Hepatic Fibrosis
Non-Small Cell Lung Cancer
Protein Kinase A Signaling
Small Cell Lung Cancer Signaling
HER-2 Signaling in Breast Cancer
FAK Signaling
Calcium Signaling
T Cell Receptor Signaling
Role of PKR Interferon Induction
Pancreatic Adenocarcinoma
MIF Regulation of Innate Immunity
Role of Tissue Factor in Cancer
Role of Oct4 in Mammalian Embryo
Renin-Angiotensin Signaling
Role of Rig1 Receptors Antiviral
Melanoma Signaling
TNFR1 Signaling
Hereditary Breast Cancer Signaling
CD28 Signaling in T Helper Cells
PI3K/AKT Signaling
ATM Signaling
Role of Osteoblast, Osteoclasts
Endometrial Cancer Signaling
Ovarian Cancer Signaling
Lymphotoxin ß Receptor Signaling
Induction of Apoptosis by HIV1
Aryl Hydrocarbon Receptor
Phospholipase C Signaling
Myc Mediated Apoptosis Signaling

**Figure 3. Reduced Caveolin-1 expression leads to increased ß-Catenin expression.** (A) Schematic of the 6 Cav1 isoforms coded in the mouse. Arrows represent the T2/Onc insertions that contributed to CIS formation. (B) Heat map of microarray data of *Cav1* expression in mouse tissues on top (nerve, neurofibromas, and MPNSTs) and *CAV1* expression in bulk human tissues below (nerve, dermal neurofibromas, plexiform-neurofibromas, and MPNSTs). (C) Immunofluorescent analysis of Cav1 and ß-Catenin expression from MPSNT cell lines derived from tumors containing a *Cav1* insertion (lower) and from control non-SB derived MPNST cell lines (upper). (D) Western blot of Cav1 expression in 2 immortalized rat Schwann cell lines targeted with 3 different *Cav1-shRNA* constructs. The non-silencing shRNA served as a control (NS), Actin expression served as loading control. (E) Immunofluorescent analysis of *ß-Catenin* expression (green) and the *Cav1-shRNA* (red). Panel on left shows 2 cells expressing *Cav1-shRNA* (red) and 2 cells that are not expressing the shRNA. The panel on right illustrates ß-Catenin expression of the cells from the left panel.

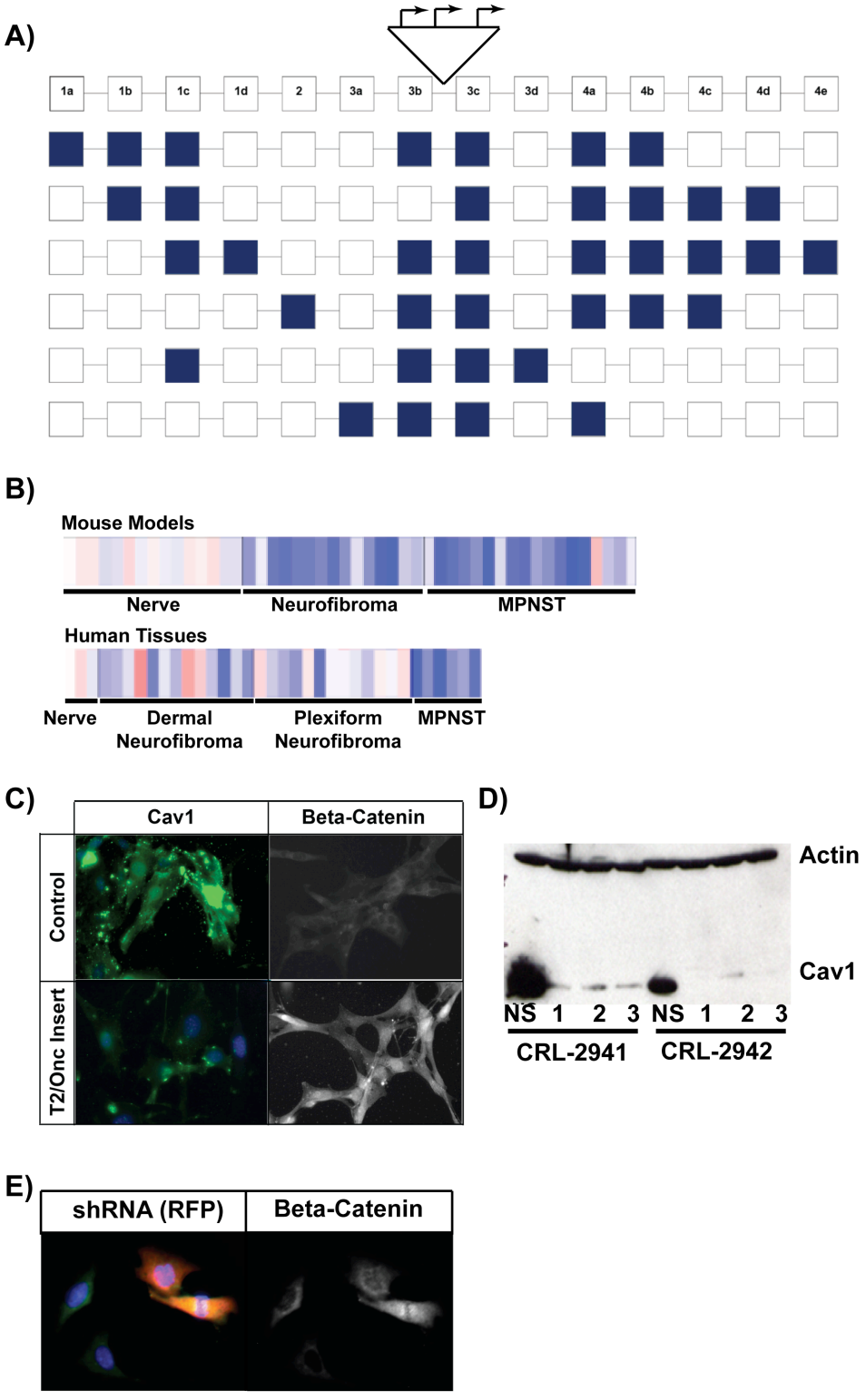
A)
1a
1b
1c
1d
2
3a
3b
3c
3d
4a
4b
4c
4d
4e
B)
Mouse Models
Nerve
Neurofibroma
MPNST
Human Tissues
Nerve
Dermal Neurofibroma
Plexiform Neurofibroma
MPNST
C)
Cav1
Beta-Catenin
Control
T2/Onc Insert
D)
Actin
Cav1
NS 1 2 3 NS 1 2 3
CRL-2941
CRL-2942
E)
shRNA (RFP)
Beta-Catenin

**Figure 4. Reduced *Cav1* expression with *EGFR* overexpression cooperate to form neurofibromas and PNSTs in vivo.**

(A) Histological analysis of the paraspinal DRG from each of the 3 genotypic cohorts to determine grade of tumor. (B) Scatter-plot depicting the widths of DRG from 2 mice from each genotypic cohort. (C) Histological analysis for alterations in downstream signaling within the DRG of each genotype.

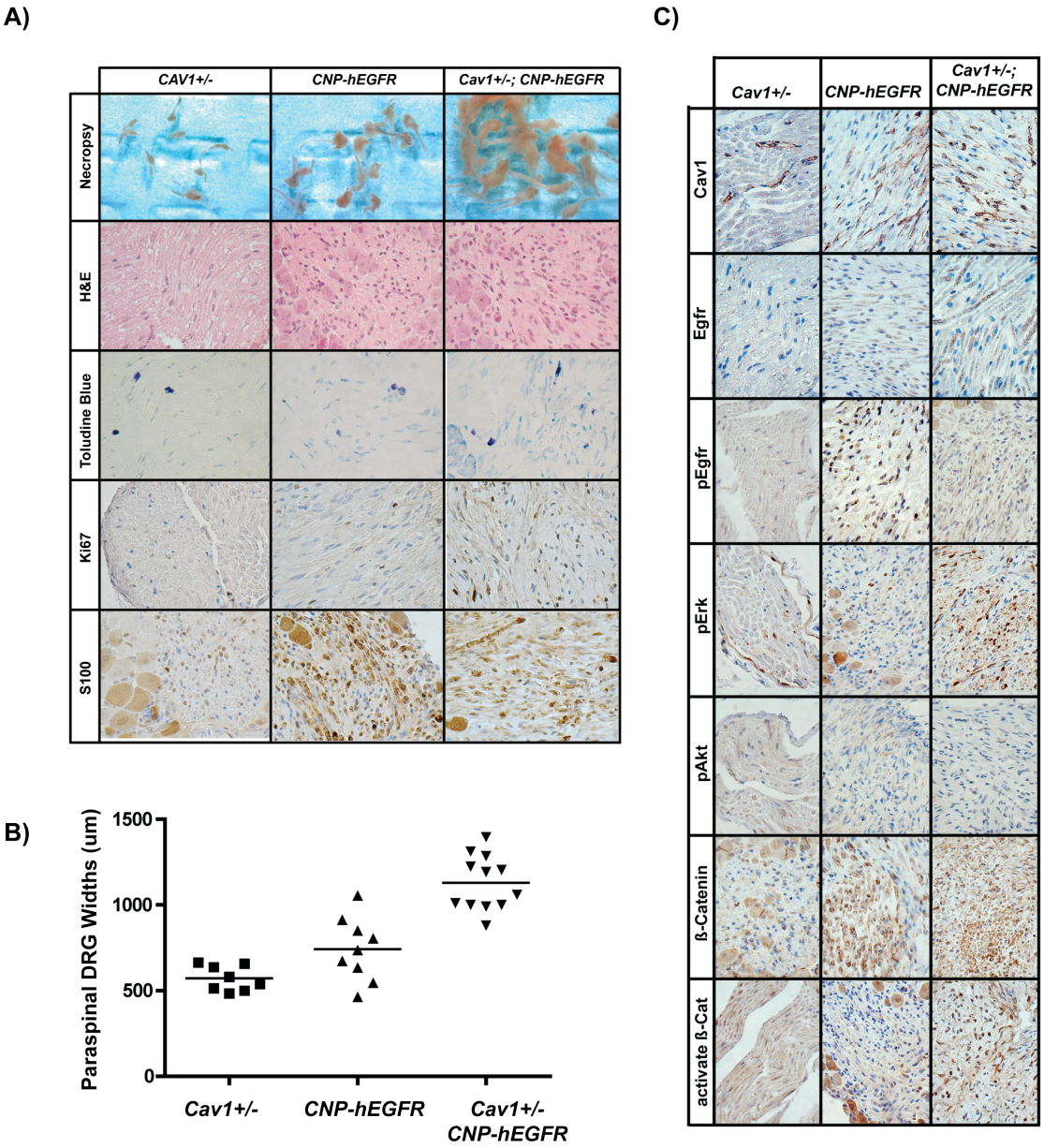
A)
CAV1+/-
CNP-hEGFR
Cav1+/-; CNP-hEGFR
Necropsy
H&E
Toludine Blue
Ki67
S100
B)
Paraspinal DRG Widths (um)
1500
1000
500
0
Cav1+/-
CNP-hEGFR
Cav1+/-
CNP-hEGFR
C)
Cav1+/-
CNP-hEGFR
Cav1+/-;
CNP-hEGFR
Cav1
Egfr
pEgfr
pErk
pAkt
ß-Catenin
activate ß-Cat

# Chapter 6.
# Concluding Remarks

At the start of my thesis project, little was known about the use of the *Sleeping Beauty* system for cancer gene discover. Collier et al. and Dupuy et al. pioneered the first SB screens identifying genes involved in sarcoma, lymphoma, and leukemia development [Collier, L.S. 2005; Dupuy, A.J. 2005]. From that point, there were still many major unresolved questions. We did not know whether the SB system would be amenable to identifying genes involved in epithelial cell cancers. Could it be specifically targeted to specific cell types? Are genetic predisposition backgrounds needed for all cancer screens? Can we model all stages of human cancer progression? A culmination of my thesis work and the work of many others has been able to address these questions. Epithelial cell cancers can be induced by SB mutagenesis and cell type specific expression of SB can be achieved. In addition, we learned genetic predisposition backgrounds are not needed to model all cancer types such as liver, colorectal, and osteosarcoma [Starr, T.K. 2009; Keng, V.W. 2009, Branden Moriarity unpublished results]. Importantly, we know that the SB mutagenesis system not only histologically but also genetically models human cancer progression [Starr, T.K. 2009; Keng, V.W. 2009; Rahrmann, E.P. 2009; unpublished results].

The focus of this thesis was identification of new genes and genetic pathways altered in prostate cancer and malignant peripheral nerve sheath tumor formation utilizing a *Sleeping Beauty* somatic mutagenesis forward genetic screen. Mutagenesis of prostate epithelial cells gave rise to proliferative cell lesions that resembled early stages of prostate cancer. From these lesions, *Pde4d*, *Klhl13*, *Braf*, and *Nras* were identified as CISs. Moreover, *Pde4d* was shown to be a pro-proliferative factor in human prostate cancer cell lines and to be overexpressed in human prostate cancers. *SB* mutagenesis in Schwann cells gave rise to all stages of Schwann cell tumorigenesis including benign neurofibromas, plexiform neurofibromas, and aggressive MPNSTs. From these tumors, hundreds of CISs were identified including known tumor suppressors *Nf1*, *Pten,* and *Cav1*. Experiments with loss of *Cav1* demonstrated cooperativity with *EGFR* overexpression *in vivo* for Schwann cell tumorigenesis. This chapter will further discuss significant findings and focus on unanswered questions and future directions.

**PDE4D as a therapeutic target for prostate cancer.**

*Sleeping Beauty* mutagenesis in prostate epithelial cells identified *Pde4d* as a CIS in proliferative prostate epithelial cell lesions that histologically resemble early stages of prostate cancer [Rahrmann, E.P. 2009]. *PDE4D* was shown to be over-expressed in human prostate cancer cell lines and tumors of all grades [Rahrmann, E.P. 2009]. In addition, *PDE4D* knockdown by *shRNAs* decreased proliferation, migration, and tumor formation abilities of human prostate cancer cell lines in xenograft models [Rahrmann,E.P. 2009]. Therefore studies using inhibitors of PDE4D may prove effective in reducing human prostate cancer cell growth and migration *in vitro* and *in vivo* [Burgin, A.B. 2009].

Recently, genetically engineered mouse models of glioma demonstrated that overexpression of *PDE4A1* lead to decreased cAMP levels and increased tumorigenesis [Warrington, N.M. 2010]. Furthermore, Warrington et al. showed that treating an *NF1* mouse model of glioma with Rolipram, pan-PDE inhibitor, reduced tumor growth [Warrington, N.M. 2010]. These findings suggest that inhibiting phosphodiesterase function in some cancers may provide a benefit in disrupting cancer cell growth. Currently, PDE4 inhibitors are in clinical trials for treating a variety of ailments including depression, asthma, COPD, Crohn's disease, Alzheimer's disease, memory enhancement, and rheumatoid arthritis [Press, N.J. 2009]. Phase III clinical trial reports on depression, asthma, and COPD have shown small improvements in patients treated with PDE4 inhibitors (Rolipram, Roflumilast, Cilomilast) [Press, N.J. 2009]. Studies on the use of these inhibitors for cancer patients that have early stages of prostate cancer are warranted and may provide a benefit by delaying if not preventing prostate cancer progression.

**Determining the role of *KLHL13* in prostate cancer.**

Kelch-like 13, KLHL13, is an adaptor protein in the Cullin3-based E3 unbiquitin-protein ligase complex required for mitotic progression and cytokenesis [Furukawa, M. 2003; Sumara, I. 2007; Maerki, S. 2009]. This complex specifically ubiquitinates Aurora kinase B, AURKB [Maerki, S. 2009; Sumara, I. 2007]. Mutations that lead to overexpression and disregulation of AURKB cause spindle defects, chromosomal

missegregation, and malignant transformation of cells [Yeung, S.C.J. 2008]. Transposon insertions within *Klhl13* from proliferative prostate epithelial cell lesions predicted a loss-of-function affect on *Klhl13* gene expression [Rahrmann, E.P. 2009]. SAGE and Microarray analyses of human normal prostate tissue versus prostate cancer demonstrated reduced expression of *KLHL13* in human prostate cancer samples [Safran, M. 2003]. Moreover, the target of KLHL13 for ubiquitination, AURKB, is overexpressed in high grade prostate cancer tumors as well as human prostate caner cell lines [Chieffi, P. 2006]. *In vitro* studies with inhibitors of AURKB demonstrated reduced growth of human prostate cancer cell lines [Chieffi, P. 2006]. Taken together, I hypothesize KLHL13 functions as a tumor suppressor to regulate AURKB expression in prostate epithelial cells. Specifically, loss of *Klhl13* expression may directly lead to increased or stabilized expression of AURKB by reduced ubiquitination and proteasomal degradation causing transformation of prostate epithelial cells. Studies assessing the expression of *KLHL13* in human prostate cancer samples and *in vitro* studies modulating *KLHL13* expression may provide insight into a mechanism for ARUKB overexpression in human prostate cancer. Results from these experiments will lead to a better understanding on the mechanism of ARUKB regulation by KLHL13 in prostate development.

**Determining the role of *N-Ras* in prostate epithelial cell fate.**

*Braf* and *Nras* were identified as CISs from proliferative prostate epithelial cell lesions [Chapter 3]. Immunohistochemistry of prostate human prostate cancer samples demonstrated *BRAF* overexpression occurs in human prostate cancer. In addition, overexpression of *BRAF* in urogenital sinus organs showed significant increase in proliferation. In addition to altered proliferation, transposon mutagenized mice developed goblet-like cells (intestinal epithelial cells) within prostate glands. Interestingly, these samples were analyzed for T2/Onc insertions and transposon insertions within the *Nras* gene were associated with the altered epithelial cell phenotype.

Goblet-like cell phenotypes occur in transgenic mouse models of *H-Ras* overexpression in prostate epithelial cells or loss of $p63^{-/-}$ l [Scherl, A. 2004; Kurita, T. 2004]. Moreover, the presence of goblet-like cells within human prostate tumors has

been documented [Saito, S. 1999; Saez,C. 1998]. However, overexpression of a mutant form of *Kras* in prostate epithelial cells did not lead to goblet-like cell differentiation [Pearson, H.B. 2009]. In addition, the H-Ras transgenic mouse model did not observe 100% penetrance of the goblet-like cell phenotype [Scherl, A. 2004]. This discrepancy in phenotype penetrance based on specific Ras expression suggests other cooperating genetic alterations are needed for altering prostate epithelial cell fate.

Further analysis of transposon insertions from the goblet-like cell phenotypes observed in transposon mutagenized prostates are warranted. Additional genes mutated by T2/Onc but not deemed CISs may cooperate with overexpression of *Nras* to alter prostate epithelial cell fate. To further define the role of *NRAS* in transdifferentiation of prostate epithelial cells to goblet-like cells, a mouse model specifically overexpressing *Nras* in the prostate epithelial cells is needed. Breeding these transgenic mice to transgenic mice of cooperating genes, identified from the analysis of transposon insertion sites in goblet-like cells, may demonstrate altered epithelial cell fate. Microarray analysis of prostates with goblet-like cells compared to control prostates may illustrate a genetic signature for epithelial cell fate. Elucidation of the mechanisms of epithelial cell fate will provide insight into the normal developmental pathways of epithelial cells.

**Dependence of *CNPase-hEGFR;Trp53*$^{+/-}$ derived MPNSTs on EGFR signaling.**

In human MPNSTs, *EGFR* gene amplification occurs frequently [Tawbi,H. 2008; Perry,A. 2002; Tabone-Eglinger,S. 2008]. To determine if EGFR is a good therapeutic target for treatment of MPNSTs, we must demonstrate that EGFR signaling is required for tumor maintenance. To address this concern, *CNPase-hEGFR;Trp53*$^{+/-}$ MPNST-derived cell lines will be transduced with a doxycyclin inducible *shRNA* targeting *EGFR*. Dependence on EGFR signaling on tumorigenicity will be assessed by monitoring for alterations in proliferation, apoptosis, anchorage independent growth, and tumorigenicity in nude mouse xenografts with cells expressing the *shRNA-EGFR*. Controls will be non-doxycyclin treated cells and cells transduced with a non-silencing shRNA.

If cells are dependent on EGFR signaling for survival and growth, reduction in *EGFR* expression would lead to reduced proliferation, anchorage independent growth,

reduced tumor formation in mice, and increased apoptosis. Furthermore, these experiments will be repeated with small molecule inhibitors targeting EGFR. Results from these experiments will determine if *CNPase-hEGFR;Trp53*$^{+/-}$ -derived MPNSTs are dependent on EGFR signaling for survival and growth.

**The role of *EGFR* overexpression and TP53 loss of function in human Schwann cell transformation.**

Overexpression of *EGFR* and loss of Trp53 function in Schwann cells cooperated in mice to form MPNSTs [Chapter 5]. Moreover, these tumors histologically and cytogenetically resembled human MPNSTs. To address whether *EGFR* overexpression and TP53 loss of function cooperate in human Schwann cell transformation, *EGFR* and *TP53* expression will be modulated in an immortalized human Schwann cell line (HSC2λ). HSC2λ was generated from normal human Schwann cells and immortalized with *TERT* and *CDK4* (developed by laboratory of Dr. Margaret Wallace, unpublished). Previous studies in immortalized human esophageal cell lines demonstrated that *EGFR* overexpression, loss of TP53 function, and TERT activation cooperated to transform immortalized esophageal cell lines [Okawa,T. 2007; Ohashi,S.]. In addition, overexpression of *EGFR* and loss-of-function *TP53* mutations are frequently observed in human MPNSTs [Esteve,A. 1993; Itakura,Y. 1994; Parenti,A.R. 1995].

A multi-gene plasmid that over-expresses wild-type *EGFR* under the *CAGGs* promoter, possesses a doxycyclin inducible shRNA targeting *TP53*, and a puromycin selectable marker has been generated. This plasmid will be transfected into HSC2λ. Cells will be assessed for alterations in expression of *EGFR* and *TP53* by RT-PCR and immunoblotting. Phenotypic analysis of the cells will include monitoring for changes in proliferation, anchorage independent growth, and tumorigenicity by xenografts into nude mice. Controls will include cells with single gene plasmids, the multigene plasmid expressed without the presence of doxycyclin, and mock-transfected HSC2λ.

The doxycyclin inducible *TP53-shRNA* was developed in order to assess the dependence transformed cells have on loss of TP53. If *EGFR* overexpression and loss of TP53 cooperate to transform HSC2λ cells, the cells can be used in a xenograft model for

tumor formation. Mice injected with the cells will be placed on doxycyclin chow to induce the *TP53* shRNA. After tumor formation occurs, mice will be given normal chow to allow for restoration of *TP53* expression and will be monitored for tumor formation. I hypothesize that tumors will be dependent on loss of *TP53* expression and that restoration of *TP53* expression will reduce tumor growth if not cause regression of the tumor. Experiments with *Trp53* restoration in bovine leukemia virus cells demonstrated reduced tumor growth in mice [Dees, C. 1996]. Overall, completion of these experiments will provide a better understanding of the role of *EGFR* and *TP53* in Schwann cell tumorigenesis in humans.

**Further defining the role of *CAV1* in Schwann cell tumorigenesis.**

From the SB-mutagenesis screen for MPNST genes, *Cav1* was identified as repeatedly mutated by T2/Onc [Chapter 5]. Transposon insertions within *Cav1* lead to reduced *Cav1* expression and increased ß-catenin levels in cell lines derived from tumors [Chapter 5]. More specifically, there was an increase in ß-catenin expression in the nuclei of the cells. This phenotype was recapitulated in shRNA experiments in immortalized Rat Schwann cells. Moreover, *Cav1*$^{+/-}$*; CNPase-hEGFR* mice developed high penetrance of neurofibromas and PNSTs. Tumors from these mice also demonstrated increased ß-catenin levels and increased activated ß-catenin compared to single transgenic control mice. Overall, to address the mechanism of action for the synergy of *Cav1* reduction and *EGFR* overexpression in tumor formation, the role of ß-catenin expression and function in Schwann cells will be investigated.

ß-Catenin expression was noticeably increased in *Cav1-T2/Onc* cell lines, cell lines with T2/Onc insertions within the *Cav1* gene causing *Cav1* deficiency, from SB-derived tumors and immortalized Rat Schwann cells transduced with a *Cav1-shRNA*. Since SB-derived tumors also expressed EGFR and immortalized Rat Schwann cells express higher levels of EGFR, this may suggest that either *Cav1* reduction and/or *EGFR* overexpression may lead to increased transcription of ß-catenin in Schwann cells. IHC for ß-catenin on dorsal root ganglion from *Cav1*$^{+/-}$ and *CNPase-hEGFR* mice demonstrated that *EGFR* overexpression was correlated with increased staining for ß-

Catenin compared to *Cav1*$^{+/-}$ mice. These data suggest that EGFR is either increasing transcription of *ß-catenin* or stabilizing ß-catenin from being degraded. To address these possibilities, an immortalized human Schwann cell line (HSC2λ), that expresses *CAV1* and does not express *EGFR*, will be transduced with either a plasmid overexpressing *EGFR* or shRNA against *CAV1* and analyzed by RT-PCR to look at transcript levels of *ß-catenin* and immunoblot analysis for protein expression of ß-catenin. Results from this experiment will determine if transcription or protein stabilization is leading to increased ß-catenin expression.

In addition to overall increased ß-catenin expression in *Cav1* knockdown and EGFR overexpressing cell lines, ß-catenin appeared to be localized to the nucleus suggesting transcriptionally activated ß-catenin. To address if the nuclear localized ß-catenin is working as a transcription factor, *Cav1*-T2/onc cell lines and modified HSC2λ cells will be transduced with transcriptional reporter plasmids (TOP-FLASH). These reporter plasmids have ß-catenin binding sites in which transcriptionally activated ß-catenin binds to the promoter region and induces luciferase expression. In addition to reporter assays, RT-PCR for expression of ß-catenin transcriptional targets *Myc* and *Cyclin D1* will be assessed. Results from these experiments will determine if the nuclear localized ß-catenin observed in *Cav1* knockdown/*EGFR* overexpression cell lines is transcriptionally active.

Moreover, to determine if overexpression of transcriptionally active ß-catenin is sufficient for Schwann cell tumorigenesis, plasmids with a mutant form of ß-catenin that cannot be degraded will be transfected into HSC2λ cells. Alterations in proliferation and anchorage independent growth will be assessed to determine the affects of activated ß-catenin expression. In addition, we are currently generating a transgenic mouse that conditionally expresses an activated form of ß-catenin. These transgenic mice will be bred to *CNPase-Cre* and *Dhh-Cre* mice to induce expression of the activated ß-catenin in Schwann cells. Mice will be aged and assessed for tumor formation. Overall, these experiments will help delineate the role of ß-catenin in Schwann cell tumorigenesis.

**New mouse models of MPNST development/progression.**

The main goal of SB screens is to identify new therapeutic targets for treatment of human diseases. In order to accomplish this goal, we must first better understand the genetics of MPNST formation/progression. Data from the SB-MPNST screen identified over a hundred CISs that are associated with MPNST formation. From this list, co-occurring CISs (co-CISs), CISs that are present in the same tumor at statistically significant levels, were identified. *Pten* and *Nf1*, known tumor suppressor genes in MPNST development, were identified as co-CISs. Using this information, we developed a new mouse model of MPNST formation by biallelic inactivation of conditionally expressing *Pten* and *Nf1* alleles in Schwann cells utilizing *Dhh-Cre*. These mice developed rapid MPNSTs by 21 days (unpublished observations by Dr. Vincent Keng). Since disregulation of both Nf1 and Pten lead to increased signaling through the PI3K/AKT/mTOR signaling pathway, mice were treated with the mTOR synthetic inhibitor RAD001 [Johannessen, C.M. 2008; Johannessen, C.M. 2005]. Compared to vehicle control treated mice, RAD001 treatments had only slight effects on increasing median survival from 16 days to 19 days and minimal tumor reduction from 22 tumors/animal to 19 tumors/animal (unpublished observation by Adrienne Watson). These data suggest that the mTOR pathway alone may not be the only pathway altered. Combination therapies with RAD001 are warranted. Though much work needs to be done to fully characterize this new MPNST model and how RAD001 specifically affects tumor formation, creation of new mouse models and therapeutic testing is the next important step in finding/testing new therapeutic targets for treating human patients.

Besides *Pten* and *Nf1*, additional genes were identified as co-CISs (Chapter 5, Figure 2A). Interestingly, *Nf1*, *Pten*, and *CBP* are co-CISs with each other. Moreover, *Taok1* is a co-CIS with *Nf1*, *CBP*, and *Pten*. *Stag2* is a co-CIS with *Nf1* and *CBP*. One interesting note is that each of these genes has suggested tumor suppressive roles. Therefore, combinations of conditionally expressing alleles of these co-CIS will be inactivated specifically in Schwann cells to generate new mouse models of MPNST development. These new MPNST models will utilize different genetic pathways for

tumor formation/progression that will be useful in testing a variety of therapeutics for treatment of human MPNSTs.

**Summary**

In summary, this work demonstrated that a *Sleeping Beauty* forward genetic mutagenesis screen in prostate epithelium and Schwann cells can identify new genes and pathways relevant in human cancers. PDE4D provides a therapeutic target for the treatment of prostate cancer in human patients, and further analysis of CISs from Schwann cell tumors will identify new therapeutic targets for the treatment of MPNSTs.

**BIBLIOGRAPHY**


Aarhus, M., et al. "Global Gene Expression Profiling and Tissue Microarray Reveal Novel Candidate Genes and Down-Regulation of the Tumor Suppressor Gene CAV1 in Sporadic Vestibular Schwannomas." *Neurosurgery* 67.4 : 998,1019; discussion 1019.

Abate-Shen, C., and M. M. Shen. "Molecular Genetics of Prostate Cancer." *Genes & development* 14.19 (2000): 2410.

Agarwal, M. L., et al. "The p53 Network." *J Biol Chem* 273.1 (1998): 1-4.

Agelaki, S., et al. "Caveolin-1 Regulates EGFR Signaling in MCF-7 Breast Cancer Cells and Enhances Gefitinib-Induced Tumor Cell Inhibition." *Cancer Biol Ther* 8.15 (2009): 1470-7.

Akagi, K., et al. "RTCGD: Retroviral Tagged Cancer Gene Database." *Nucleic acids research* 32.suppl 1 (2004): D523.

Ananda, P., et al. “Cancer is a preventable disease that requires major lifestyle changes.” *Pharm Res* 25.9 (2008): 2097-2116.

Anderson, R. G. "The Caveolae Membrane System." *Annu Rev Biochem* 67 (1998): 199-225.

Asatiani, E., et al. "Deletion, Methylation, and Expression of the NKX3. 1 Suppressor Gene in Primary Human Prostate Cancer." *Cancer research* 65.4 (2005): 1164.

Aumuller, G., and J. Greenberg. "Seasonal Changes in the Fine Structure of the Accessory Sex Gland in the Mole (Talpa Europaea)." *Cell Tissue Res* 175.3 (1976): 403-16.

Badache, A., and G. H. De Vries. "Neurofibrosarcoma‐derived Schwann Cells Overexpress platelet‐derived Growth Factor (PDGF) Receptors and are Induced to Proliferate by PDGF BB." *Journal of cellular physiology* 177.2 (1998): 334-42.

Badache, A., N. Muja, and G. H. De Vries. "Expression of Kit in Neurofibromin-Deficient Human Schwann Cells: Role in Schwann Cell Hyperplasia Associated with Type 1 Neurofibromatosis." *Oncogene* 17.6 (1998): 795-800.

Ballester, R., et al. "The NF1 Locus Encodes a Protein Functionally Related to Mammalian GAP and Yeast IRA Proteins." *Cell* 63.4 (1990): 851-9.

Bang, Y. J., et al. "Cyclic AMP Induces Transforming Growth Factor Beta 2 Gene Expression and Growth Arrest in the Human Androgen-Independent Prostate Carcinoma Cell Line PC-3." *Proceedings of the National Academy of Sciences of the United States of America* 89.8 (1992): 3556.

Bang, YJ, et al. "Terminal Neuroendocrine Differentiation of Human Prostate Carcinoma Cells in Response to Increased Intracellular Cyclic AMP." *Proceedings of the National Academy of Sciences of the United States of America* 91.12 (1994): 5330.

Basu, T. N., et al. "Aberrant Regulation of Ras Proteins in Malignant-Tumor Cells from Type-1 Neurofibromatosis Patients." *Nature* 356.6371 (1992): 713-5.

Belur, L. R., et al. "Gene Insertion and Long-Term Expression in Lung Mediated by the Sleeping Beauty Transposon System." *Molecular Therapy* 8.3 (2003): 501-7.

Berman, D. M., et al. "Roles for Hedgehog Signaling in Androgen Production and Prostate Ductal Morphogenesis." *Dev Biol* 267.2 (2004): 387-98.

Bhatia-Gaur, R., et al. "Roles for Nkx3.1 in Prostate Development and Cancer." *Genes Dev* 13.8 (1999): 966-77.

Bijl, J., et al. "High Incidence of Proviral Integrations in the Hoxa Locus in a New Model of E2a–PBX1-Induced B-Cell Leukemia." *Genes & development* 19.2 (2005): 224.

Birindelli, S., et al. "Rb and TP53 Pathway Alterations in Sporadic and NF1-Related Malignant Peripheral Nerve Sheath Tumors." *Lab Invest* 81.6 (2001): 833-44.

Blobel, G. A. "CREB-Binding Protein and p300: Molecular Integrators of Hematopoietic Transcription." *Blood* 95.3 (2000): 745-55.

Bolger, G., et al. "A Family of Human Phosphodiesterases Homologous to the Dunce Learning and Memory Gene Product of Drosophila Melanogaster are Potential Targets for Antidepressant Drugs." *Molecular and cellular biology* 13.10 (1993): 6558.

Bolger, G. B., et al. "Characterization of Five Different Proteins Produced by Alternatively Spliced mRNAs from the Human cAMP-Specific Phosphodiesterase PDE4D Gene." *Biochemical Journal* 328.Pt 2 (1997): 539.

Bowen, C., et al. "Loss of NKX3. 1 Expression in Human Prostate Cancers Correlates with Tumor Progression1, 2." *Cancer research* 60.21 (2000): 6111.

Brannan, C. I., et al. "Targeted Disruption of the Neurofibromatosis Type-1 Gene Leads to Developmental Abnormalities in Heart and various Neural Crest-Derived Tissues." *Genes & development* 8.9 (1994): 1019.

Brekke, H. R., et al. "Identification of p53 as a Strong Predictor of Survival for Patients with Malignant Peripheral Nerve Sheath Tumors." *Neuro Oncol* 11.5 (2009): 514-28.

Buresh, R. A., et al. "Sulfatase 1 is an Inhibitor of Ductal Morphogenesis with Sexually Dimorphic Expression in the Urogenital Sinus." *Endocrinology* 151.7 (2010): 3420.

Burger, M., et al. "Mitogen-Activated Protein Kinase Signaling is Activated in Prostate Tumors but Not Mediated by B-RAF Mutations." *European urology* 50.5 (2006): 1102-10.

Burgin, A. B., et al. "Design of Phosphodiesterase 4D (PDE4D) Allosteric Modulators for Enhancing Cognition with Improved Safety." *Nature biotechnology* 28.1 (2009): 63-70.

Callahan, R., and G. H. Smith. "MMTV-Induced Mammary Tumorigenesis: Gene Discovery, Progression to Malignancy and Cellular Pathways." *Oncogene* 19.8 (2000): 992-1001.

Camp, R. L., G. G. Chung, and D. L. Rimm. "Automated Subcellular Localization and Quantification of Protein Expression in Tissue Microarrays." *Nature medicine* 8.11 (2002): 1323-8.

Cantiani, L., et al. "Caveolin-1 Reduces Osteosarcoma Metastases by Inhibiting c-Src Activity and Met Signaling." *Cancer Res* 67.16 (2007): 7675-85.

Capozza, F., et al. "Absence of Caveolin-1 Sensitizes Mouse Skin to Carcinogen-Induced Epidermal Hyperplasia and Tumor Formation." *Am J Pathol* 162.6 (2003): 2029-39.

Carlson, C. M., et al. "Transposon Mutagenesis of the Mouse Germline." *Genetics* 165.1 (2003): 243.

Cerveira, N., et al. "TMPRSS2-ERG Gene Fusion Causing ERG Overexpression Precedes Chromosome Copy Number Changes in Prostate Carcinomas and Paired HGPIN Lesions." *Neoplasia (New York, NY)* 8.10 (2006): 826.

Chieffi, P., et al. "Aurora B Expression Directly Correlates with Prostate Cancer Malignancy and Influence Prostate Cell Proliferation." *The Prostate* 66.3 (2006): 326-33.

Cho, N. Y., et al. "BRAF and KRAS Mutations in Prostatic Adenocarcinoma." *International journal of cancer* 119.8 (2006): 1858-62.

Cichowski, K., et al. "Mouse Models of Tumor Development in Neurofibromatosis Type 1." *Science* 286.5447 (1999): 2172.

Collier, L. S., et al. "Whole-Body Sleeping Beauty Mutagenesis can Cause Penetrant leukemia/lymphoma and Rare High-Grade Glioma without Associated Embryonic Lethality." *Cancer research* 69.21 (2009): 8429.

Collier, L. S., et al. "Cancer Gene Discovery in Solid Tumours using Transposon-Based Somatic Mutagenesis in the Mouse." *Nature* 436.7048 (2005): 272-6.

Couet, J., M. Sargiacomo, and M. P. Lisanti. "Interaction of a Receptor Tyrosine Kinase, EGF-R, with Caveolins. Caveolin Binding Negatively Regulates Tyrosine and serine/threonine Kinase Activities." *J Biol Chem* 272.48 (1997): 30429-38.

De Marzo, A. M., et al. "Proliferative Inflammatory Atrophy of the Prostate: Implications for Prostatic Carcinogenesis." *American Journal of Pathology* 155.6 (1999): 1985.

de Angelis, M.H., et al. “Genome-wide, large-scale production of mutant mice by ENU mutagenesis.” *Nature Genetics* 25.4 (2000): 444-447.

de Vries, A., et al. "Targeted Point Mutations of p53 Lead to Dominant-Negative Inhibition of Wild-Type p53 Function." *Proc Natl Acad Sci U S A* 99.5 (2002): 2948-53.

DeClue, J. E., et al. "Epidermal Growth Factor Receptor Expression in Neurofibromatosis Type 1-Related Tumors and NF1 Animal Models." *Journal of Clinical Investigation* 105.9 (2000): 1233-60.

Dees, C., et al. "Wild Type p53 Reduces the Size of Tumors Caused by Bovine Leukemia Virus-Infected Cells." *Cancer letters* 101.1 (1996): 115-22.

Deguchi, K., et al. "MOZ-TIF2-Induced Acute Myeloid Leukemia Requires the MOZ Nucleosome Binding Motif and TIF2-Mediated Recruitment of CBP." *Cancer Cell* 3.3 (2003): 259-71.

Doles, J., et al. "Functional Compensation in Hedgehog Signaling during Mouse Prostate Development." *Dev Biol* 295.1 (2006): 13-25.

Donjacour, A. A., A. A. Thomson, and G. R. Cunha. "FGF-10 Plays an Essential Role in the Growth of the Fetal Prostate." *Dev Biol* 261.1 (2003): 39-54.

Doorn, P. F., et al. "Malignant Peripheral Nerve Sheath Tumors in Patients with and without Neurofibromatosis." *Eur J Surg Oncol* 21.1 (1995): 78-82.

Dotto, G. P. "Notch Tumor Suppressor Function." *Oncogene* 27.38 (2008): 5115.

Druker, B. J., and N. B. Lydon. "Lessons Learned from the Development of an ab1 Tyrosine Kinase Inhibitor for Chronic Myelogenous Leukemia." *Journal of Clinical Investigation* 105.1 (2000): 3-8.

Ducatman, B. S., et al. "Malignant Peripheral Nerve Sheath Tumors. A Clinicopathologic Study of 120 Cases." *Cancer* 57.10 (1986): 2006-21.

Dupuy, A. J., et al. "Mammalian Mutagenesis using a Highly Mobile Somatic Sleeping Beauty Transposon System." *Nature* 436.7048 (2005): 221-6.

Dupuy, A. J., et al. "Mammalian Germ-Line Transgenesis by Transposition." *Proceedings of the National Academy of Sciences of the United States of America* 99.7 (2002): 4495.

Dupuy, A. J., S. Fritz, and D. A. Largaespada. "Transposition and Gene Disruption in the Male Germline of the Mouse." *Genesis* 30.2 (2001): 82-8.

Dupuy, A. J., et al. "A Modified Sleeping Beauty Transposon System that can be used to Model a Wide Variety of Human Cancers in Mice." *Cancer Res* 69.20 (2009): 8150-6.

Edwards, J., et al. "Gene Amplifications Associated with the Development of Hormone-Resistant Prostate Cancer." *Clinical cancer research* 9.14 (2003): 5271.

Engelman, J. A., et al. "Caveolin-Mediated Regulation of Signaling Along the p42/44 MAP Kinase Cascade in Vivo:: A Role for the Caveolin-Scaffolding Domain." *FEBS letters* 428.3 (1998): 205-11.

Engelman, J. A., et al. "Reciprocal Regulation of Neu Tyrosine Kinase Activity and Caveolin-1 Protein Expression in Vitro and in Vivo." *Journal of Biological Chemistry* 273.32 (1998): 20448.

Engelman, J. A., et al. "Recombinant Expression of Caveolin-1 in Oncogenically Transformed Cells Abrogates Anchorage-Independent Growth." *Journal of Biological Chemistry* 272.26 (1997): 16374.

Esteve, A., et al. "Correlation of p53 Mutations with Epidermal Growth Factor Receptor Overexpression and Absence of mdm2 Amplification in Human Esophageal Carcinomas." *Mol Carcinog* 8.4 (1993): 306-11.

Evans, D. G., et al. "Malignant Peripheral Nerve Sheath Tumours in Neurofibromatosis 1." *J Med Genet* 39.5 (2002): 311-4.

Fan, L., et al. "Hedgehog Signaling Promotes Prostate Xenograft Tumor Growth." *Endocrinology* 145.8 (2004): 3961-70.

Ferner, R. E., and D. H. Gutmann. "International Consensus Statement on Malignant Peripheral Nerve Sheath Tumors in Neurofibromatosis." *Cancer Res* 62.5 (2002): 1573-7.

Ferner, R. E., and M. J. O'Doherty. "Neurofibroma and Schwannoma." *Curr Opin Neurol* 15.6 (2002): 679-84.

Fiucci, G., et al. "Caveolin-1 Inhibits Anchorage-Independent Growth, Anoikis and Invasiveness in MCF-7 Human Breast Cancer Cells." *Oncogene* 21.15 (2002): 2365-75.

Fonte, C., et al. "Involvement of {Beta}-Catenin and Unusual Behavior of CBP and p300 in Glucocorticosteroid Signaling in Schwann Cells." *Proc Natl Acad Sci U S A* 102.40 (2005): 14260-5.

Fonte, C., et al. "Opposite Effects of CBP and p300 in Glucocorticoid Signaling in Astrocytes." *J Steroid Biochem Mol Biol* 104.3-5 (2007): 220-7.

Forus, A., et al. "Comparative Genomic Hybridization Analysis of Human Sarcomas: I. Occurrence of Genomic Imbalances and Identification of a Novel Major Amplicon at 1q21-q22 in Soft Tissue Sarcomas." *Genes Chromosomes Cancer* 14.1 (1995): 8-14.

Fowler, M., et al. "RUNX1 (AML-1) and RUNX2 (AML-3) Cooperate with prostate-derived Ets Factor to Activate Transcription from the PSA Upstream Regulatory Region." *Journal of cellular biochemistry* 97.1 (2006): 1-17.

Freestone, S. H., et al. "Sonic Hedgehog Regulates Prostatic Growth and Epithelial Differentiation." *Dev Biol* 264.2 (2003): 352-62.

Friedman, J. M., et al. *Neurofibromatosis: Phenotype, Natural History, and Pathogenesis*. Johns Hopkins University Press, 1999.

Fukuda, T., et al. "Coexpression of HGF and c-Met/HGF Receptor in Human Bone and Soft Tissue Tumors." *Pathology international* 48.10 (1998): 757-62.

Furukawa, M., et al. "Targeting of Protein Ubiquitination by BTB–Cullin 3–Roc1 Ubiquitin Ligases." *Nature cell biology* 5.11 (2003): 1001-7.

Galbiati, F., et al. "Targeted Downregulation of Caveolin-1 is Sufficient to Drive Cell Transformation and Hyperactivate the p42/44 MAP Kinase Cascade." *The EMBO journal* 17.22 (1998): 6633-48.

Galbiati, F., B. Razani, and M. P. Lisanti. "Emerging Themes in Lipid Rafts and Caveolae." *Cell* 106.4 (2001): 403-11.

Gallee, MP, et al. "Monoclonal Antibody Ki-67 Defined Growth Fraction in Benign Prostatic Hyperplasia and Prostatic Cancer." *The Journal of urology* 142.5 (1989): 1342.

García-Cardeña, G., et al. "Dissecting the Interaction between Nitric Oxide Synthase (NOS) and Caveolin." *Journal of Biological Chemistry* 272.41 (1997): 25437.

Geurts, A. M., et al. "Gene Mutations and Genomic Rearrangements in the Mouse as a Result of Transposon Mobilization from Chromosomal Concatemers." *PLoS Genet* 2.9 (2006): e156.

Gioeli, D., et al. "Activation of Mitogen-Activated Protein Kinase Associated with Prostate Cancer Progression." *Cancer research* 59.2 (1999): 279.

Goeritz, F., et al. "Seasonal Timing of Sperm Production in Roe Deer: Interrelationship among Changes in Ejaculate Parameters, Morphology and Function of Testis and Accessory Glands." *Theriogenology* 59.7 (2003): 1487-502.

Gregorakis, A. K., E. H. Holmes, and G. P. Murphy. "Prostate-Specific Membrane Antigen: Current and Future Utility." *Semin Urol Oncol* 16.1 (1998): 2-12.

Gregorian, C., et al. "PTEN Dosage is Essential for Neurofibroma Development and Malignant Transformation." *Proc Natl Acad Sci U S A* 106.46 (2009): 19479-84.

Gu, W., X. L. Shi, and R. G. Roeder. "Synergistic Activation of Transcription by CBP and p53." *Nature* 387.6635 (1997): 819-23.

Gutmann, D. H. "The Neurofibromatoses: When Less is More." *Human molecular genetics* 10.7 (2001): 747.

Hagel, C., et al. "Histopathology and Clinical Outcome of NF1-Associated Vs. Sporadic Malignant Peripheral Nerve Sheath Tumors." *Journal of neuro-oncology* 82.2 (2007): 187-92.

Hakozaki, M., et al. "Establishment and Characterization of a Novel Human Malignant Peripheral Nerve Sheath Tumor Cell Line, FMS-1, that Overexpresses Epidermal

Growth Factor Receptor and Cyclooxygenase-2." *Virchows Arch* 455.6 (2009): 517-26.

Harris, J. W., et al. "Construction of a Tc1-Like Transposon Sleeping Beauty-Based Gene Transfer Plasmid Vector for Generation of Stable Transgenic Mammalian Cell Clones." *Anal Biochem* 310.1 (2002): 15-26.

He, W. W., et al. "A Novel Human Prostate-Specific, Androgen-Regulated Homeobox Gene (NKX3.1) that Maps to 8p21, a Region Frequently Deleted in Prostate Cancer." *Genomics* 43.1 (1997): 69-77.

Hellawell, G. O., et al. "Expression of the Type 1 Insulin-Like Growth Factor Receptor is Up-Regulated in Primary Prostate Cancer and Commonly Persists in Metastatic Disease." *Cancer research* 62.10 (2002): 2942.

Hind, D., et al. "The use of Irinotecan, Oxaliplatin and Raltitrexed for the Treatment of Advanced Colorectal Cancer: Systematic Review and Economic Evaluation." *Health Technol Assess* 12.15 (2008): 1-182.

Ho, S. M., et al. "Developmental Exposure to Estradiol and Bisphenol A Increases Susceptibility to Prostate Carcinogenesis and Epigenetically Regulates Phosphodiesterase Type 4 Variant 4." *Cancer research* 66.11 (2006): 5624.

Ho, C. C., et al. "Up-Regulated Caveolin-1 Accentuates the Metastasis Capability of Lung Adenocarcinoma by Inducing Filopodia Formation." *Am J Pathol* 161.5 (2002): 1647-56.

Holtkamp, N., et al. "Mutation and Expression of PDGFRA and KIT in Malignant Peripheral Nerve Sheath Tumors, and its Implications for Imatinib Sensitivity." *Carcinogenesis* 27.3 (2006): 664.

Holtkamp, N., et al. "Subclassification of Nerve Sheath Tumors by Gene Expression Profiling." *Brain pathology* 14.3 (2004): 258-64.

Holtkamp, N., et al. "MMP-13 and p53 in the Progression of Malignant Peripheral Nerve Sheath Tumors." *Neoplasia* 9.8 (2007): 671-7.

Huijbregts, R. P. H., et al. "DEVELOPMENT/PLASTICITY/REPAIR-Hypertrophic Neuropathies and Malignant Peripheral Nerve Sheath Tumors in Transgenic Mice Overexpressing Glial Growth Factor b3 in Myelinating Schwann Cells." *Journal of Neuroscience* 23.19 (2003): 7269-80.

Hummel, T. R., et al. "Gene Expression Analysis Identifies Potential Biomarkers of Neurofibromatosis Type 1 Including Adrenomedullin." *Clin Cancer Res* 16.20 : 5048-57.

Huson, SM, and R. A. C. Hughes. *The Neurofibromatoses: A Pathogenetic and Clinical Overview*. Chapman & Hall Medical, London, 1994.

Huss, J. W., et al. "The Gene Wiki: Community Intelligence Applied to Human Gene Annotation." *Nucleic acids research* 38.suppl 1 (2010): D633.

Itakura, Y., et al. "Epidermal Growth Factor Receptor Overexpression in Esophageal Carcinoma. an Immunohistochemical Study Correlated with Clinicopathologic Findings and DNA Amplification." *Cancer* 74.3 (1994): 795-804.

Ivics, Z., et al. "Molecular Reconstruction of Sleeping Beauty, a Tc1-Like Transposon from Fish, and its Transposition in Human Cells." *Cell* 91.4 (1997): 501-10.

Jacks, T., et al. "Tumour Predisposition in Mice Heterozygous for a Targeted Mutation in Nf1." *Nature genetics* 7.3 (1994): 353-61.

Jemal, A., et al. "Cancer Statistics, 2006." *CA: a cancer journal for clinicians* 56.2 (2006): 106-30.

Jemal, A., et al. "Cancer Statistics, 2010." *CA: a cancer journal for clinicians* (2010): caac. 20073v1.

Jeong, JH, et al. "BRAF Activation Initiates but does Not Maintain Invasive Prostate." (2008)

Joesting, M. S., et al. "Secreted Frizzled Related Protein 1 is a Paracrine Modulator of Epithelial Branching Morphogenesis, Proliferation, and Secretory Gene Expression in the Prostate." *Dev Biol* 317.1 (2008): 161-73.

Joesting, M. S., et al. "Identification of SFRP1 as a Candidate Mediator of Stromal-to-Epithelial Signaling in Prostate Cancer." *Cancer Res* 65.22 (2005): 10423-30.

Johannessen, C. M., et al. "TORC1 is Essential for NF1-Associated Malignancies." *Current Biology* 18.1 (2008): 56-62.

Johannessen, C. M., et al. "The NF1 Tumor Suppressor Critically Regulates TSC2 and mTOR." *Proceedings of the National Academy of Sciences of the United States of America* 102.24 (2005): 8573.

Johansson, F. K., et al. "Identification of Candidate Cancer-Causing Genes in Mouse Brain Tumors by Retroviral Tagging." *Proceedings of the National Academy of Sciences of the United States of America* 101.31 (2004): 11334.

Johansson, G., et al. "Effective in Vivo Targeting of the Mammalian Target of Rapamycin Pathway in Malignant Peripheral Nerve Sheath Tumors." *Molecular cancer therapeutics* 7.5 (2008): 1237.

Jones, C., et al. "Molecular Cytogenetic Identification of Subgroups of Grade III Invasive Ductal Breast Carcinomas with Different Clinical Outcomes." *Clin Cancer Res* 10.18 Pt 1 (2004): 5988-97.

Jonkers, J., and A. Berns. "Retroviral Insertional Mutagenesis as a Strategy to Identify Cancer Genes." *Biochim Biophys Acta* 1287.1 (1996): 29-57.

Jost, A. "A New Look at the Mechanisms Controlling Sex Differentiation in Mammals." *Johns Hopkins Med J* 130.1 (1972): 38-53.

Justice, M.J., et al. “Mouse ENU mutagenesis.” *Human Molecular Genetics* 8.10 (1999): 1955-1963.

Kadono, T., et al. "Expressions of various Growth Factors and their Receptors in Tissues from Neurofibroma." *Dermatology* 201.1 (2000): 10-4.

Kadono, T., et al. "The Growth Regulation of Neurofibroma Cells in Neurofibromatosis Type-1: Increased Responses to PDGF-BB and TGF-[Beta] 1." *Biochemical and biophysical research communications* 198.3 (1994): 827-34.

Kang-Decker, N., et al. "Loss of CBP Causes T Cell Lymphomagenesis in Synergy with p27Kip1 Insufficiency." *Cancer Cell* 5.2 (2004): 177-89.

Karhadkar, S. S., et al. "Hedgehog Signalling in Prostate Regeneration, Neoplasia and Metastasis." *Nature* 431.7009 (2004): 707-12.

Kasper, L. H., et al. "CREB Binding Protein Interacts with Nucleoporin-Specific FG Repeats that Activate Transcription and Mediate NUP98-HOXA9 Oncogenicity." *Mol Cell Biol* 19.1 (1999): 764-76.

Kee, B. L., J. Arias, and M. R. Montminy. "Adaptor-Mediated Recruitment of RNA Polymerase II to a Signal-Dependent Activator." *J Biol Chem* 271.5 (1996): 2373-5.

Keizman, D., et al. "Expression and Significance of EGFR in Malignant Peripheral Nerve Sheath Tumor." *J Neurooncol* 94.3 (2009): 383-8.

Keng, V. W., et al. "A Conditional Transposon-Based Insertional Mutagenesis Screen for Genes Associated with Mouse Hepatocellular Carcinoma." *Nature biotechnology* 27.3 (2009): 264-74.

Khan, E. M., et al. "Epidermal Growth Factor Receptor Exposed to Oxidative Stress Undergoes Src- and Caveolin-1-Dependent Perinuclear Trafficking." *J Biol Chem* 281.20 (2006): 14486-93.

Kim, D. H., and A. Lerner. "Type 4 Cyclic Adenosine Monophosphate Phosphodiesterase as a Therapeutic Target in Chronic Lymphocytic Leukemia." *Blood* 92.7 (1998): 2484.

Kim, K. H., et al. "Mutations of the BRAF Gene in Papillary Thyroid Carcinoma and in Hashimoto's Thyroiditis." *Pathology international* 55.9 (2005): 540-5.

Kluwe, L., R. Friedrich, and V. F. Mautner. "Loss of NF1 Allele in Schwann Cells but Not in Fibroblasts Derived from an NF1-Associated Neurofibroma." *Genes Chromosomes Cancer* 24.3 (1999): 283-5.

Kluwe, L., R. E. Friedrich, and V. F. Mautner. "Allelic Loss of the NF1 Gene in NF1-Associated Plexiform Neurofibromas." *Cancer Genet Cytogenet* 113.1 (1999): 65-9.

Konishi, N., et al. "Comparison of Ras Activation in Prostate Carcinoma in Japanese and American Men." *The Prostate* 30.1 (1997): 53-7.

Kourea, H. P., et al. "Deletions of the INK4A Gene Occur in Malignant Peripheral Nerve Sheath Tumors but Not in Neurofibromas." *American Journal of Pathology* 155.6 (1999): 1855.

Kurita, T., et al. "Role of p63 and Basal Cells in the Prostate." *Development* 131.20 (2004): 4955.

Kuslak, S. L., and P. C. Marker. "Fibroblast Growth Factor Receptor Signaling through MEK–ERK is Required for Prostate Bud Induction." *Differentiation* 75.7 (2007): 638-51.

Lajoie, P., et al. "Plasma Membrane Domain Organization Regulates EGFR Signaling in Tumor Cells." *J Cell Biol* 179.2 (2007): 341-56.

Lakkis, M. M., and J. A. Epstein. "Neurofibromin Modulation of Ras Activity is Required for Normal Endocardial-Mesenchymal Transformation in the Developing Heart." *Development* 125.22 (1998): 4359.

Lamm, M. L., et al. "Sonic Hedgehog Activates Mesenchymal Gli1 Expression during Prostate Ductal Bud Formation." *Dev Biol* 249.2 (2002): 349-66.

Lappe-Siefke, C., et al. "Disruption of Cnp1 Uncouples Oligodendroglial Functions in Axonal Support and Myelination." *Nat Genet* 33.3 (2003): 366-74.

Largaespada, D. A., and L. S. Collier. "Transposon-Mediated Mutagenesis in Somatic Cells: Identification of Transposon-Genomic DNA Junctions." *Methods Mol Biol* 435 (2008): 95-108.

Lee, S. W., et al. "Tumor Cell Growth Inhibition by Caveolin Re-Expression in Human Breast Cancer Cells." *Oncogene* 16.11 (1998): 1391-7.

Legius, E., et al. "TP53 Mutations are Frequent in Malignant NF1 Tumors." *Genes Chromosomes Cancer* 10.4 (1994): 250-5.

Leong, K. G., and W. Q. Gao. "The Notch Pathway in Prostate Development and Cancer." *Differentiation* 76.6 (2008): 699-716.

Levine, A. J. "P53, the Cellular Gatekeeper for Growth and Division." *Cell* 88.3 (1997): 323-31.

Li, L., et al. "Caveolin-1 Maintains Activated Akt in Prostate Cancer Cells through Scaffolding Domain Binding Site Interactions with and Inhibition of serine/threonine Protein Phosphatases PP1 and PP2A." *Molecular and cellular biology* 23.24 (2003): 9389.

Li, S., J. Couet, and M. P. Lisanti. "Src Tyrosine Kinases, Gα Subunits, and H-Ras Share a Common Membrane-Anchored Scaffolding Protein, Caveolin." *Journal of Biological Chemistry* 271.46 (1996): 29182.

Li, L., et al. "Caveolin-1 Mediates Testosterone-Stimulated survival/clonal Growth and Promotes Metastatic Activities in Prostate Cancer Cells." *Cancer Res* 61.11 (2001): 4386-92.

Ling, B. C., et al. "Role for the Epidermal Growth Factor Receptor in Neurofibromatosis-Related Peripheral Nerve Tumorigenesis." *Cancer Cell* 7.1 (2005): 65-75.

Liu, T., et al. "Lack of BRAF Activating Mutations in Prostate Adenocarcinoma: A Study of 93 Cases." *Applied Immunohistochemistry & Molecular Morphology* 17.2 (2009): 121.

Liu, X., and M. A. Gorovsky. "Mapping the 5′ and 3′ Ends of Tetrahymena Thermophila mRNAs using RNA Ligase Mediated Amplification of cDNA Ends (RLM-RACE)." *Nucleic acids research* 21.21 (1993): 4954.

Lothe, R. A., et al. "Gain of 17q24-Qter Detected by Comparative Genomic Hybridization in Malignant Tumors from Patients with Von Recklinghausen's Neurofibromatosis." *Cancer Res* 56.20 (1996): 4778-81.

Lothe, R. A., et al. "Biallelic Inactivation of TP53 Rarely Contributes to the Development of Malignant Peripheral Nerve Sheath Tumors." *Genes Chromosomes Cancer* 30.2 (2001): 202-6.

Lu, Z., et al. "Downregulation of Caveolin-1 Function by EGF Leads to the Loss of E-Cadherin, Increased Transcriptional Activity of Beta-Catenin, and Enhanced Tumor Cell Invasion." *Cancer Cell* 4.6 (2003): 499-515.

Lyon, M. F., and S. G. Hawkes. "X-Linked Gene for Testicular Feminization in the Mouse." *Nature* 227.5264 (1970): 1217-9.

Maerki, S., et al. "The Cul3–KLHL21 E3 Ubiquitin Ligase Targets Aurora B to Midzone Microtubules in Anaphase and is Required for Cytokinesis." *The Journal of cell biology* 187.6 (2009): 791.

Magro, G., et al. "Multinucleated Floret-Like Giant Cells in Sporadic and NF1-Associated Neurofibromas: A Clinicopathologic Study of 94 Cases." *Virchows Arch* 456.1 : 71-6.

Mantripragada, K. K., et al. "High-Resolution DNA Copy Number Profiling of Malignant Peripheral Nerve Sheath Tumors using Targeted Microarray-Based Comparative Genomic Hybridization." *Clinical Cancer Research* 14.4 (2008): 1015.

Marker, P. C., et al. "Hormonal, Cellular, and Molecular Control of Prostatic Development." *Dev Biol* 253.2 (2003): 165-74.

Mawrin, C., et al. "Immunohistochemical and Molecular Analysis of p53, RB, and PTEN in Malignant Peripheral Nerve Sheath Tumors." *Virchows Archiv* 440.6 (2002): 610-5.

McCaughan, J. A., et al. "Further Evidence of the Increased Risk for Malignant Peripheral Nerve Sheath Tumour from a Scottish Cohort of Patients with Neurofibromatosis Type 1." *J Med Genet* 44.7 (2007): 463-6.

McDavid, K., et al. "Prostate Cancer Incidence and Mortality Rates and Trends in the United States and Canada." *Public health reports* 119.2 (2004): 174.

Mechtersheimer, G., et al. "Analysis of Chromosomal Imbalances in Sporadic and NF1-Associated Peripheral Nerve Sheath Tumors by Comparative Genomic Hybridization." *Genes Chromosomes Cancer* 25.4 (1999): 362-9.

Memarzadeh, S., et al. "Enhanced Paracrine FGF10 Expression Promotes Formation of Multifocal Prostate Adenocarcinoma and an Increase in Epithelial Androgen Receptor." *Cancer Cell* 12.6 (2007): 572-85.

Menon, AG, et al. "Chromosome 17p Deletions and p53 Gene Mutations Associated with the Formation of Malignant Neurofibrosarcomas in Von Recklinghausen Neurofibromatosis." *Proceedings of the National Academy of Sciences of the United States of America* 87.14 (1990): 5435.

Mertens, F., et al. "Cytogenetic Findings in Malignant Peripheral Nerve Sheath Tumors." *Int J Cancer* 61.6 (1995): 793-8.

Messiaen, L. M., et al. "Exhaustive Mutation Analysis of the NF1 Gene Allows Identification of 95% of Mutations and Reveals a High Frequency of Unusual Splicing Defects." *Human mutation* 15.6 (2000): 541-55.

Mikkers, H., et al. "High-Throughput Retroviral Tagging to Identify Components of Specific Signaling Pathways in Cancer." *Nature genetics* 32.1 (2002): 153-9.

Mikol, D. D., et al. "Caveolin-1 Expression in Schwann Cells." *Glia* 27.1 (1999): 39-52.

Miller, S. J., et al. "Large-Scale Molecular Comparison of Human Schwann Cells to Malignant Peripheral Nerve Sheath Tumor Cell Lines and Tissues." *Cancer research* 66.5 (2006): 2584.

Morris, J. M. "The Syndrome of Testicular Feminization in Male Pseudohermaphrodites." *Am J Obstet Gynecol* 65.6 (1953): 1192-211.

Nakajima, T., et al. "RNA Helicase A Mediates Association of CBP with RNA Polymerase II." *Cell* 90.6 (1997): 1107-12.

Nancarrow, D. J., et al. "Genome-Wide Copy Number Analysis in Esophageal Adenocarcinoma using High-Density Single-Nucleotide Polymorphism Arrays." *Cancer research* 68.11 (2008): 4163.

Némoz, G., et al. "Identification of Cyclic AMP-Phosphodiesterase Variants from the PDE4D Gene Expressed in Human Peripheral Mononuclear Cells." *FEBS letters* 384.1 (1996): 97-102.

Nielsen, G. P., et al. "Malignant Transformation of Neurofibromas in Neurofibromatosis 1 is Associated with CDKN2A/p16 Inactivation." *American Journal of Pathology* 155.6 (1999): 1879.

Niles, RM, et al. "Inhibition of Human Prostatic Epithelial Cell Replication by cAMP and Selected Analogs." *Experimental cell research* 102.1 (1976): 95-103.

Nowak, S. J., and V. G. Corces. "Phosphorylation of Histone H3: A Balancing Act between Chromosome Condensation and Transcriptional Activation." *TRENDS in Genetics* 20.4 (2004): 214-20.

Ogryzko, V. V., et al. "The Transcriptional Coactivators p300 and CBP are Histone Acetyltransferases." *Cell* 87.5 (1996): 953-9.

Ohashi, S., et al. "Epidermal Growth Factor Receptor and Mutant p53 Expand an Esophageal Cellular Subpopulation Capable of Epithelial-to-Mesenchymal Transition through ZEB Transcription Factors." *Cancer Res* 70.10 : 4174-84.

Ohlfest, J. R., et al. "Phenotypic Correction and Long-Term Expression of Factor VIII in Hemophilic Mice by Immunotolerization and Nonviral Gene Transfer using the Sleeping Beauty Transposon System." *Blood* 105.7 (2005): 2691.

Okamoto, T., et al. "Caveolins, a Family of Scaffolding Proteins for Organizing "Preassembled Signaling Complexes" at the Plasma Membrane." *J Biol Chem* 273.10 (1998): 5419-22.

Okawa, T., et al. "The Functional Interplay between EGFR Overexpression, hTERT Activation, and p53 Mutation in Esophageal Epithelial Cells with Activation of Stromal Fibroblasts Induces Tumor Development, Invasion, and Differentiation." *Genes Dev* 21.21 (2007): 2788-803.

Olive, K. P., et al. "Mutant p53 Gain of Function in Two Mouse Models of Li-Fraumeni Syndrome." *Cell* 119.6 (2004): 847-60.

Palanisamy, N., et al. "Rearrangements of the RAF Kinase Pathway in Prostate Cancer, Gastric Cancer and Melanoma." *Nature medicine* 16.7 (2010): 793-8.

Parenti, A. R., et al. "P53 Overexpression in the Multistep Process of Esophageal Carcinogenesis." *Am J Surg Pathol* 19.12 (1995): 1418-22.

Park, W. Y., et al. "Up-Regulation of Caveolin Attenuates Epidermal Growth Factor Signaling in Senescent Cells." *J Biol Chem* 275.27 (2000): 20847-52.

Pearson, H. B., T. J. Phesse, and A. R. Clarke. "K-Ras and Wnt Signaling Synergize to Accelerate Prostate Tumorigenesis in the Mouse." *Cancer research* 69.1 (2009): 94.

Peng, PD, et al. "Efficient Nonviral Sleeping Beauty Transposon-Based TCR Gene Transfer to Peripheral Blood Lymphocytes Confers Antigen-Specific Antitumor Reactivity." *Gene therapy* 16.8 (2009): 1042-9.

Perry, A., et al. "Differential NF1, p16, and EGFR Patterns by Interphase Cytogenetics (FISH) in Malignant Peripheral Nerve Sheath Tumor (MPNST) and Morphologically Similar Spindle Cell Neoplasms." *J Neuropathol Exp Neurol* 61.8 (2002): 702-9.

Petrij, F., et al. "Rubinstein-Taybi Syndrome Caused by Mutations in the Transcriptional Co-Activator CBP." *Nature* 376.6538 (1995): 348-51.

Pike, L. J., X. Han, and R. W. Gross. "Epidermal Growth Factor Receptors are Localized to Lipid Rafts that Contain a Balance of Inner and Outer Leaflet Lipids: A Shotgun Lipidomics Study." *J Biol Chem* 280.29 (2005): 26796-804.

Pinto, A. E., et al. "Frequent 7q Gains in Flow Cytometric multiploid/hypertetraploid Breast Carcinomas: A Study of Chromosome Imbalances by Comparative Genomic Hybridisation." *J Clin Pathol* 59.4 (2006): 367-72.

Plaat, B. E., et al. "Computer-Assisted Cytogenetic Analysis of 51 Malignant Peripheral-Nerve-Sheath Tumors: Sporadic Vs. Neurofibromatosis-Type-1-Associated Malignant Schwannomas." *Int J Cancer* 83.2 (1999): 171-8.

Podlasek, C. A., et al. "Prostate Development Requires Sonic Hedgehog Expressed by the Urogenital Sinus Epithelium." *Dev Biol* 209.1 (1999): 28-39.

Porter, D. E., et al. "Survival in Malignant Peripheral Nerve Sheath Tumours: A Comparison between Sporadic and Neurofibromatosis Type 1-Associated Tumours." *Sarcoma* 2009 (2009): 756395.

Press, N. J., and K. H. Banner. "2 PDE4 Inhibitors-A Review of the Current Field." *Progress in medicinal chemistry* 47 (2009): 37-74.

Pytel, P., J. B. Taxy, and T. Krausz. "Divergent Differentiation in Malignant Soft Tissue Neoplasms: The Paradigm of Liposarcoma and Malignant Peripheral Nerve Sheath Tumor." *Int J Surg Pathol* 13.1 (2005): 19-28.

Rahrmann, E. P., et al. "Identification of PDE4D as a Proliferation Promoting Factor in Prostate Cancer using a Sleeping Beauty Transposon-Based Somatic Mutagenesis Screen." *Cancer research* 69.10 (2009): 4388.

Rao, U. N. M., E. Sonmez-Alpan, and G. K. Michalopoulos. "Hepatocyte Growth Factor and c-MET in Benign and Malignant Peripheral Nerve Sheath Tumors." *Human pathology* 28.9 (1997): 1066-70.

Razani, B., et al. "Caveolin-1 Expression is Down-Regulated in Cells Transformed by the Human Papilloma Virus in a p53-Dependent Manner. Replacement of Caveolin-1 Expression Suppresses HPV-Mediated Cell Transformation." *Biochemistry* 39.45 (2000): 13916-24.

Rhodes, D. R., et al. "ONCOMINE: A Cancer Microarray Database and Integrated Data-Mining Platform." *Neoplasia (New York, NY)* 6.1 (2004): 1.

Richter, W., S. L. C. Jin, and M. Conti. "Splice Variants of the Cyclic Nucleotide Phosphodiesterase PDE4D are Differentially Expressed and Regulated in Rat Tissue." *Biochemical Journal* 388.Pt 3 (2005): 803.

Rutkowski, J. L., et al. "Genetic and Cellular Defects Contributing to Benign Tumor Formation in Neurofibromatosis Type 1." *Hum Mol Genet* 9.7 (2000): 1059-66.

Saez, C., et al. "Sialomucins are Characteristically O-Acylated in Poorly Differentiated and Colloid Prostatic Adenocarcinomas." *Modern pathology : an official journal of the United States and Canadian Academy of Pathology, Inc* 11.12 (1998): 1193-7.

Safran, M., et al. "Human Gene-Centric Databases at the Weizmann Institute of Science: GeneCards, UDB, CroW 21 and HORDE." *Nucleic acids research* 31.1 (2003): 142.

Saito, S., and H. Iwaki. "Mucin-Producing Carcinoma of the Prostate: Review of 88 Cases." *Urology* 54.1 (1999): 141-4.

Sanchez, P., et al. "Inhibition of Prostate Cancer Proliferation by Interference with SONIC HEDGEHOG-GLI1 Signaling." *Proc Natl Acad Sci U S A* 101.34 (2004): 12561-6.

Sawyers, C. L. "Chronic Myeloid Leukemia." *New England Journal of Medicine* 340.17 (1999): 1330-40.

Scherer, P. E., et al. "Caveolin Isoforms Differ in their N-Terminal Protein Sequence and Subcellular Distribution. Identification and Epitope Mapping of an Isoform-Specific Monoclonal Antibody Probe." *Journal of Biological Chemistry* 270.27 (1995): 16395.

Scherl, A., et al. "Prostatic Intraepithelial Neoplasia and Intestinal Metaplasia in Prostates of probasin-RAS Transgenic Mice." *The Prostate* 59.4 (2004): 448-59.

Schindler, T., et al. "Structural Mechanism for STI-571 Inhibition of Abelson Tyrosine Kinase." *Science* 289.5486 (2000): 1938.

Schlesinger, C., D. G. Bostwick, and K. A. Iczkowski. "High-Grade Prostatic Intraepithelial Neoplasia and Atypical Small Acinar Proliferation: Predictive Value for Cancer in Current Practice." *The American Journal of Surgical Pathology* 29.9 (2005): 1201.

Schmidt, H., et al. "Gains in Chromosomes 7, 8q, 15q and 17q are Characteristic Changes in Malignant but Not in Benign Peripheral Nerve Sheath Tumors from Patients with Recklinghausen's Disease." *Cancer Lett* 155.2 (2000): 181-90.

Schmidt, H., et al. "Cytogenetic Characterization of Six Malignant Peripheral Nerve Sheath Tumors: Comparison of Karyotyping and Comparative Genomic Hybridization." *Cancer Genet Cytogenet* 128.1 (2001): 14-23.

Schmidt, H., et al. "Genomic Imbalances of 7p and 17q in Malignant Peripheral Nerve Sheath Tumors are Clinically Relevant." *Genes Chromosomes Cancer* 25.3 (1999): 205-11.

Shen, Y., et al. "KRAS and BRAF Mutations in Prostate Carcinomas of Chinese Patients." *Cancer genetics and cytogenetics* 198.1 (2010): 35-9.

Sherman, L. S., et al. "Single Cell Ras-GTP Analysis Reveals Altered Ras Activity in a Subpopulation of Neurofibroma Schwann Cells but Not Fibroblasts." *Journal of Biological Chemistry* 275.39 (2000): 30740.

Shou, J., et al. "Dynamics of Notch Expression during Murine Prostate Development and Tumorigenesis." *Cancer research* 61.19 (2001): 7291.

Singh, U. P. "Reproductive Biology of the Male Sheath-Tailed Bat, Taphozous Longimanus (Emballonuridae) from India." *Biomed Environ Sci* 10.1 (1997): 14-26.

Sjöblom, T., et al. "The Consensus Coding Sequences of Human Breast and Colorectal Cancers." *Science* 314.5797 (2006): 268.

Starr, T. K., et al. "A Transposon-Based Genetic Screen in Mice Identifies Genes Altered in Colorectal Cancer." *Science* 323.5922 (2009): 1747.

Stonecypher, M. S., et al. "Activation of the Neuregulin-1/ErbB Signaling Pathway Promotes the Proliferation of Neoplastic Schwann Cells in Human Malignant Peripheral Nerve Sheath Tumors." *Oncogene* 24.36 (2005): 5589-605.

Storlazzi, CT, et al. "Identification of a Novel Amplicon at Distal 17q Containing the BIRC5/SURVIVIN Gene in Malignant Peripheral Nerve Sheath Tumours." *The Journal of pathology* 209.4 (2006): 492-500.

Su, W., et al. "Malignant Peripheral Nerve Sheath Tumor Cell Invasion is Facilitated by Src and Aberrant CD44 Expression." *Glia* 42.4 (2003): 350-8.

Subramanian, S., et al. "Genome-Wide Transcriptome Analyses Reveal p53 Inactivation Mediated Loss of miR-34a Expression in Malignant Peripheral Nerve Sheath Tumours." *J Pathol* 220.1 : 58-70.

Sumara, I., et al. "A Cul3-Based E3 Ligase Removes Aurora B from Mitotic Chromosomes, Regulating Mitotic Progression and Completion of Cytokinesis in Human Cells." *Developmental cell* 12.6 (2007): 887-900.

Tabone-Eglinger, S., et al. "Frequent EGFR Positivity and Overexpression in High-Grade Areas of Human MPNSTs." *Sarcoma* 2008 (2008): 849156.

Tahir, S. A., et al. "Secreted Caveolin-1 Stimulates Cell survival/clonal Growth and Contributes to Metastasis in Androgen-Insensitive Prostate Cancer." *Cancer Res* 61.10 (2001): 3882-5.

Takeuchi, T., et al. "Extracellular Matrix Dermatopontin Modulates Prostate Cell Growth in Vivo." *Journal of endocrinology* 190.2 (2006): 351.

Tawbi, H., et al. "Epidermal Growth Factor Receptor Expression and Mutational Analysis in Synovial Sarcomas and Malignant Peripheral Nerve Sheath Tumors." *Oncologist* 13.4 (2008): 459-66.

Tirado, O. M., et al. "Caveolin-1 (CAV1) is a Target of EWS/FLI-1 and a Key Determinant of the Oncogenic Phenotype and Tumorigenicity of Ewing's Sarcoma Cells." *Cancer Res* 66.20 (2006): 9937-47.

Tomlins, S. A., et al. "TMPRSS2: ETV4 Gene Fusions Define a Third Molecular Subtype of Prostate Cancer." *Cancer research* 66.7 (2006): 3396.

Tomlins, S. A., et al. "Recurrent Fusion of TMPRSS2 and ETS Transcription Factor Genes in Prostate Cancer." *Science* 310.5748 (2005): 644.

Tsujimura, A., et al. "Proximal Location of Mouse Prostate Epithelial Stem Cells: A Model of Prostatic Homeostasis." *J Cell Biol* 157.7 (2002): 1257-65.

ÜCKERT, S., et al. "Characterization and Functional Relevance of Cyclic Nucleotide Phosphodiesterase Isoenzymes of the Human Prostate." *The Journal of urology* 166.6 (2001): 2484-90.

Uckert, S., et al. "Immunohistochemical Distribution of cAMP-and cGMP-Phosphodiesterase (PDE) Isoenzymes in the Human Prostate." *European urology* 49.4 (2006): 740-5.

Upadhyaya, M., et al. "Germline and Somatic NF1 Gene Mutation Spectrum in NF1-Associated Malignant Peripheral Nerve Sheath Tumors (MPNSTs)." *Hum Mutat* 29.1 (2008): 74-82.

Uren, AG, et al. "Retroviral Insertional Mutagenesis: Past, Present and Future." *Oncogene* 24.52 (2005): 7656-72.

Urich, H., and RD Tien. "Tumors of the Cranial, Spinal and Peripheral Nerve Sheaths." *Russell and Rubinstein's Pathology of Tumors of the Nervous System.London: Arnold* 2 (1998): 141–193.

Van Cutsem, E., et al. "K-RAS Status and Efficacy in the First-Line Treatment of Patients with Metastatic Colorectal Cancer (mCRC) Treated with FOLFIRI with Or without Cetuximab: The CRYSTAL Experience." *J Clin Oncol* 26.15 suppl (2008): 5s.

Verdijk, R. M., et al. "TP53 Mutation Analysis of Malignant Peripheral Nerve Sheath Tumors." *J Neuropathol Exp Neurol* 69.1 : 16-26.

Vogel, K. S., et al. "Mouse Tumor Model for Neurofibromatosis Type 1." *Science* 286.5447 (1999): 2176.

Wallace, M. R., et al. "Culture of Cytogenetically Abnormal Schwann Cells from Benign and Malignant NF1 Tumors." *Genes Chromosomes Cancer* 27.2 (2000): 117-23.

Wallenius, V., et al. "Overexpression of the Hepatocyte Growth Factor (HGF) Receptor (Met) and Presence of a Truncated and Activated Intracellular HGF Receptor Fragment in Locally aggressive/malignant Human Musculoskeletal Tumors." *American Journal of Pathology* 156.3 (2000): 821.

Wang, B. E., et al. "Inhibition of Epithelial Ductal Branching in the Prostate by Sonic Hedgehog is Indirectly Mediated by Stromal Cells." *J Biol Chem* 278.20 (2003): 18506-13.

Warren, M., et al. "Protein Expression of Matriptase and its Cognate Inhibitor HAI-1 in Human Prostate Cancer: A Tissue Microarray and Automated Quantitative

Analysis." *Applied Immunohistochemistry & Molecular Morphology* 17.1 (2009): 23.

Warrington, N. M., et al. "Cyclic AMP Suppression is Sufficient to Induce Gliomagenesis in a Mouse Model of Neurofibromatosis-1." *Cancer research* 70.14 (2010): 5717.

Watanabe, T., et al. "Malignant Peripheral Nerve Sheath Tumour Arising within Neurofibroma. an Immunohistochemical Analysis in the Comparison between Benign and Malignant Components." *Journal of clinical pathology* 54.8 (2001): 631.

Watson, M. A., et al. "Gene Expression Profiling Reveals Unique Molecular Subtypes of Neurofibromatosis Type I-associated and Sporadic Malignant Peripheral Nerve Sheath Tumors." *Brain pathology* 14.3 (2004): 297-303.

Weir, B. A., et al. "Characterizing the Cancer Genome in Lung Adenocarcinoma." *Nature* 450.7171 (2007): 893-8.

Weiss-Messer, E., et al. "Growth Hormone (GH) Receptors in Prostate Cancer: Gene Expression in Human Tissues and Cell Lines and Characterization, GH Signaling and Androgen Receptor Regulation in LNCaP Cells." *Molecular and cellular endocrinology* 220.1-2 (2004): 109-23.

Wild, R., et al. "Quantitative Assessment of Angiogenesis and Tumor Vessel Architecture by Computer-Assisted Digital Image Analysis: Effects of VEGF-Toxin Conjugate on Tumor Microvessel Density." *Microvascular research* 59.3 (2000): 368-76.

Willett, C. G., et al. "Direct Evidence that the VEGF-Specific Antibody Bevacizumab has Antivascular Effects in Human Rectal Cancer." *Nature medicine* 10.2 (2004): 145-7.

Williams, T. M., et al. "Loss of Caveolin-1 Gene Expression Accelerates the Development of Dysplastic Mammary Lesions in Tumor-Prone Transgenic Mice." *Mol Biol Cell* 14.3 (2003): 1027-42.

Williams, T. M., et al. "Combined Loss of INK4a and Caveolin-1 Synergistically Enhances Cell Proliferation and Oncogene-Induced Tumorigenesis: Role of INK4a/CAV-1 in Mammary Epithelial Cell Hyperplasia." *J Biol Chem* 279.23 (2004): 24745-56.

Williams, T. M., et al. "Caveolin-1 Gene Disruption Promotes Mammary Tumorigenesis and Dramatically Enhances Lung Metastasis in Vivo. Role of Cav-1 in Cell Invasiveness and Matrix Metalloproteinase (MMP-2/9) Secretion." *J Biol Chem* 279.49 (2004): 51630-46.

Wu, J., et al. "Plexiform and Dermal Neurofibromas and Pigmentation are Caused by Nf1 Loss in Desert Hedgehog-Expressing Cells." *Cancer Cell* 13.2 (2008): 105-16.

Wu, X., et al. "Transcription Start Regions in the Human Genome are Favored Targets for MLV Integration." *Science* 300.5626 (2003): 1749.

Xu, G. F., et al. "The Neurofibromatosis Type 1 Gene Encodes a Protein Related to GAP." *Cell* 62.3 (1990): 599-608.

Yeung, S. C. J., C. Gully, and M. H. Lee. "Aurora-B Kinase Inhibitors for Cancer Chemotherapy." *Mini reviews in medicinal chemistry* 8.14 (2008): 1514-25.

Zhang, L., et al. "Cyclic Nucleotide Phosphodiesterase Profiling Reveals Increased Expression of Phosphodiesterase 7B in Chronic Lymphocytic Leukemia." *Proceedings of the National Academy of Sciences* 105.49 (2008): 19532.

Zheng, H., et al. "Induction of Abnormal Proliferation by Nonmyelinating Schwann Cells Triggers Neurofibroma Formation." *Cancer Cell* 13.2 (2008): 117-28.

Zhu, Y., et al. "Neurofibromas in NF1: Schwann Cell Origin and Role of Tumor Environment." *Science* 296.5569 (2002): 920.

Zou, C., et al. "Clinical, Pathological, and Molecular Variables Predictive of Malignant Peripheral Nerve Sheath Tumor Outcome." *Ann Surg* 249.6 (2009): 1014-22.